INFORMATION TO USERS

This manuscript has been reproduced from the microfilm master. UMI films the text directly from the original or copy submitted. Thus, some thesis and dissertation copies are in typewriter face, while others may be from any type of computer printer.

The quality of this reproduction is dependent upon the quality of the copy submitted. Broken or indistinct print, colored or poor quality illustrations and photographs, print bleedthrough, substandard margins, and improper alignment can adversely affect reproduction.

In the unlikely event that the author did not send UMI a complete manuscript and there are missing pages, these will be noted. Also, if unauthorized copyright material had to be removed, a note will indicate the deletion.

Oversize materials (e.g., maps, drawings, charts) are reproduced by sectioning the original, beginning at the upper left-hand corner and continuing from left to right in equal sections with small overlaps.

Photographs included in the original manuscript have been reproduced xerographically in this copy. Higher quality 6" x 9" black and white photographic prints are available for any photographs or illustrations appearing in this copy for an additional charge. Contact UMI directly to order.

Bell & Howell Information and Learning
300 North Zeeb Road, Ann Arbor, MI 48106-1346 USA
800-521-0600

High-Rate Digital Acoustic Communications in a Shallow Water Channel

by

YOUNG-HOON YOON
BSEE, Kyung-pook National University, South Korea, 1984
MSEE, Kyung-pook National University, South Korea, 1986

A Dissertation Submitted in Partial Fulfillment of the
Requirements for the Degree of

DOCTOR OF PHILOSOPHY

in the Department of
Electrical and Computer Engineering

We accept this dissertation as conforming
to the required standard

Dr. A. Zielinski, Supervisor (Department of Electrical and Computer Engineering)

Dr. T. A. Gulliver, Departmental Member (Department of Electrical and Computer Engineering)

Dr. S. Stuchly, Departmental Member (Department of Electrical and Computer Engineering)

Dr. A. Doige, Outside Member (Department of Mechanical Engineering)

Dr. L. Wu, External Examiner (National Research Council, Ottawa)

© YOUNG-HOON YOON, 1999
University of Victoria

All rights reserved. This dissertation may not be reproduced in whole or in part, by photocopying or other means, without the permission of the author.

Supervisor: Dr. Adam Zielinski

ABSTRACT

The subject of this dissertation is coherent digital acoustic communication in the underwater environment. The objective of the research is to develop algorithms for reliable communication in the shallow underwater channel. Investigation is focused on channel depth less than 100 m and distances between transmitter and receiver from 5 km to 50 km.

Based on the characteristics of the underwater acoustic channel and using a conventional approach, the achievable transmission range and the required acoustic power is determined for given channel conditions and system parameters.

A channel model suitable for the investigation of shallow water communication is developed which takes into account transmitter-receiver geometry, environmental conditions and system parameters. The model is based on multiple reflections in the channel with weightings according to signal attenuation due to spreading, reflection losses and absorption. Time-variability is introduced by incorporating Doppler frequency shifts due to transmitter/receiver motion.

A new method of evaluating performance of a system operating in such multipath conditions is proposed by introduction of a signal-to-multipath ratio (SMR), which is a measure of intersymbol interference (ISI) caused by the multipath. The SMR allows assessment of system performance for various receiver/transmitter positions and channel parameters. It can be used, for instance, to find the transmitter/receiver depth for optimum transmission. A suitable equalizer can improve a SMR. For example, a decision feedback equalizer (DFE) using a least mean square (LMS) and fast optimized LMS criterion is effective in coping with ISI as demonstrated by computer simulations. Hardware complexities of several equalizer algorithms are investigated for a selected channel. The performance degradation due to the presence of Gaussian noise in addition to

multipath is analyzed by simulation.

A novel structure of an equalizer suitable for the time-variant underwater acoustic channel is proposed. By adaptively adjusting the number of equalizer taps depending on the channel condition, the proposed structure offers reduced hardware complexity. Computer simulations demonstrate the effectiveness of this approach.

It is anticipated that the results of this work will find application in the design of high data rate transmission systems for ocean bottom instrumentation, the design of telemetry for autonomous underwater vehicles, and others.

Examiners:

Dr. A. Zielinski, Supervisor (Department of Electrical and Computer Engineering)

Dr. T. A. Gulliver, Departmental Member (Department of Electrical and Computer Engineering)

Dr. S. Stuchly, Departmental Member (Department of Electrical and Computer Engineering)

Dr. A. Doige, Outside Member (Department of Mechanical Engineering)

Dr. L. Wu, External Examiner (National Research Council, Ottawa)

Table of Contents

List of Tables

List of Figures

Abbreviations

ALAN	-	acoustic local area network
AUV	-	autonomous underwater vehicle
BER	-	bit error rate
BPF	-	bandpass filter
DFE	-	decision feedback equalizer
DPLL	-	digital phase locked loop
DPSK	-	differential phase shift keying
FIR	-	finite impulse response
FLOPS	-	floating point operations per second
FOLMS	-	fast self-optimized LMS
FSE	-	fractionally-spaced equalizer
I-Q loop	-	inphase-quadrature loop
ISI	-	intersymbol interference
LMS	-	least mean square
LPF	-	low pass filter
MSE	-	mean square error
PLL	-	phase locked loop
PSK	-	phase shift keying
QAM	-	quadrature amplitude modulation
QPSK	-	quadrature phase shift keying
RDR	-	range to depth ratio
RLS	-	recursive least square

SMR - signal-to-multipath ratio

SNR - signal to noise ratio

UWA - underwater acoustic

WHOI - Woods Hole oceanographic institution

Acknowledgments

I would like to thank my supervisor, Dr. Zielinski of the Department of Electrical and Computer Engineering, for his encouragement, guidance, and advice during the course of this research and for his help in the preparation of this dissertation.

Financial assistance received from ETRI (Electronics and Telecommunications Research Institute in Korea), Dr. Zielinski (through the Natural Science and Engineering Research Council of Canada) at the University of Victoria and the BC Advanced Systems Institute is gratefully acknowledged.

To my parents and daughters

Chapter 1

Introduction

1.1 Motivation

In parallel to increased ocean related activities, demand for reliable underwater communications is increasing. Such communications are required for transmission of measurement data from underwater sensors, telemetry, control of autonomous underwater vehicles, voice and video transmission, and others [23, 78]. The goal of the research presented here is to contribute to the development of a reliable, coherent communication system which offers good bandwidth utilization and transmission performance.

Acoustic signals in the underwater environment are attenuated. Attenuation rises rapidly with increased frequency and distance [84]. This sets an upper limit for carrier frequency and therefore a limit to data transmission throughput. Transmitted signals suffer from phase shifts and amplitude fluctuations produced by multipath propagation and Doppler shifts due to receiver and transmitter motion [19]. In addition, effects of ambient noise caused by shipping, industrial noise, wind noise and biological noise [78] must be accounted for.

Even though many of the well-established principles of wireless radio communications can be utilized and have been adapted for application in underwater channels,

particular attention must be paid to the distinct characteristics of such channels [19, 78]. Table 1.1 compares typical parameters of terrestrial electromagnetic mobile communication with underwater acoustic communication systems. The underwater channel clearly shows a wider multipath spread and a larger Doppler frequency to carrier frequency ratio (f_d/f_c) compared with terrestrial electromagnetic mobile channels.

Spread spectrum techniques are used in a terrestrial electromagnetic mobile communication to mitigate the effects of multipath propagation. However, these techniques are not suitable for underwater communication because of bandwidth limitations imposed by acoustic transducers [31]. Beamforming is an effective technique when reflected signals arrive from distinctively different angles, but it is not effective for use in a shallow water channel where the various multipaths have very small arrival angles.

Frequency shift keying (FSK) has been frequently used since no carrier phase recovery circuit is required. However, FSK has poor bandwidth utilization. To increase the bandwidth efficiency of underwater acoustic communication systems, phase-coherent modulation such as phase shift keying (PSK) and quadrature amplitude modulation (QAM) has been employed. Coherent communication, however, requires recovery and tracking of the carrier phase. For this task, a phase locked-loop (PLL) is commonly utilized [60, 65]. The effect of multipath and Doppler shifts can be reduced by means of adaptive equalization and synchronization jointly optimized. More specifically, a receiver structure which employs a decision-feedback equalizer (DFE) combined with a digital phase-locked loop (DPLL) has been shown to be effective [38, 77].

Equalization methods are suited to data transmission in channels where differences in path length between the direct path and various multipaths are small. The length of channel impulse response of underwater channels (multipath spread T_m) shown in Table 1.1 requires a different equalizer design from that of terrestrial communications. Multipath spread T_m in the underwater acoustic channel may amount to 100-2000 symbols. Equalizers in such a channel need many coefficients to be updated in real-time which requires complex hardware. Several studies on reducing hardware complexity

have been performed recently [44, 54, 81]. Signal delay spread can vary greatly with different sea conditions. This large variation of signal delay spread will translate into inefficiency of an equalizer operation if the number of equalizer taps is fixed. In other words, if an equalizer is designed with a large number of taps to cope with the worst case signal delay spread, such an equalizer will consume more power with many redundant taps when the signal delay spread is reduced as the channel condition becomes favorable. This study proposes an adaptive algorithm for reducing the number of redundant taps when channel conditions improve.

Table 1.1: Comparison between typical terrestrial electromagnetic mobile and underwater acoustic communication systems

Parameters	Terrestrial Mobile	Underwater Acoustic
carrier frequency (f_c)	1 GHz	10 kHz
channel bandwidth	30 kHz	2 kHz
signalling rate	24.3 ksymbols/s	2 ksymbols/s
multipath spread (T_m)	10 μs [53, 63] (0.24 symbols)	50 - 1000 ms [72] (100 - 2000 symbols)
vehicle speed (v)	100 km/h (highway)	18 km/h (submersible)
Doppler frequency (f_d)	92.6 Hz	33.3 Hz
f_d/f_c	9.26×10^{-6}	3.33×10^{-3}
cycles/symbol	41152	5

1.2 General Considerations

Here, we describe the reasons for using acoustic signals for underwater communication and the advantages of digital systems.

1.2.1 Rationale for using acoustic signals

Electromagnetic waves and optical pulses can be used underwater but they are subject to large absorption by seawater. Because salt water is conductive, only the lowest radio wavelengths (30 Hz to 300 Hz) will propagate any distance. In coastal waters, the absorption coefficient of electromagnetic waves can be as high as 10 dB/m or greater [25]. Signals propagated in this band require large transmitter powers and large antennae. The optical communications is largely affected by scattering since numerous scattering particles exist in the sea. Sound transmission is the most effective means of directing energy transfer over long distances in water [26]. Acoustic signal attenuation due to absorption is 10^{-2} to 10^{-3} dB/m at the frequency range between 1 kHz and 50 kHz. Acoustic signals have been primarily used and technologies related to sound generation and detection have been extensively developed.

1.2.2 Rationale for digital systems

There are several advantages to digital communications over comparable analog communications. Digital systems offer:

- Higher degree of flexibility

  Signal-processing capabilities such as error control coding and adaptive equalization can be used. This offers the user the potential for low error rates and high reliability. Improved performance can also make longer transmission ranges possible.

- Economical advantages

  The availability and advancements in high-speed digital microprocessors, memory and integrated logic circuits enhance the economic benefits of digital communication systems.

- Encryption for security

  Digital data can easily be encrypted for security such as communications between submerged military submarines.

1.3 Literature Review

The special issues on acoustic communications in the IEEE Journal of Oceanic Engineering (Vol.21, No.2, April 1996) and on oceanic acoustic data telemetry (Vol.19, No.1, January 1991) describe recent advances and research activities in the area of underwater communications. An extensive bibliographical review is available [30, 78]. This literature review is conducted on three different subjects: underwater channel modeling, equalization and synchronization.

1.3.1 Underwater acoustic channel modeling

Considerable effort has been undertaken to model the shallow water channel [9, 37, 39, 42, 74]. Such channel is defined as a channel which has large range-to-depth ratio. In system design one must consider multipath propagation as well as spatial and temporal variability of acoustic signals in the underwater channel [19, 25]. Multipath propagation causes intersymbol interference (ISI) while channel variability causes phase fluctuations of received signals. The multipath structure depends on the channel geometry, environmental conditions and the frequency of the transmitted signals. The channel geometry is given by ocean depth, transmitter and receiver depth and the distance between transmitter and receiver. Environmental conditions include the effects of

water pressure, temperature and water density distribution [25, 37].

An adequate channel model suitable for computer simulations offers several advantages:

(1) it will save the high cost of experimentation with underwater communications systems;

(2) it will provide an ability to deal with selected effects separately; and

(3) it will generate an ability to compare performances of different system configurations under the same channel conditions.

However, modeling can be inaccurate to some degree due to model imperfection and input parameter uncertainties. Therefore, a model should be used carefully as a guideline to evaluate system performance. In modeling a shallow channel, the multipath propagation of sound as well as amplitude and phase fluctuations are the most important characteristics to be considered.

For an acoustic channel with non-constant sound speed profile, the ray-tracing method is commonly utilized to find acoustic rays between transmitter and receiver [37, 74]. The acoustic rays of interest leave the transmitter and reach the receiver directly or via reflections at the sea surface or at the bottom (eigenrays). The received signal is a summation of a number of time-varying phasors with random amplitude and phase. To model the fluctuations of amplitude and phase in acoustic propagation in the ocean, a Rayleigh fading model has been frequently utilized for a shallow water channel [39, 42]. According to Falahati [39], each individual statistically independent acoustic ray (eigenray) can be modeled by a single Rayleigh fading simulator while incorporating the Doppler shift due to the movement of transmitter and/or receiver.

A stochastic underwater acoustic channel model which accounts for fluctuations of the received signal using a combination of linear and nonlinear transforms performed on a Gaussian variable was proposed [42]. This model is flexible and able to reproduce arbitrary fluctuations measured in real experimentation as well as Rayleigh fading. Recently, Bjerrum-Niese *et al.* [9] developed a simulation tool for high data-rate acoustic

communication in a shallow water, time varying channel. Their channel model was developed based on physical aspects of the acoustic channel, emphasizing fluctuations of the signal transmission caused by time-varying multipath effects. Finally, a simple but effective channel model is proposed suitable for shallow water channels [91]. This was further generalized by Bjerrum-Niese *et al.* using a numerical ray tracing model in a layered shallow water channel [8].

1.3.2 Equalization

As a method of reducing ISI, an equalizer has been commonly employed [56, 72, 80]. In some cases, equalization has been performed together with beamforming (beamsteering) [7, 66, 78]. While a beamforming technique is an effective method in channels with a small range-to-depth ratio (less than 10), it becomes increasingly inefficient to resolve the very small inter-arrival angles of various multipaths in a channel with a large range-to-depth ratio (larger than 10). For this reason, equalization is most appropriate where differences in arriving angles and path lengths between adjacent path signals are small.

A linear equalizer operating under a least mean squares (LMS) algorithm [69, 78] and a DFE operating under a LMS [45] or a recursive least squares (RLS) algorithm [78] has been tested on several different channels. LMS algorithms have lower computational complexity whereas RLS algorithms and their variations offer better convergence and numerical stability but at the cost of higher complexity [70].

Carrier frequencies between 10 kHz and 50 kHz have been employed achieving data rates between 1 kbps (deep, long range channel) and 40 kbps (shallow water, medium range channel) [78]. Phase-coherent detection methods based on joint synchronization and equalization algorithms have been successfully tested by Northeastern University and Woods Hole Oceanographic Institution [77]. The joint algorithm utilized the combination of a DFE and a DPLL for the minimization of ISI and the carrier phase estimation. Because of this success, research has been broadened to include a

multichannel DFE and acoustic local area networks (ALAN) [79]. The multichannel DFE is an extension of single sensor reception by utilizing spatial diversity; that is, by the processing of many received input signals using an array of sensors.

Another important issue regarding equalizer design for shallow water acoustic communication is hardware complexity [44, 54]. Hardware complexity is related to the number of coefficients (equalizer taps) requiring update in real time. The channel impulse response in several cases requires more than a hundred taps to be updated [44]. In order to reduce the computational load of the equalizer, the unique characteristics of acoustic channels can be exploited. That is, the multipath structure in shallow water is often sparse; signal arrivals tend to be clustered in groups with gaps in time between adjacent groups. Also, the channel response and ambient noise are often stable over several seconds which allows the equalizer parameters to be updated less frequently, once trained. Different adaptation algorithms offer different computational complexity, convergence and tracking property [20, 73]. We wish to select the least computationaly complex algorithm for which the error rate performance is still acceptable. The hybrid of LMS and RLS algorithms which takes advantage of the property of fast converging RLS and low computational complexity of LMS has been proposed [41]. The receiver selects the adaptation algorithm automatically depending on channel conditions and the state of an equalizer. The performance of LMS is sensitive to the choice of step size. In other words, a smaller step size provides the smaller tracking performance while a large step size gives the faster convergence. To address this problem, self-optimized LMS algorithm [11, 20, 44] has been utilized at some increase in computational complexity.

Recently, self-optimization or blind recovery has received considerable attention [11, 43, 58, 82]. Self-optimization enables a receiver to adjust to changes in channel conditions with less frequent insertion of training sequences. As result, self-optimization or blind recovery receiver algorithms increase data throughput.

1.3.3 Synchronization

Noncoherent detection of FSK signals does not require tracking of the carrier phase, and therefore it has traditionally been employed as a modulation method for underwater acoustic communications [23, 64]. However, to overcome the effect of multipath propagation (that is, ISI), signal design with guard times have to be used. Guard times are inserted between successive pulses to ensure that reverberation vanishes before each subsequent pulse is received. However, this reduces data throughput. Recently, in order to increase the bandwidth efficiency of underwater acoustic communication systems, research on phase-coherent modulation techniques such as phase shift keying and quadrature amplitude modulation has been actively pursued [40, 78, 80]. Depending on the carrier synchronization method, a phase-coherent system can be divided into two categories: differentially coherent and purely phase-coherent systems. Differentially coherent detection has simple carrier recovery, but it has worse performance compared with purely coherent detection [19].

The Doppler effect arising from the relative motion between transmitter and receiver as well as the change of channel characteristics in time due to the moving ocean surface impose the difficulty of tracking the carrier phase in the presence of a complex multipath structure [57, 75]. Several algorithms have been developed for joint adaptive equalization and synchronization [75, 78]. A second order DPLL is frequently employed for carrier synchronization.

In order to achieve better performance from the synchronizer, rapid acquisition combined with accurate and reliable tracking is required [33, 61, 65, 75]. Acquisition is the process of acquiring lock from unlocked conditions whereas tracking is the process of maintaining synchronization after initial acquisition. Rapid acquisition of synchronization allows the length of a training sequence to be minimized while accurate and reliable phase tracking is needed to minimize tracking error and probability of a cycle slip or losing lock. Losing synchronization reduces efficiency in the data detection process because inaccurate synchronization directly reduces the probability of making correct decisions. In addition, loss of synchronization may sometimes lead to successive errors before synchronization is recovered.

1.4 Original Contributions

This dissertation covers two major topics: shallow water channel modeling and the techniques of communication in a shallow water channel and performance evaluation. The objective of this study is to develop algorithms for achieving reliable communications in a shallow underwater channel. The investigation is focused on the case of channel depth of less than 100 m and distance between transmitter and receiver from 5 to 50 km. The reason why this case was selected is that many activities occur in the shallow region of the continental shelf. Due to the effective bandwidth utilization required for achieving high speed data transmission, coherent N-ary PSK modulation is chosen throughout this research.

Major Contributions

Major contributions of this research include:

(1) Channel Modeling

A novel channel model suitable for the investigation of shallow water communications has been developed [91]. Geometric and environmental conditions of the channel are taken into consideration. The model utilizes the impulse response of the channel with weightings according to signal attenuation due to multiple reflection losses and absorption. The method of computing signal delays and attenuations is derived. For the time-variant channel, the effect of Doppler shift due to the relative motion between a transmitter and a receiver is considered. The channel model assumes the constant sound profile and smooth bottom which is often the case in many shallow water areas. Even though the assumption of a constant sound profile reduces the accuracy of the model, it provides insight into signal propagation without using an elaborate ray tracing algorithm.

(2) A New Measure of Performance

A new method of performance evaluation of multipath corrupted signals is introduced [91, 93]. This simple but effective performance measure is based on the concept of a signal-to-multipath ratio (SMR). The definition of SMR is based on the assumption that the signal at the receiver is analyzed within an observation window of duration equal to that of the signalling element. SMR is a measure of ISI caused by the multipath and gives a lower bound (worst case) on transmission performance. It allows assessment of system performance for various receiver/transmitter positions and channel parameters. Neglecting ambient noise, SMR can be used to determine the condition of error-free transmission (distinct phase constellations corresponding to different symbols transmitted). It enables us to find the transmitter/receiver depth for optimum signal transmission. The SMR is also used to assess the effect of a directional receiver. The SMR concept has been adopted by other researchers [8].

(3) Channel Equalizer with Adaptive Number of Tabs

When the sea state is changing due to changes in wind speed, the extent of signal delay spread varies greatly. A novel equalizer structure with an adaptive number of equalizer taps suitable for a time-varying underwater acoustic channel is proposed. This structure can adjust the number of equalizer taps depending on the sea state. That is, the number of equalizer taps is adaptively reduced when signal delay spread becomes smaller with a favorable channel condition. This allows the design of a computationaly efficient and less power consuming system required for the prolonged battery life of a remotely operated system. Performance of the proposed structure is evaluated by computer simulations. The effectiveness of a directional receiver with a proposed structure is also demonstrated.

Minor Contributions

Minor contributions of this research include:

(1) Achievable Transmission Range

Taking into consideration the relevant characteristics of underwater acoustic channels, we investigated the achievable transmission range at different channel conditions and system requirements. The dependency of achievable transmission range on frequency used, wind speed and required SNR is presented. When designing a remote transmitter/receiver, the power budget is an important factor because low power consumption is essential for prolonged operation. We also investigated the required acoustic power for certain transmission range at given SNR values. The effect of time variation of wind speed on the system response is described. The large variation of the signal delay spread at several different wind speeds is confirmed.

(2) Decision Feedback Equalizer (DFE)

DFEs using several different algorithms for coefficient update are simulated to demonstrate their effectiveness in coping with ISI caused by multipath propagation. Convergence characteristics and steady state performance of the equalizer with LMS, fast self-optimized LMS (FOLMS) and RLS algorithms are investigated. The hardware complexity required to implement an equalizer based on those algorithms is determined. The performance degradation due to Gaussian noise in addition to multipath is analyzed by simulations.

(3) Joint Adaptive Equalization and Carrier Synchronization

As an anti-multipath technique for a time variant underwater acoustic channel, the algorithm of joint adaptive equalization and a carrier synchronization for the N-ary PSK modulated signal is simulated. The effects of the variation of wind speed on received signal and the directionality of the receiver are investigated. The adaptive property of the equalizer in response to varying channel conditions is demonstrated by computer simulation.

1.5 Organization of the Dissertation

Chapter 1. Introduction

Chapter 1 describes the motivation of this research and presents a literature review, focusing particularly on an underwater acoustic channel model, equalization and synchronization. Some general considerations on the utilization of acoustic signals for signal transmission and the advantage of digital communications over analog communications are briefly reviewed. The scope, original contributions and organization of this dissertation are described.

Chapter 2. Digital Acoustic Communication Systems

In Chapter 2, relevant characteristics of an underwater acoustic channel for communications are described. Based on these characteristics, we investigate the achievable transmission range at given channel conditions and system requirements. The achievable transmission range as a function of the wind speed is investigated. We also investigate the required acoustic power for a certain transmission range at given SNR values. The overall functional structure of digital acoustic communication is described. The configuration of a N-ary PSK modulated communication system with an equalizer is presented. Filter characteristics at the transmitter and receiver are also derived.

Chapter 3. Model for Shallow Water Communication Channel

Chapter 3 introduces a model of a shallow water channel suitable for computer analysis. We initially develop the static channel model with deterministic propagation paths. A time variant channel model which accounts for the change of channel in time is then developed. The method of computation of signal attenuation and delay based on channel geometry, environmental conditions and system parameters is described. To limit the number of terms in the computation of a received signal, a condition to find the number of terms with significant amplitudes is derived. A case of the channel model

is studied to investigate signal attenuation and arriving angles with respect to time delay and wind speed. The case when a directional receiver with a simplified beam pattern is employed at the receiver is also studied. We will see that the use of a directional receiver is better suited for a channel with a small range-to-depth ratio while the equalization methods are better suited for a channel with a large range-to-depth ratio. The time-variability of the channel response incorporates the Doppler shifts due to transmitter/receiver motion.

Chapter 4. Performance Analysis of Digital Acoustic Communication

Performance measures for ISI are reviewed in Chapter 4. A new concept of performance evaluation for multipath corrupted signals is introduced using a SMR. The condition of error-free transmission based on the SMR is derived assuming that effects of ambient noise are negligible compared with effects of ISI. A sample N-ary PSK communication system is analyzed by investigating SMRs for various channel conditions. The computation of SMR at a given channel and system allows us to find the optimum location of transmitter and receiver. The SMR is also studied when a directional receiver is employed.

Chapter 5. Simulation of the Equalizer for Shallow Water Acoustic Communication

Chapter 5 investigates an equalization method for a communication system in a static time-invariant underwater channel as a counter measure to multipath. The equalizer structure and its algorithms are described. The hardware complexity associated with an equalizer is investigated. A DFE with LMS, FOLMS and square-root RLS algorithms, frequently employed for the update of an equalizer's coefficients, is investigated. A DFE structure is simulated using the channel model described in Chapter 3. Scatter diagrams obtained before and after equalization demonstrate the effectiveness of an equalizer in coping with ISI. Convergence characteristics are explored by investigating the variations of mean squared error with time. The effect of step size of the

equalizer on transient and steady state performance is studied. The transient performance is evaluated by the convergence speed while steady state performance is evaluated by variance of self noise. The effectiveness of the FOLMS algorithm is noted for its improved transient and steady state performance with only a small increase in hardware complexity.

Chapter 6. Anti-multipath Technique for a Time-varying Underwater Channel

Here, the time variation of the underwater acoustic channel is considered. The effect of time variation of wind speed on the system impulse response is investigated. The modified structure of the joint equalization and carrier synchronization of N-ary PSK modulated signals in a time variant underwater acoustic channel is explored. A novel equalizer structure with an adaptive number of taps is proposed. This structure will adjust the number of equalizer taps adaptively depending on the sea state. The method of updating equalizer coefficients and adjusting the number of taps of the equalizer is described. The performance of the proposed structure in a time-varying underwater acoustic channel is investigated by computer simulations. The effectiveness with a proposed structure combined with a directional receiver is confirmed.

Chapter 7. Summary and Future Research Considerations

Chapter 7 concludes the dissertation with a summary of the results and suggestions for future research.

Chapter 2

Digital Acoustic Communication Systems

2.1 Introduction

The purpose of a communication system is to send information from a data source to the data user. A high rate of transmission and a low probability of error are desirable performance measures. However, the acoustic channel has a finite bandwidth and signals in the underwater environment are attenuated, and exposed to ambient noise and distortion. These require a trade-off between the achievable data rate and the error probability. A functional block diagram for digital acoustic communication is shown in Figure 2.1. The information (data) source produces a discrete sequence or analog waveform which is encoded, transmitted over an acoustic channel, reconstructed, and delivered to a remote data user. Examples of data sources are:

(1) measurement data from acoustic instruments such as ocean bottom seismometers and pollution monitors in environmental systems;

(2) control/command data from/to a surface user on sea or land;

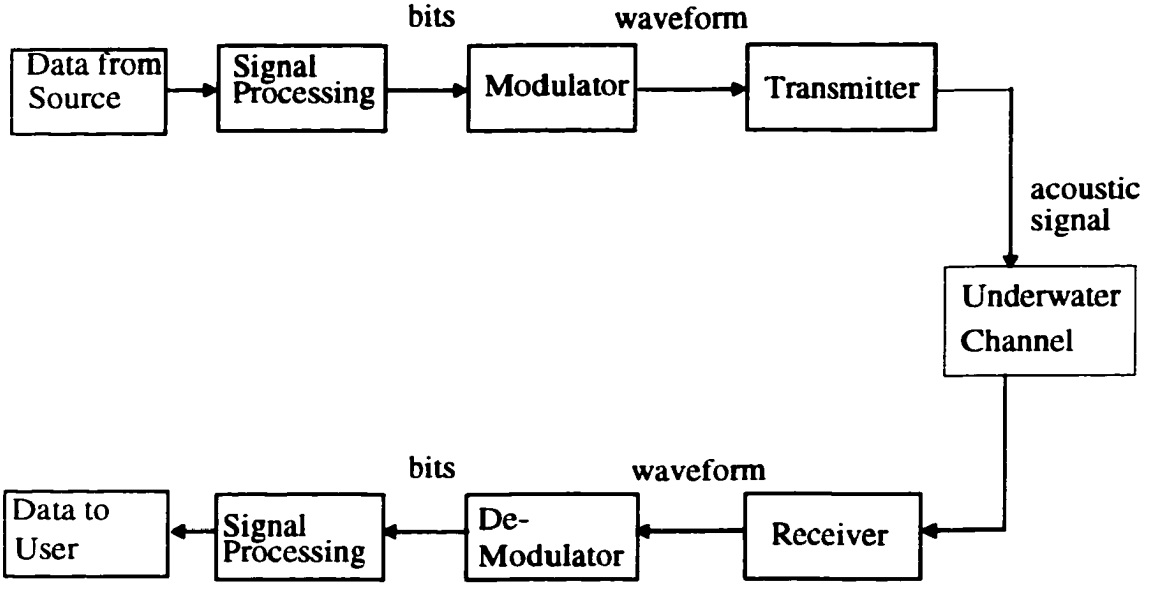

Figure 2.1: Functional block diagram for digital acoustic communication

(3) speech signals of communicating divers;

(4) real-time video transmission from acoustically controlled autonomous underwater vehicles (AUVs).

As efficient communication systems are being developed, the areas of their application grow, and so do performance requirements of the system.

Signal processing may include signal compression to reduce the amount of information transmitted, error detection and correction coding, and equalization or array processing to improve system performance. The data input to the processing block may be supplied by an analog source which is sampled and converted to digital data. The processed information bits are fed to the digital modulator. Modulation is the process by which some characteristics of a carrier are varied in accordance with the incoming modulating data. The transmitted signal can have varying frequency (frequency shift keying-FSK), phases (N-ary phase shift keying; N-ary PSK) and amplitudes (amplitude shift keying-ASK) or a combination of phases and amplitudes (quadrature amplitude modulation-QAM), depending on the type of modulation.

The transmitter block in Figure 2.1 represents transducers such as an underwater acoustic projector. In order to focus a beam into a certain direction, a transducer array can be used.

The acoustic channel characteristics play an important role in reliable system design. Transmission losses due to geometrical spreading and absorption in the presence of ambient noise impose a maximum achievable transmission range. Multipath propagation is also encountered which is caused by the reflection of acoustic energy at the surface and bottom. The reverberation due to multipath signal propagation results in intersymbol interference in the received signal. Finally, the relative motion between the transmitter and receiver introduces Doppler frequency spreading.

The receiver block in Figure 2.1 represents transducers such as a hydrophone or an array of hydrophones. Receiving arrays are very effective in removing intersymbol interference (ISI) when arriving angles of reflected signals are large. Even in a shallow

water channel, a directional receiver can be used to shorten the duration of the channel impulse response by nulling out the multipath arriving from angles that are large in relation to the direct path signal. The signal received in this manner can be processed by an equalizer with a smaller number of taps.

The important characteristics of the underwater acoustic channel and the power requirements for signal transmission are briefly described in Section 2.2. In Section 2.3, the specific system outline employed for this study is described.

2.2 Underwater Acoustic Channel

In this section, relevant characteristics of the underwater channel used for the acoustic communications are briefly described. Based on these characteristics, we investigate the achievable transmission range at given channel conditions and system requirements. The factors that limit range and rate of acoustic signal transmission include transmission losses, ambient noise and cavitation threshold. Intersymbol-interference due to multipath propagation and Doppler spreading due to relative motion of transmitter/receiver are other impairments to the achievement of high data rate transmission.

2.2.1 Transmission losses

As an acoustic wave propagates outward from the source, its intensity decreases. The rate of this intensity spreading depends on the channel geometry. Let us define a shallow underwater channel as a channel with a range-depth ratio (RDR) approximately larger than 10. In a shallow water channel, transmission loss (TL) is governed by the cylindrical spreading law, that is [31, 85],

$$TL = 10\log r \tag{2.1}$$

where r is a transmission range.

In addition to the spreading loss, the attenuation of the signal is caused by the conversion of some portion of the radiated energy into heat and lost to the medium during propagation. This attenuation due to absorption is a function of frequency and limits the usable frequency for a particular transmission range. The absorption coefficient $\alpha(f)$ in dB/m is given by [1]

$$\alpha(f) = \left[\frac{2.34\times 10^{-6} S f_T f^2}{f_T^2 + f^2} + \frac{3.38\times 10^{-6} f^2}{f_T}\right](1 - 6.54\times 10^{-4} P)8.686 \qquad (2.2)$$

where S is the salinity in ppt, f is the frequency in kHz, T is the temperature in °C, P is the pressure in atm. and

$$f_T = 21.9\times 10^{[6 - 1520/(T+273)]}. \qquad (2.3)$$

The transmission loss is then the sum of the spreading loss and the attenuation

$$TL(f) = 10\log r + r\alpha(f). \qquad (2.4)$$

2.2.2 Ambient noise

The signal-to-noise ratio (SNR) at the receiver is dependent on the ambient noise in a channel. Ambient noise in an underwater channel is caused by several sources [28]. Their values in dB re 1 μPa per $\sqrt{\text{Hz}}$, termed as noise spectral level (NSL), are given below where frequency f is expressed in kHz.

- Turbulence noise:

$$NSL_1 = 17 - 30\log f. \qquad (2.5\text{ a})$$

- Shipping noise:

$$NSL_2 = 40 + 20(D - 0.5) + 26\log f - 60\log(f + 0.03), \qquad (2.5\text{ b})$$

where D is the shipping density with a value between 0 (light) and 1(heavy).

- Surface agitation noise:

$$NSL_3 = 50 + 7.5w^{0.5} + 20\log f - 40\log(f + 0.4), \qquad (2.5\text{ c})$$

where w is the wind speed in m/s.

- Thermal noise:

$$NSL_4 = -15 + 20\log f. \qquad (2.5\text{ d})$$

The total noise level due to various contributions is:

$$NSL = 10\log \sum_{i=1}^{4} 10^{\frac{NSL_i}{10}}. \qquad (2.6)$$

For $f = 10$ kHz, $w = 10$ m/s and $D = 0$ (light shipping), the total spectral noise level is 53 dB re 1 μPa per $\sqrt{\text{Hz}}$. The total in-band noise level NLB for a narrow band is given by

$$NLB = NSL + 10\log B, \qquad (2.7)$$

where B is the bandwidth in Hz. Figure 2.2 shows the result of the calculation of total in-band noise with a typical value [19, 68] of the quality factor $Q = f/B = 5$ in the frequency range of interest for underwater acoustic communication. We see that ambient noise level decreases with frequency except when wind speed $w = 0$ knots which shows increasing noise level with a frequency larger than approximately 30 kHz.

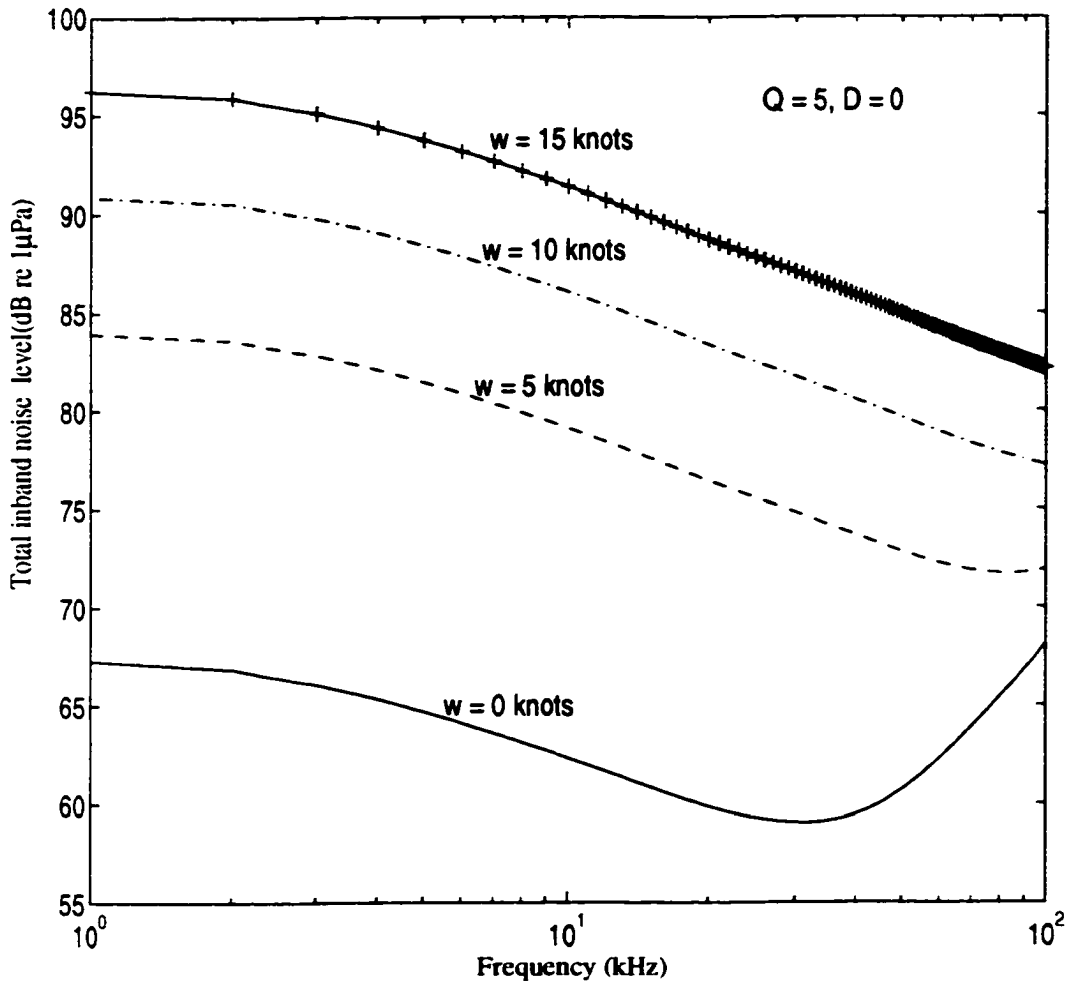

Figure 2.2: Total in-band noise level as a function of frequency

2.2.3 Achievable transmission range

In this section, the achievable transmission range for underwater communication is investigated considering the carrier frequency, acoustic power transmitted and wind speed. When the power radiated by a sonar projector exceeds the cavitation level, cavitation bubbles begin to form on the surface and just in front of the projector. This limits the acoustic power which can be transmitted. The cavitation threshold I_T in watts/cm^2 at depth z is [17, 84]:

$$I_T = 0.3\gamma(P_c(0) + 9.236 \times 10^{-3} z)^2 \tag{2.8}$$

where γ is a factor expressing the near-field effect on the cavitation limit with a value between 0.3 and 0.6, $P_c(0)$ is ambient pressure in atm. at the water surface, and z is the depth in metres. When multiplied by the face area of the projector (in cm^2), the cavitation threshold represents the maximum power (in watts) of the projector. At water surface with an atmospheric acoustic pressure of 1 atm., the cavitation threshold is $I_{T0} = 0.33$ W/cm^2. Let us assume that a total radiated acoustic power W at the onset of cavitation, distributed uniformly over an effective projector area A. With a threshold I_{T0} at water surface ($z = 0$), the relationship between maximum power W and depth z in metres is given by:

$$W_{max} = A \cdot I_{T0} \cdot (1 + 9.236 \times 10^{-3} z)^2. \tag{2.9}$$

For instance, a piston projector with a 10 cm diameter face is limited by cavitation to maximum power of about 26 watts when operated near the water surface.The cavitation threshold increases rapidly with depth, enabling greater power to be used. At a depth of 20 m, the projector can radiate 232 watts, approximately 8.9 times its maximum power at the surface. A typical acoustic transducer produces pressure of 190 dB

re 1μPa at 1 metre away on the maximum pressure axis, requiring 71 watts of acoustic power.

The maximum detectable range for a given signal-to-noise ratio (SNR) can be obtained using Eq. (2.4), Eq. (2.7) and an expression for SNR,

$$SNR = SL - TL - NLB + DI \tag{2.10}$$

where TL is transmission loss as previously defined and DI represents directivity index.

Figure 2.3 shows the maximum detectable range vs. frequency for SNR = 0 dB. Results indicate that maximum detectable range decreases with increasing frequency. This is due to the larger attenuation at higher frequencies. Unfortunately, although reducing frequency allows for an increase in transmission range, it also results in decreased information throughput. With an operating frequency of 50 kHz, communication range is limited to several kilometres. Figure 2.3 also shows that the detectable range decreases with the increased noise associated with higher wind.

As an example of underwater communications, assume that $f = 10$ kHz, $w = 20$ knots and $D = 0$ (light shipping). Then, total spectral noise is 53 dB re 1 μPa per $\sqrt{\text{Hz}}$ and the total in-band noise is 86 dB re 1μPa when a typical value of quality factor $Q = 5$ is employed [19, 68]. Assuming $DI = 0$ dB (omni-directional transducer) and $SL = 190$ dB re 1μPa, the practically achievable maximum transmission range is about 70 km. This range decreases to 60 km for heavy shipping noise ($D = 1$).

When designing a remote transmitter, the power budget is an important factor to be considered because low power consumption is essential for prolonged operation. Figure 2.4 gives the acoustic power required to achieve certain transmission ranges at given SNR values. Depending on applications, the desired communication performance requires different power associated with different values of SNR. Even with a

few tens of watts of acoustic power, signal transmission up to several tens of kilometres is possible. Figure 2.5 shows the relationship between achievable transmission range and wind speed. As wind speed increases, the achievable range decreases due to the increased ambient noise caused by surface agitation.

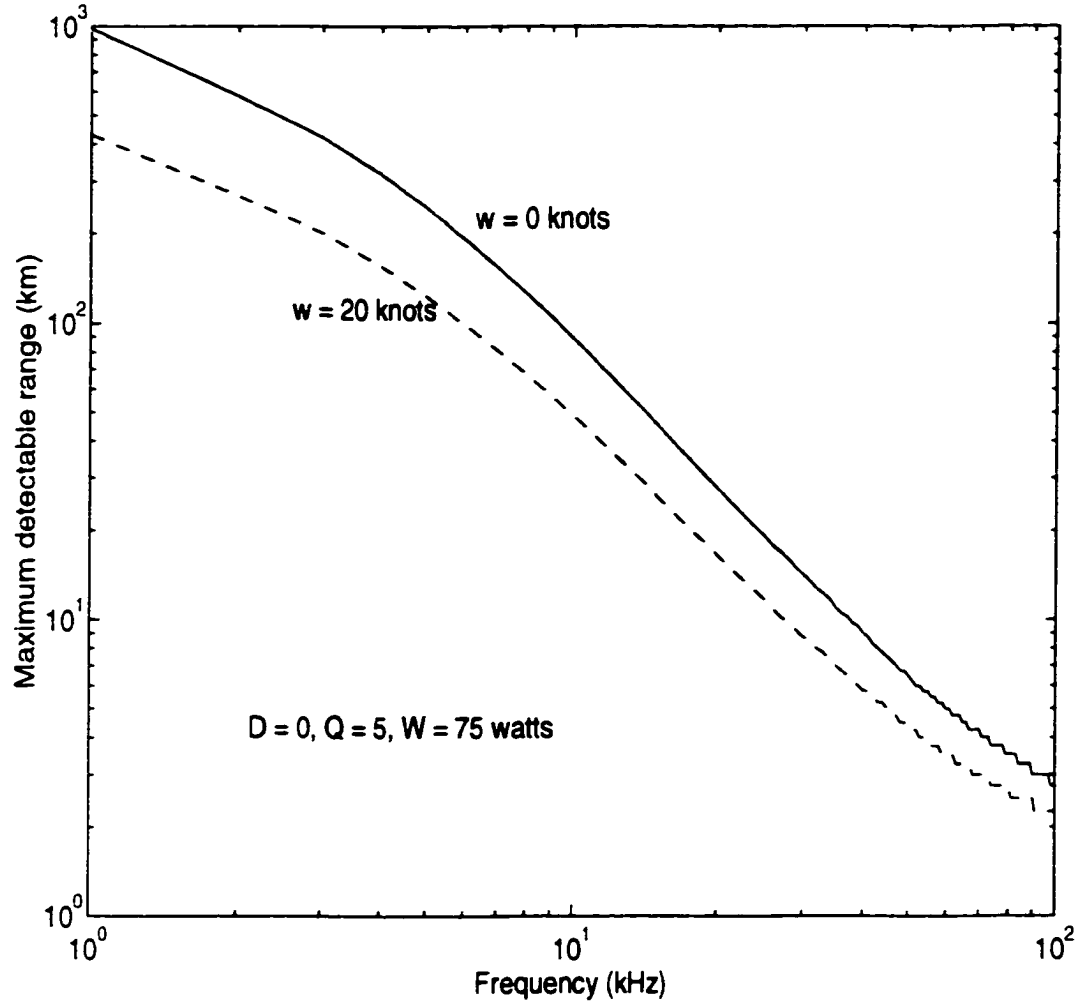

Figure 2.3: Maximum detectable range vs. frequency

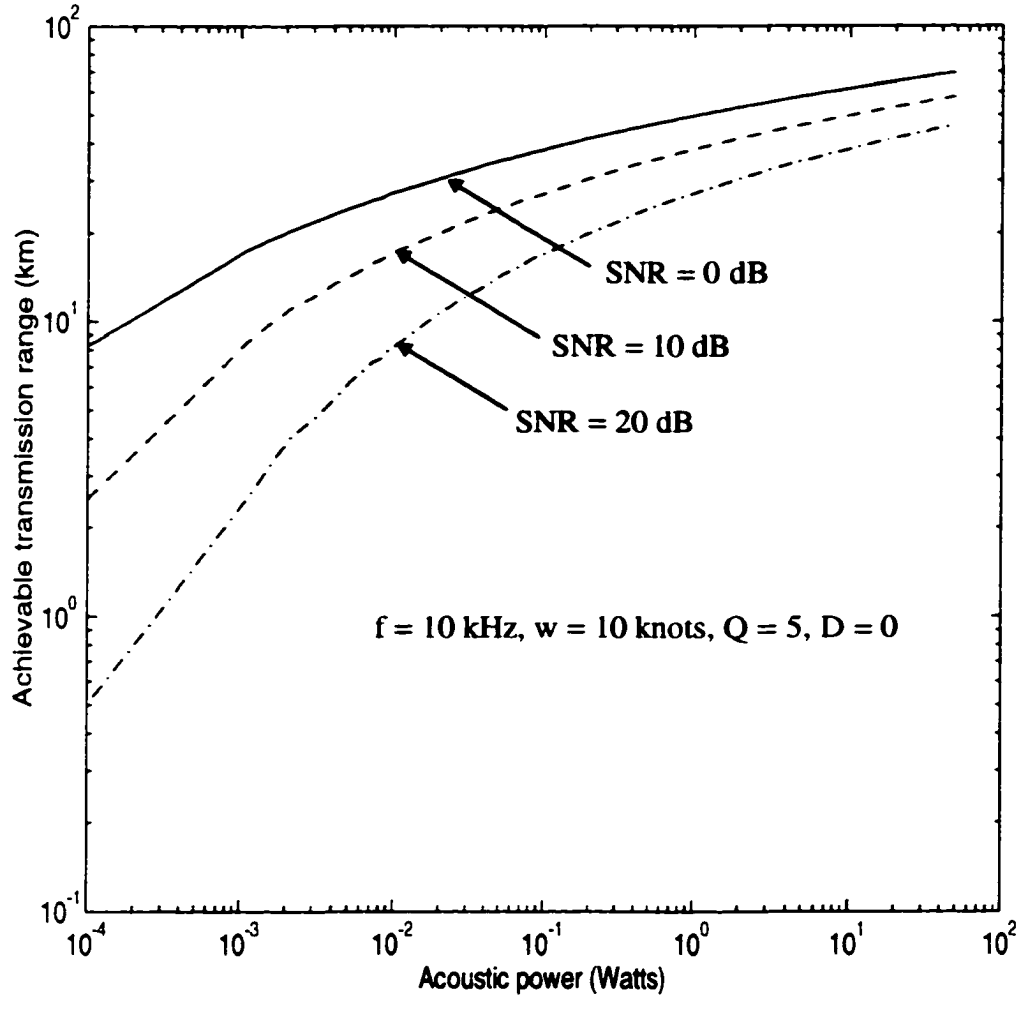

Figure 2.4: Acoustic power vs. achievable transmission range

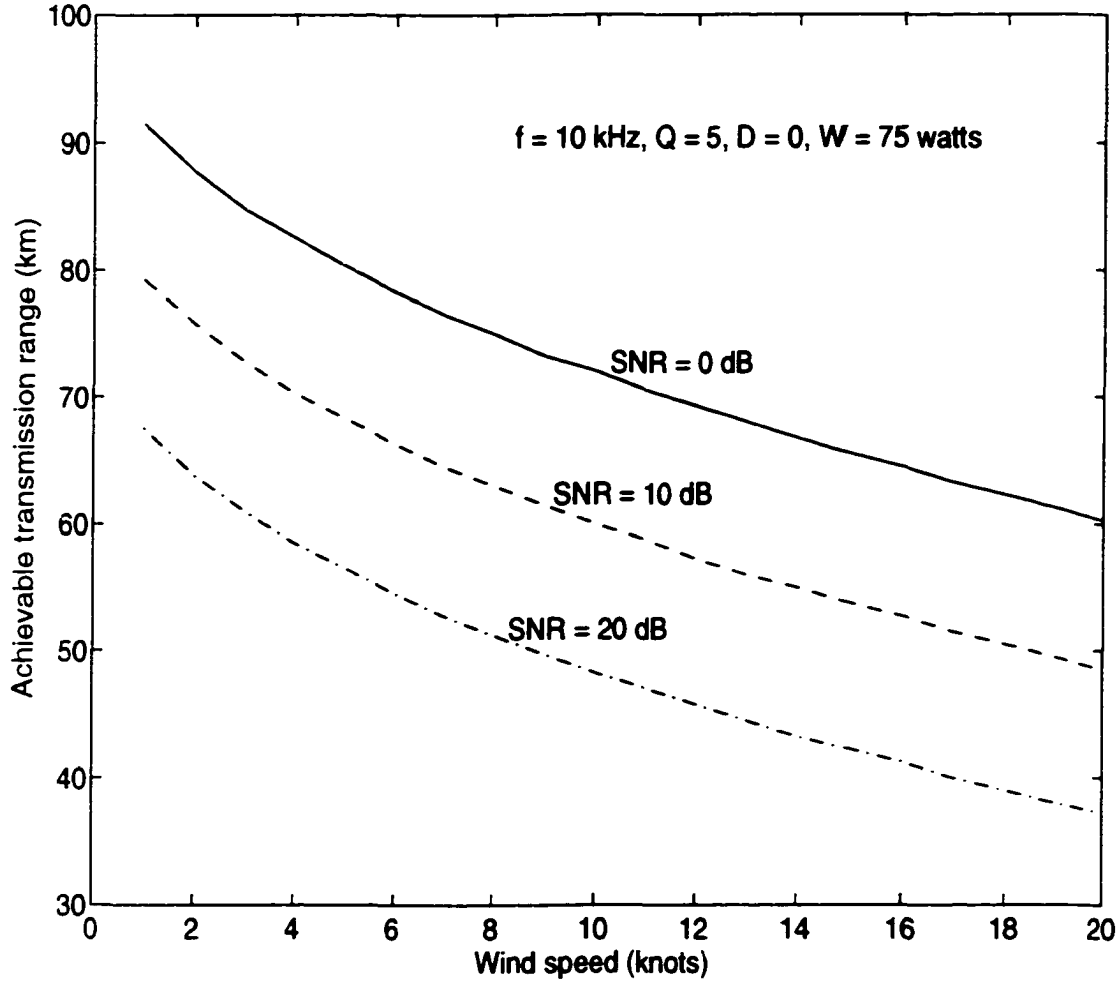

Figure 2.5: Achievable transmission vs. wind speed

2.2.4 Other important characteristics

Multipath signal propagation due to reflection at the surface/bottom imposes a challenging task for underwater acoustic communications. This results in severe intersymbol interference.

In addition, the relative motion between transmitter and receiver introduces Doppler frequency spreading. The Doppler shift causes a phase shift in the received carrier frequency which must be tracked and removed to allow reliable signal detection. These characteristics will be further studied in subsequent chapters.

2.3 System Configuration

In this section, a communication system under investigation is described. The overall system configuration with N-ary phase shift keyed modulation is described. Filter characteristics at transmitter and receiver is also explained.

2.3.1 Overall system configuration

The system configuration, utilizing N-ary phase shift keyed (N-ary PSK) modulation and adaptive equalization [39], is shown in Figure 2.6. The encoder accepts the sequence of input binary data. It has two outputs; in-phase, I, and quadrature, Q. Each symbol out of N symbols is coded by a distinct n-tuple (n is bits-per-symbol given by $\log_2$N) input binary data. For each symbol, a unique combination of I and Q is assigned. We can use a complex notation $D = I + jQ$ to describe these N points separated in the complex plane by modulating phase $\Phi = \frac{2\pi}{N}(m-1)$ where $m = 1, 2, \ldots, N$. The encoded data stream of I and Q is then used to modulate a sequence of δ-pulses transmitted every signalling period T. To limit their bandwidth,

such modulated sequences are then low-pass filtered by LPFs with impulse responses $h_H(t)$. The same low pass filters are applied at the receiver. The filter characteristics will be further explained in Section 2.3.2.

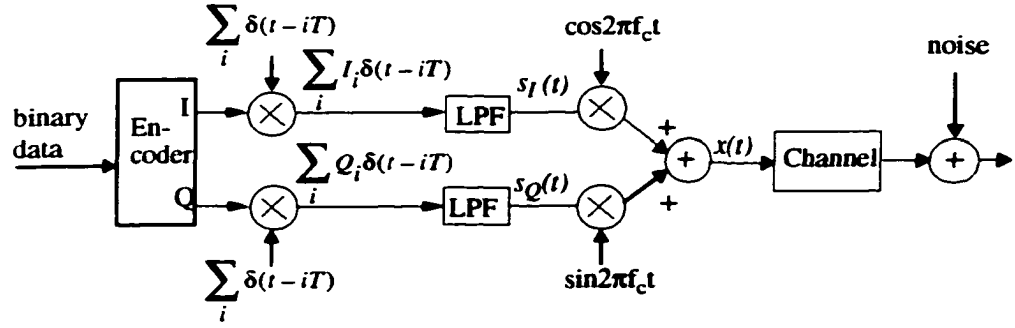

(a)

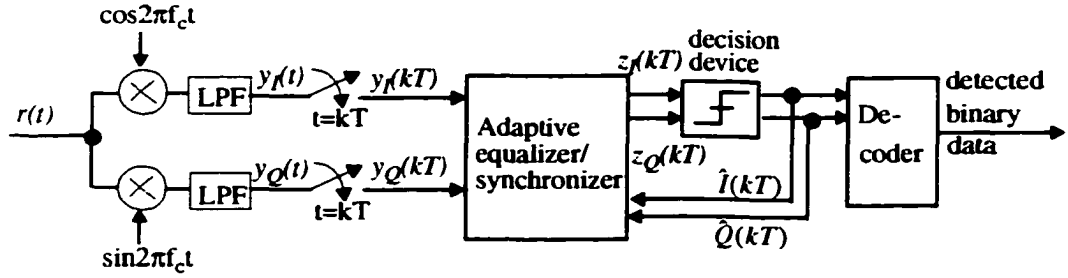

(b)

Figure 2.6: Overall system configuration with N-ary PSK modulation.

(a) Transmitter (b) Receiver.

The in-phase and quadrature signals at the output of the transmitting low pass filters are

$$\begin{aligned} s_I(t) &= \sum_i I_i h_H(t - iT) \text{ and} \\ s_Q(t) &= \sum_i Q_i h_H(t - iT). \end{aligned} \tag{2.11}$$

The filtered signals are then multiplied by a carrier frequency, added and transmitted through the underwater acoustic channel. At the receiver, the receiver filter limits the noise component outside the signal frequency band.

The combined system impulse response $h(t)$ which includes the transmitting filter, channel and receiving filter is

$$h(t) = h_H(t) * h_c(t) * h_H(t), \tag{2.12}$$

where * denotes the convolution operator and $h_c(t)$ is the impulse response of the channel. The demodulated signal $y(t)$ at the receiver is the superposition of the impulse response of Eq. (2.12) to each transmitted symbol and additive white Gaussian noise $n(t)$:

$$\begin{aligned} y(t) &= y_I(t) + jy_Q(t) \\ &= \sum_i d_i h(t - iT) + n(t) \end{aligned} \tag{2.13}$$

where d_i is the complex data sequence, $h(t)$ the complex impulse response. Sampling the received signal $y(t)$ at each time instant $t = kT + t_o$ where t_o accounts for the channel delay, we obtain the data signal at the input of the equalizer:

$$
\begin{aligned}
y(kT + t_o) &= \sum_i d_i h(kT + t_o - iT) + n(kT + t_o) \\
&= d_k h(t_o) + \sum_{i \neq k} d_i h(kT + t_o - iT) + n(kT + t_o).
\end{aligned}
\tag{2.14}
$$

The first term in Eq. (2.14) is the desired signal at the k-th sampling instant, and the second term represents the intersymbol interference (ISI) from neighboring symbols. The purpose of an equalizer is to minimize ISI by reducing the second term of Eq. (2.14). The complex output of the equalizer $z(kT)$ is fed into the decision device. The decision regarding a transmitted symbol is based on the distance to the reference points. The symbol with the shortest distance is selected. Finally, the decoder generates a stream of recovered data bits.

2.3.2 Modified raised cosine filter

For the transmitter and receiver filter, each filter must be selected to get maximum signal-to-noise power ratio at the detector input. For a known channel the appropriate choice of filter is based on the Nyquist criterion for minimizing intersymbol interference caused by filters and a channel [73]. Assuming that attenuation, delay, or distortion introduced by a transmission channel can be properly compensated using an equalizer/synchronizer, we use modified raised-cosine filters (LPFs) with a roll-off factor $\beta = 1$ and impulse response $h_H(t)$. We start with an overall transfer function for transmitting and receiving filters [53];

$$
H(f) = \begin{cases} \frac{T}{2}[1 + \cos \pi f T] & -\frac{1}{T} < f < \frac{1}{T}, \\ 0 & \text{elsewhere} \end{cases}
\tag{2.15}
$$

where T is the symbol period. The overall transfer function can be split equally between

the transmitting and receiving filters as $\sqrt{H(f)}$ [53].

Using the trigonometric relation $\cos 2\alpha = 2(\cos\alpha)^2 - 1$, the transfer function for the transmitting and receiving filters becomes

$$H_T(f) = H_R(f) = \begin{cases} \sqrt{T}\cos\frac{\pi f T}{2} & -\frac{1}{T} < f < \frac{1}{T} \\ 0 & \text{elsewhere} \end{cases}. \tag{2.16}$$

The impulse response of each filter is obtained through the inverse Fourier transform of Eq. (2.16), that is,

$$\begin{aligned} h_T(t) &= h_R(t) \\ &= \int_{-\frac{1}{T}}^{\frac{1}{T}} \sqrt{T}\cos\left(\frac{\pi f T}{2}\right) e^{j2\pi f t} df \\ &= \frac{1}{\sqrt{T}}\left\{ \frac{\sin\pi\left(\frac{2t}{T}+\frac{1}{2}\right)}{\pi\left(\frac{2t}{T}+\frac{1}{2}\right)} + \frac{\sin\pi\left(\frac{2t}{T}-\frac{1}{2}\right)}{\pi\left(\frac{2t}{T}-\frac{1}{2}\right)} \right\}. \end{aligned} \tag{2.17}$$

This result is the root-raised cosine impulse response and should be limited to some practical duration for implementation, that is, $-T_a < t < T_a$. This truncation causes sidelobes in the frequency spectrum. To reduce sidelobes levels, the impulse response of the filter is modified using the Hamming window [39, 53]

$$w_H(t) = 0.54 + 0.46\cos\left(\frac{\pi t}{T_a}\right), \qquad -T_a < t < T_a. \tag{2.18}$$

The windowed impulse response becomes

$$h_H(t) = h_T(t)w_H(t) = h_R(t)w_H(t). \tag{2.19}$$

We use this modified raised cosine filter in the transmitter and receiver.

Figure 2.7 shows the overall impulse response of the filters and the frequency response of the root-raised cosine filter. Figure 2.8 shows a signal waveform and an eye diagram at the output of the receiving filter when QPSK modulated data is transmitted through the ideal channel, assuming unity power of the transmitted signal (i.e., the amplitude of in-phase and quadrature signal is 0.707). The eye opening may be used as an indication of system "robustness." For good transmission, the eye opening should allow for a correct decisions. As intersymbol interference and noise are added by the channel, the eye opening will close. The sampling of the received signal is performed at the point where the opening of the eye is greatest. The eye pattern when a signal is transmitted through a shallow water channel will be presented in Chapter 5.

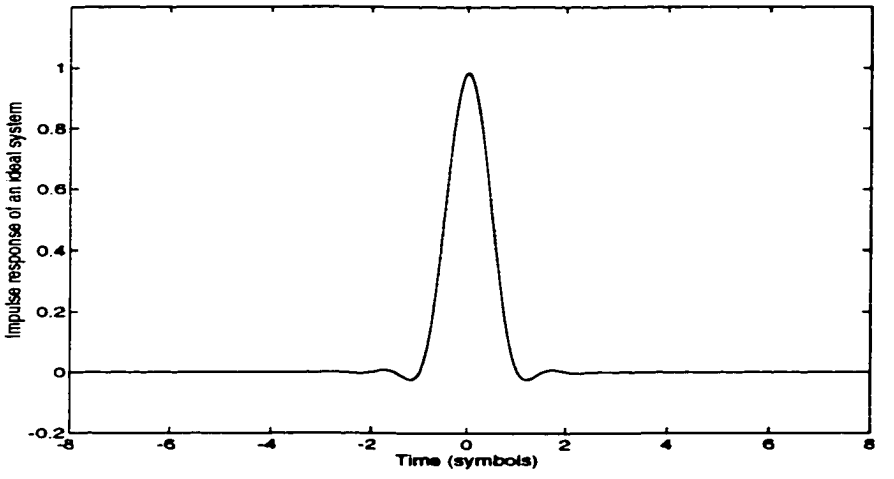

(a)

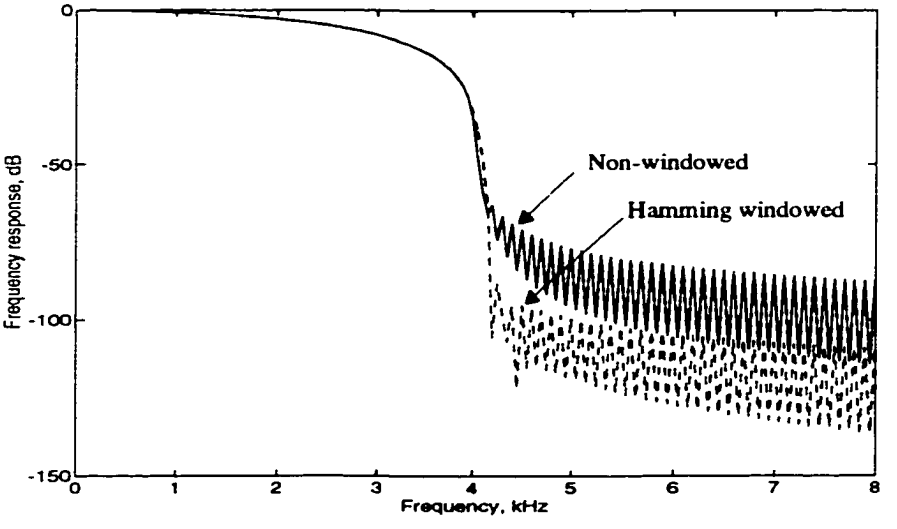

(b)

Figure 2.7: (a) Impulse response of the transmit and receive filters (b) Frequency response of ideal root-raised cosine low-pass filter.

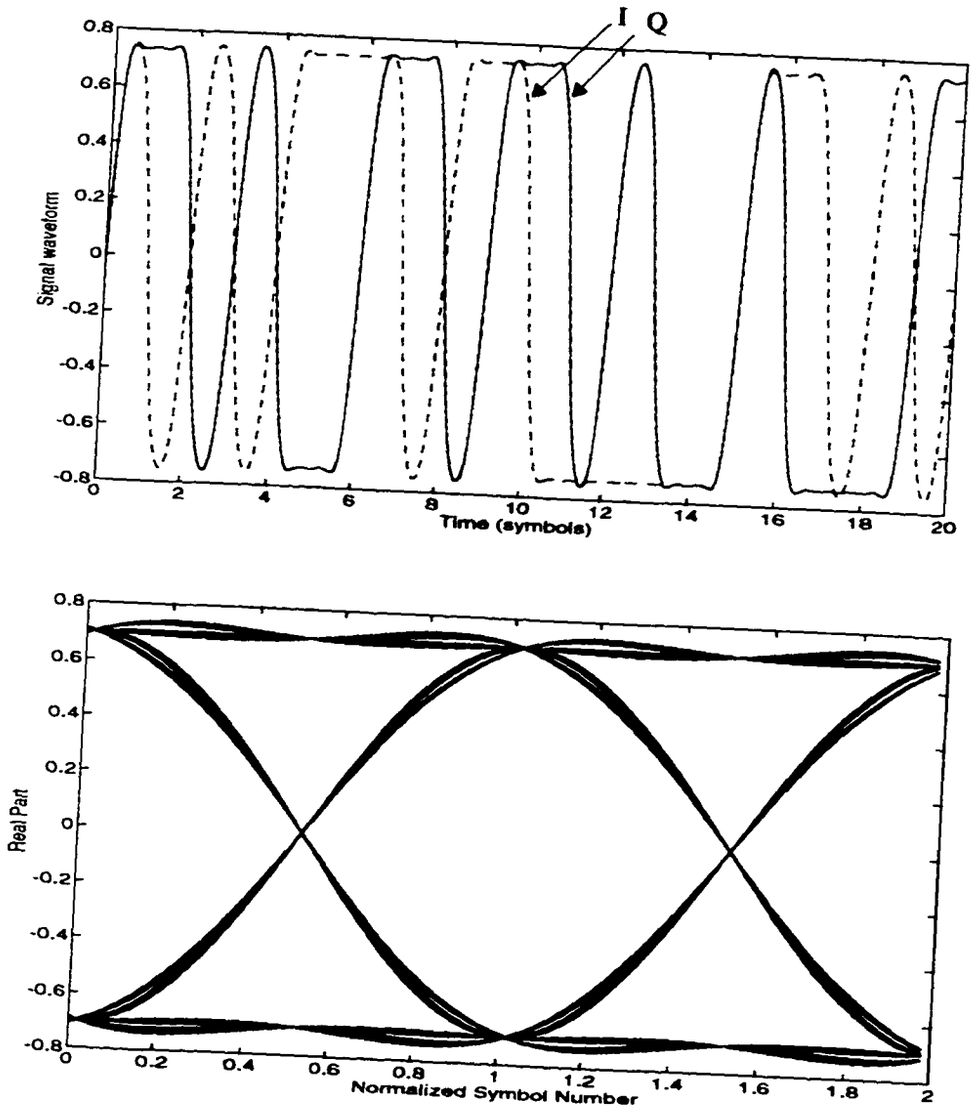

Figure 2.8: Signal waveform and eye pattern for a QPSK signal

2.4 Summary

A brief explanation of digital acoustic underwater communication systems was given based on functional blocks.

Relevant characteristics of the underwater acoustic channel for the communication systems were described to investigate the power budget requirement. A trade-off between the achievable transmission range and data throughput exists. Several kilometres with $f = 50$ kHz and several tens of kilometres with $f \leq 10$ kHz might be possible using only 75 watts of acoustic power. Also, we investigated the required acoustic power for certain transmission range at given SNR values. The effect on achievable transmission range due to the wind speed variation was investigated.

The system configuration investigated throughout research was described. Filter characteristics at transmitter and receiver were also explained

Chapter 3

Model for Shallow Water Acoustic Channel

3.1 Introduction

Multipath signal propagation depends on the channel geometry and on the frequency of a transmitted signal. In a shallow underwater channel, propagation will occur primarily as surface/bottom reflections in addition to a direct path. In a deep channel, sound rays bend according to a sound velocity profile. In this study, we confine ourselves to a shallow underwater channel with a constant sound velocity profile.

In this chapter, a model suitable for computer analysis that describes a shallow underwater channel is introduced. Firstly, we develop a static channel model with deterministic propagation paths. Then, a time variant channel model which accounts for the change of channel in time is developed. The static channel model considers the following parameters:

- channel geometry; ocean depth, transducers locations,

- environmental conditions; wind speed, sound speed, acoustic impedance contrasts at the boundaries,

- system parameters; operating frequency.

A case study will be presented using the proposed model. We will see that using a directional receiver is better suited for a channel with a small range-to-depth ratio (RDR) and that equalization methods are better suited for a channel with a large RDR.

To account for the time-variability of the channel response, the Doppler effect due to transmitter/receiver motion is considered. Also, change in wind speed causes a change in signal attenuation due to surface scattering by waves. This eventually produces the time-variability of the delay spread and shapes of signal responses.

3.2 Static Time-Invariant Channel Model

At first, we model the underwater acoustic channel as a linear time-invariant channel. This model provides an estimate of channel delay spread which in turn can be used to determine the number of equalizer taps. It also gives general ideas regarding signal parameters such as signal attenuation and arrival angles for different multipaths.

3.2.1 Channel geometry

Boundaries at the channel surface and bottom reflect an acoustic signal, resulting in multiple travel paths between transmitter and receiver. The receiver can thus acquire signals arriving from different paths, each signal delayed according to the channel geometry. Here, we assume the channel geometry as shown in Figure 3.1. The channel has uniform depth h and constant sound speed c. The characteristics of reflections at the boundaries depend on the value of the Rayleigh parameter given by [12, 84]:

$$R = \frac{2\pi f}{c}\sigma \sin\varphi$$

where f is the system operating frequency, σ is the rms surface wave-height (crest to trough), and φ is the grazing angle of the acoustic ray.

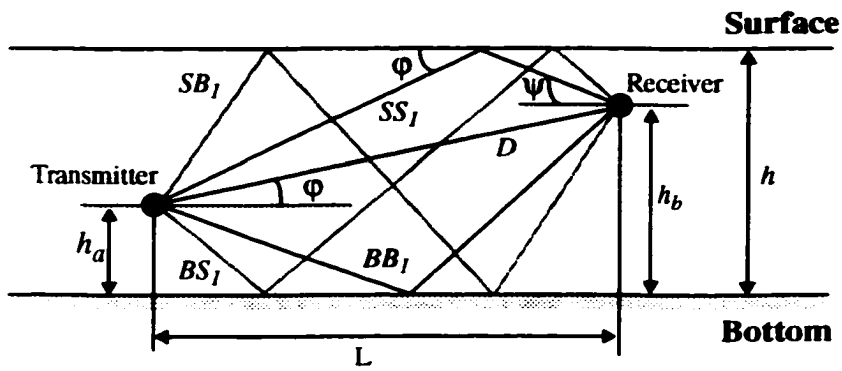

h_a: Transmitter height above the bottom
h_b: Receiver height above the bottom
L: Horizontal distance between the transmitter and receiver
φ: Grazing angle
ψ:Arriving angle

Figure 3.1: Model for shallow water acoustic channel

The relationship between σ (in metres) and wind speed w (in knots) for a fully developed sea is given by [27]:

$$\sigma = 3.6576 \times 10^{-3} w^2 . \tag{3.1}$$

For $R \gg 1$, the boundary acts as a scatterer, reflecting the signal in all directions. For $R \ll 1$, the boundary is primarily a reflector supporting coherent specular reflection [84]. A practical condition for coherent specular reflection is [18]

$$\lambda > 8H \sin\varphi \tag{3.2}$$

where λ is the wavelength given as the ratio c/f and H is the height (crest to trough) of the roughness feature. We assume regular *sinusoidal* waves such that their peak-to-peak amplitudes H are related to their rms values by $H = 2\sqrt{2}\sigma$, where σ is as given by Eq. (3.1). If the water surface becomes rough, the acoustic signal is in part specularly reflected and in part scattered and absorbed. This causes the acoustic intensity to be reduced compared with the signal reflected from a smooth water surface which supports a specular reflection [18, 29]. An empirical formula for computing surface reflection losses for a rough-water surface was formulated in [29].

A transmitted signal path can be classified as either a direct path D or a multi-path. Multi-path signals can be grouped into four types according to the form and order of reflection; we use the notation SS to denote multi-path signals which make a first and last boundary reflection from the sea-surface before arriving at the receiver. Similarly, we define the SB, BS and BB multi-paths where B denotes a reflection from the bottom. We extend this notation to define a given order of multi-path by writing SSn, SBn, BSn and BBn, n denoting an "order" for the multi-path. These four types of paths are shown in Figure 3.1 for the primary, $n = 1$, path. In all subsequent formulae, we assume that receiver height, h_b, is greater than transmitter height, h_a. However, the role

of transmitter and receiver is interchangeable. A channel model shown in Figure 3.1 can be visualized using the Lloyds mirror effect for the convenience of computation of the length of signal paths and delay time, and so on [13].

Calculation of the combined response of received direct and reflected path signals can be performed by the summation of image signals. This summation method satisfies the boundary condition at the surface and bottom as explained in [13].

3.2.2 Computation of signal losses

The length of each signal path shown in Figure 3.1 is:

$$\sqrt{L^2 + A^2} \tag{3.3}$$

The angle of arrival of the acoustic ray at the receiver is given by:

$$\psi = k\tan^{-1}(A/L). \tag{3.4}$$

In the above:

$$\begin{aligned} A &= h_b - h_a; && \text{k=-1} && \text{for D} \\ A &= 2nh - h_a - h_b; && \text{k=1} && \text{for SSn} \\ A &= 2nh - h_a + h_b; && \text{k=-1} && \text{for SBn} \\ A &= 2nh + h_a - h_b; && \text{k=1} && \text{for BSn} \end{aligned} \tag{3.5}$$

and

$$A = 2(n-1)h + h_a + h_b; \qquad \text{k=-1} \qquad \text{for BBn}. \tag{3.6}$$

We can approximate Eq. (3.3) with the assumptions that

$$\frac{A}{L} \ll 1 \text{ and } n \le N_{path} \tag{3.7}$$

where N_{path} is the significant order of multipath which affects the accuracy of the approximation. Under these restrictions, Eq. (3.3) may be expanded using the binomial expansion; that is, for each signal path:

$$\sqrt{L^2 + A^2} \approx \left[L + \frac{1}{2L} A^2 \right]. \tag{3.8}$$

Observing Eq. (3.5), the largest approximation error happens when $A = (2n+1)h$. If $\frac{L}{h} \geq 50$ and $n \leq 7$, the computation error due to the approximation is less than 0.1 percent when $L \geq 1\text{km}$. With this assumption, for direct path signal we obtain

$$D = \sqrt{L^2 + (h_b - h_a)^2} \approx \left[L + \frac{1}{2L} (h_b - h_a)^2 \right]. \tag{3.9}$$

Similarly, for the SSn path we obtain

$$SSn = \sqrt{L^2 + [2nh - (h_b - h_a)]^2} \approx \left[L + \frac{1}{2L} [2nh - (h_b - h_a)]^2 \right]. \tag{3.10}$$

The difference in arrival time between the direct path and SSn path signals can be written as follows:

$$\begin{aligned} \tau_{SSn} &= t_{SSn} - t_D = \frac{SSn - D}{c} \\ &\approx \frac{2}{Lc} [n^2 h^2 - nh(h_a + h_b) + h_a h_b] \end{aligned} \tag{3.11}$$

where t_D and t_{SSn} are arrival times of the direct path and SSn path signals, respectively. In a similar way we obtain the difference in arrival times for the remaining types of multi-paths:

$$\begin{aligned}
\tau_{SBn} &= t_{SBn} - t_D = \frac{SBn - D}{c} \\
&\approx \frac{2}{Lc}[n^2h^2 - nh(h_b - h_a)], \\
\tau_{BSn} &= t_{BSn} - t_D = \frac{BSn - D}{c} \\
&\approx \frac{2}{Lc}[n^2h^2 - nh(h_a - h_b)]
\end{aligned} \tag{3.12}$$

and

$$\begin{aligned}
\tau_{BBn} &= t_{BBn} - t_D = \frac{BBn - D}{c} \\
&\approx \frac{2}{Lc}[(n-1)^2h^2 - (n-1)h(h_a + h_b) + h_a h_b].
\end{aligned} \tag{3.13}$$

The maximum differential delay is usually defined as the channel delay spread T_m:

$$T_m = max(\tau_i) \qquad i=1, ..., N_{path} \tag{3.14}$$

where N_{path} is the number of signal paths with significant magnitudes as defined later. The delay spread T_m is often expressed in terms of signalling intervals to indicate the number of interfering symbols. This value allows us to determine the tap size of an equalizer.

The acoustic pressure decreases for each reflection are determined by the complex surface and bottom pressure reflection coefficients, r_s and r_b, respectively. In general, reflection coefficients depend on grazing angle and therefore on the order of the multi-path. The surface reflection coefficient can be evaluated using, for instance, the Bech-mann-Spezzichino model [32] in the form proposed in [29]. We observe from this mod-el that for the low grazing angles characteristic of a shallow channel, the magnitude of the reflection coefficient becomes independent of grazing angle and is given by:

$$|r_s| = \sqrt{\frac{1 + (f/f_1)^2}{1 + (f/f_2)^2}} \tag{3.15}$$

where

$$f_2 = 378w^{-2}$$

and

$$f_1 = \sqrt{10} f_2 .$$

In the above, f is the frequency of operation in kHz and w is wind speed in knots. Because of the large impedance mismatch at the boundary of the sea surface, the reflected signal has a 180° phase shift. Considering this phase shift due to reflection from the sea surface, the complex surface pressure reflection coefficient can be written as:

$$r_s = -|r_s| \tag{3.16}$$

The magnitude of the surface reflected signal vs. wind speed is shown in Figure 3.2. The magnitude of reflected signal is reduced with increased wind speed and frequency.

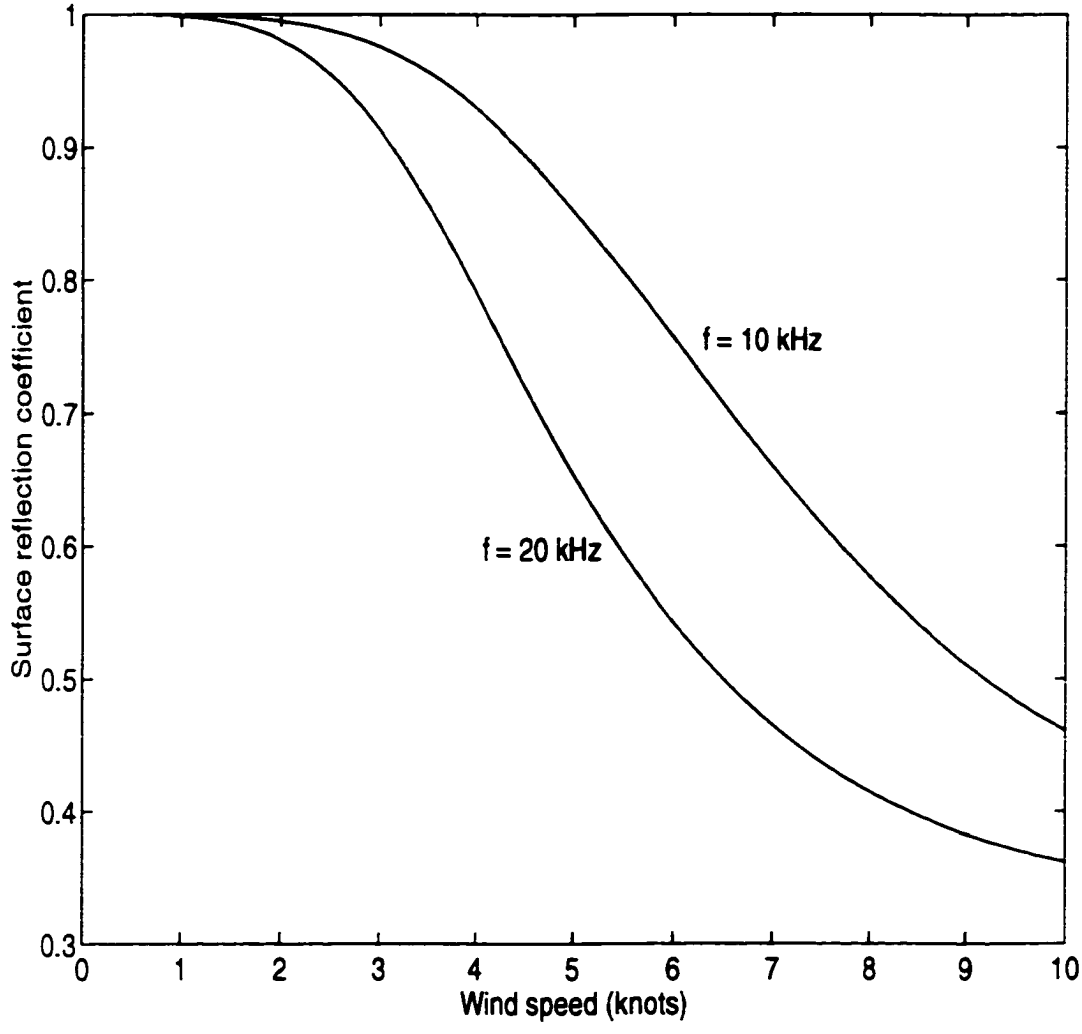

Figure 3.2: Surface reflection coefficient vs. wind speed

The bottom reflection coefficient can be evaluated using either the Rayleigh model [12] or the NUSC model [87]. In general, its value decreases with lower grazing angle. We note from the NUSC model that, for grazing angle less than 5°, operating frequency f less than 50 kHz and bottom porosity less than 0.5, the magnitude of the reflection coefficient r_b is approximately unity.

The incident angle θ is an angle as measured from normal to the reflection boundary. The critical angle is defined as the incident angle when total reflection occurs, which is given by $\theta_c = \sin^{-1}(c_w/c_b)$. The bottom reflected wave will have a nonzero phase shift ϕ when the incident angle is larger than the critical angle and the phase shift ϕ is given by [27]

$$\phi = -2\tan^{-1}\left(\frac{\sqrt{\sin\theta^2 - u^2}}{v\cos\theta}\right) \tag{3.17}$$

where $u = c_w/c_b$ is the ratio of water channel sound speed to bottom material sound speed, $v = \rho_b/\rho_w$ is the ratio of the density of bottom material and water. Therefore, for low grazing angles the bottom reflection coefficient r_b can be expressed as

$$r_b = e^{j\phi} \tag{3.18}$$

The combined pressure loss due to repeated surface and/or bottom reflections for each type of multi-path is given by:

$$R_{SSn} = r_s{}^n r_b{}^{n-1} \tag{3.19}$$

$$R_{SBn} = r_s{}^n r_b{}^n \tag{3.20}$$

$$R_{BSn} = r_s^{\,n} r_b^{\,n-1} \tag{3.21}$$

and

$$R_{BBn} = r_s^{\,n-1} r_b^{\,n} \tag{3.22}$$

where $n = 1, \ldots, \infty$.

Consider the special case of a perfectly smooth and lossless surface. The loseless surface produces a large number of signal paths which have significant magnitude. Therefore, we must consider the bottom reflected wave with large incident angles. A bottom reflected signal which has an incident angle larger than the critical angle produces no phase shift, but the signal magnitude is less than unity. In this case, the signal loss at the bottom plays an important role. The amplitude of the bottom reflected signal is

$$r_b = \frac{z_b \cos\theta - z_w \cos\theta_t}{z_b \cos\theta + z_w \cos\theta_t}; \quad \text{for } (\theta < \theta_c), \tag{3.23}$$

where

$$\theta_t = \sin^{-1}\left(\frac{c_b}{c_w}\sin\theta\right). \tag{3.24}$$

The characteristic impedance z is a product of density and sound speed, that is, $z = \rho c$. Properties of water and sediments are shown in Table 3.1 [27].

Table 3.1: Water and sediment properties

	water	coarse sand	fine sand	silt	clay
$\rho(kg/m^3)$	1000	2000	1900	1800	1400
c(m/s)	1500	1800	1700	1600	1600

Figure 3.3 shows the magnitude of the reflection coefficient and phase shift as a function of incident angle for several bottom materials. When the incident angle is close to 90°, complete reflection (no loss) with 180° phase shift occurs. When the incident angle is less than the critical angle, bottom reflected signals suffer from signal losses. Summarizing, if the ocean surface is perfectly smooth (no wind), signal losses due to bottom reflection are dominant factors in determining the resultant signal at the receiver.

Although the case of perfectly smooth (lossless) ocean was studied to verify signal propagation, signal paths with large grazing angles can be rejected with a directional receiver. With a directional receiver, the attenuation of signals in a shallow water channel will be primarily dependent on surface reflections, transmission range and operating frequency. With this assumption, Eq. (3.19) - Eq. (3.22) can be simplified as:

$$\begin{aligned} R_{SSn} &= (-1)^n(|r_s|^n|r_b|^{n-1}e^{j(n-1)\phi}) \\ &\approx (-1)^n|r_s|^n e^{j(n-1)\phi}, \end{aligned} \tag{3.25}$$

$$\begin{aligned} R_{SBn} &= (-1)^n|r_s|^n|r_b|^n e^{jn\phi} \\ &\approx (-1)^n|r_s|^n e^{jn\phi}, \end{aligned} \tag{3.26}$$

$$\begin{aligned} R_{BSn} &= (-1)^n(|r_s|^n|r_b|^n e^{jn\phi}) \\ &\approx (-1)^n|r_s|^n e^{jn\phi} \end{aligned} \tag{3.27}$$

and

$$\begin{aligned} R_{BBn} &= (-1)^{n-1}|r_s|^{n-1}|r_b|^n e^{jn\phi} \\ &\approx (-1)^{n-1}|r_s|^{n-1} e^{jn\phi} \end{aligned} \tag{3.28}$$

where $n = 1, \ldots, \infty$.

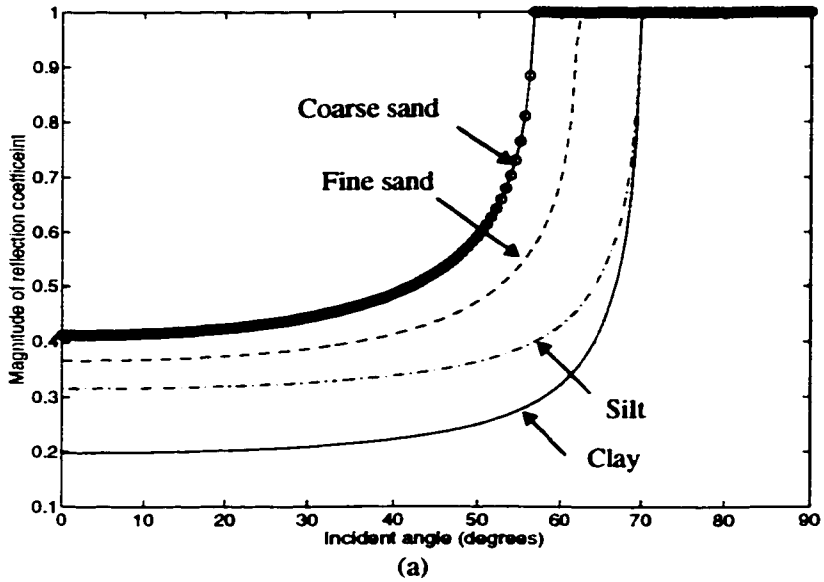

(a)

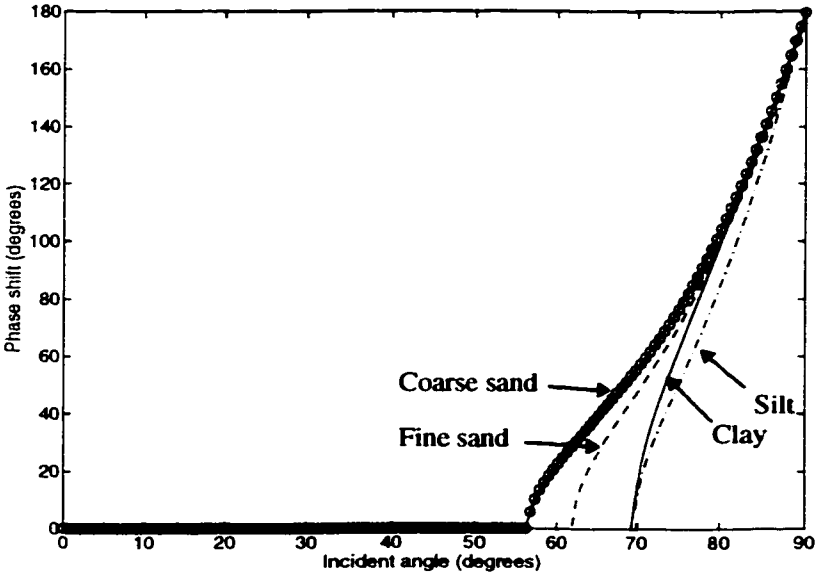

(b)

Figure 3.3: Reflection characteristics of bottom vs. incident angle

3.2.3 Computation of the combined response of the received signal

The impulse response of a multi-path channel can be modeled by the weighted sum of delayed delta functions [69]. The received signal *y(t)* can therefore be represented by a weighted sum of the delayed transmitted signal *x(t)*, that is:

$$y(t) = \sum_{i=1}^{\infty} \alpha_i x(t - \tau_i) \tag{3.29}$$

where α_i is the amplitude of the signal received via the *i*-th path normalized by the amplitude of the direct path signal ($i = 1$), and τ_i designates the difference in time of arrivals between the direct path signal ($i = 1$) and reflected signals ($i \neq 1$). The value of delays τ_i and amplitudes α_i of multi-path signals can be calculated from Eq. (3.11)-Eq. (3.13) and Eq. (3.15)-Eq. (3.22).

Let us denote the travel time of direct and reflected signal as t_D, t_{BSn}, t_{SBn} and t_{BBn} depending on the type of reflections. The received signal *y(t)* constructed in terms of the summation of reflected signals is given by:

$$y(t) = \frac{e^{j\omega(t-t_D)}}{D} + \sum_{n=1}^{\infty} \left[\frac{R_{SSn}}{SSn} e^{j\omega(t-t_{SS_n})} + \frac{R_{SBn}}{SBn} e^{j\omega(t-t_{SB_n})} \right] + \frac{R_{BSn}}{BSn} e^{j\omega(t-t_{BS_n})} + \frac{R_{BBn}}{BBn} e^{j\omega(t-t_{BB_n})}. \tag{3.30}$$

By letting the relative delay $\tau_{SSn} = t_{SSn} - t_D$, $\tau_{SBn} = t_{SBn} - t_D$, and so on, the received signal can be written as

$$y(t) = \frac{e^{j\omega(t-t_D)}}{D}\left\{1 + \sum_{n=1}^{\infty}\left[\alpha_{SSn}e^{-j\omega\tau_{SSn}} + \alpha_{SBn}e^{-j\omega\tau_{SBn}} + \alpha_{BSn}e^{-j\omega\tau_{BSn}} + \alpha_{BBn}e^{-j\omega\tau_{BBn}}\right]\right\} \tag{3.31}$$

where $\alpha_{SSn} = \frac{D}{SSn}R_{SSn}$, $\alpha_{SBn} = \frac{D}{SBn}R_{SBn}$, $\alpha_{SSn} = \frac{D}{BSn}R_{BSn}$ and $\alpha_{SSn} = \frac{D}{SSn}R_{SSn}$. The received signal normalized by the direct path signal then becomes:

$$y(t) = 1 + \sum_{n=1}^{\infty}[\alpha_{SSn}e^{-j\omega\tau_{SSn}} + \alpha_{SBn}e^{-j\omega\tau_{SBn}} + \alpha_{BSn}e^{-j\omega\tau_{BSn}} + \alpha_{BBn}e^{-j\omega\tau_{BBn}}]. \tag{3.32}$$

Signal normalization by the direct path signal is equivalent to setting the time origin as the arrival time of the first-path ray and to set magnitude of received direct path signal as unity. Since our primary objective is to study the multi-path propagation effects, this simplification is useful. However, when we design an overall communication system, the required power to account for the distance-related signal attenuation should be properly taken into consideration.

In the computation of Eq. (3.32), we can limit the number of terms to include only those with significant amplitudes. We will investigate the condition to find the number of terms for significant amplitudes. Multipath signal from each multipath type can be assumed independent so that we can rewrite Eq. (3.32) as

$$y(t) = 1 + \sum_{n=1}^{\infty}\alpha_{SSn}e^{-j\omega\tau_{SSn}} + \sum_{n=1}^{\infty}\alpha_{SBn}e^{-j\omega\tau_{SBn}} + \sum_{n=1}^{\infty}\alpha_{BSn}e^{-j\omega\tau_{BSn}} + \sum_{n=1}^{\infty}\alpha_{BBn}e^{-j\omega\tau_{BBn}} \tag{3.33}$$

Investigating Eq. (3.25) through Eq. (3.28) and Eq. (3.33), the signal for each multipath can be expressed as

$$y_a(t) = \sum_{n=1}^{\infty} a^n e^{j\Phi_n} \tag{3.34}$$

where $a = |r_s|$ and Φ_n represents phase shift caused by time delay and surface/bottom reflections. When $\Phi_n = 0$, the effect of signal addition is largest and will give us the number of significant multipath for the worst case. With this assumption, Eq. (3.34) can be represented as the sum of infinite geometrical progression, S_∞, given as [5]

$$S_\infty = \sum_{i=1}^{\infty} |a^i| = \frac{a}{1-a}, \qquad (a < 1) \tag{3.35}$$

The sum of the first N_{path} terms, S_N, is

$$S_N = \sum_{i=1}^{N_{path}} |a^i| = \frac{a\left(1 - a^{N_{path}}\right)}{1-a}. \tag{3.36}$$

If the difference in sum between N_{path} terms and infinite terms divided by infinite sum are below a certain threshold value x_o, we can neglect those terms larger than order N_{path}, that is,

$$\frac{S_\infty - S_N}{S_\infty} \le x_o. \tag{3.37}$$

Substituting Eq. (3.35) and Eq. (3.36) into Eq. (3.37), we get the expression to find an order of significant paths:

$$N_{path} \geq \frac{\log(x_o)}{\log(a)}, \qquad a < 1. \tag{3.38}$$

Let us consider a case when a directional receiver is employed at the receiver. For simplicity, we assume simplified beam pattern as depicted in Figure 3.4. This beam pattern has a constant level within the main lobe and another constant level outside of a main lobe (side lobe). That is, all multipath signals arriving outside the main lobe are subject to equal suppression. For computation of order of significant paths when a directional receiver is employed, Eq. (3.36) through Eq. (3.38) should be modified to consider attenuations of signals which arrive from outside of the main lobe. Let us denote N_{ML} as the number of signal paths arriving within a main lobe and α as an attenuation factor due to the side lobe suppression with a value of $\alpha = 10^{\beta/20}$ where β is the amount of suppression in dB. Then, the sum of infinite terms and first N_{path} terms is given as:

$$\begin{aligned} S_\infty &= \sum_{i=1}^{N_{ML}} |a^i| + \alpha \cdot \sum_{i=N_{ML}+1}^{\infty} |a^i| \\ &= \frac{a + (\alpha - 1)a^{N_{ML}+1}}{1-a}, \qquad a < 1 \end{aligned} \tag{3.39}$$

$$\begin{aligned} S_N &= \sum_{i=1}^{N_{ML}} |a^i| + \alpha \cdot \sum_{i=N_{ML}+1}^{N_{path}} |a^i| \\ &= \frac{a + (\alpha - 1)a^{N_{ML}+1} - \alpha a^{N_{path}+1}}{1-a}, \qquad a < 1 \end{aligned} \tag{3.40}$$

Letting $K = (1 + (\alpha - 1)a^{N_{ML}})/\alpha$, the order of significant multipath N_{path} when a directional receiver is used can be obtained using Eq. (3.37), Eq. (3.40) and Eq. (3.39):

$$N_{path} \geq \frac{\log(Kx_o)}{\log(a)}, a < 1. \tag{3.41}$$

In this study, we neglect those terms with which calculation error for each multi-path type is below a threshold value of 5 percent (i.e. $x_o = 0.05$).

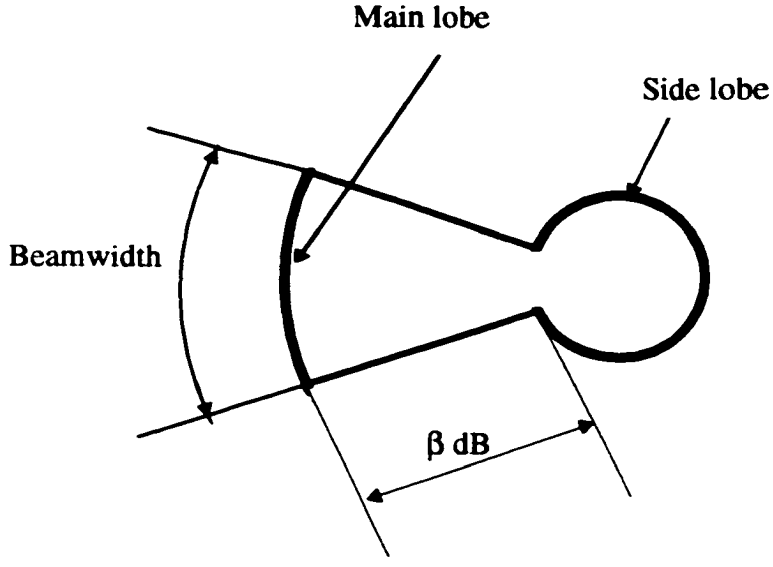

Figure 3.4: Simplified beam pattern

3.2.4 A case study

As an example, a shallow water channel with depth h = 20 m and transmission range L = 10 km is studied. We postulate that a transmitter and a receiver are located in the middle of the channel. For computation of the received signal, signal paths with a significant signal strength are considered.

Figure 3.5 shows the received signal envelope when a pulse with a duration of 0.25 ms is transmitted through an underwater channel with a wind speed of 5 knots.

Figure 3.6 shows the differential time delay and their normalized signal amplitude at delayed time. There is approximately 20 ms of maximum delay spread with wind speed w = 10 knots which corresponds to 100 symbols duration at a transmission rate of 5 ksymbols/s. The multipath effect of the reflected signal is stronger at lower wind speeds due to smaller signal attenuations at the ocean surface.

Figure 3.7 shows angles of multipath arrivals vs. differential time delay. As the differential time delay is increased, the arrival angle becomes larger. This result suggests the possibility of using a directional receiver to limit the number of signal paths at the receiver.

Let us consider a case when the side lobe level is reduced to 20 dB by a directional receiver. Figure 3.8 shows number of significant paths vs. wind speed. At low wind speed, there is a large number of significant paths which can be effectively reduced by a directional receiver.

Figure 3.9 depicts the signal delay spread vs. wind speed with a non-directional receiver or a directional receiver. At low wind speed, the signal delay spread is quite large and the benefit of a directional receiver is noticeable. If the system with an non-directional transducer is operating at a rate of 5 ksymbols per second, the signal delay spread extends over 450 symbols (90 ms) for wind speed less than 4 knots. However, using a directional receiver with a beamwidth of 5°, the signal delay spread can be reduced to 77 symbols (15.4 ms). It will eventually enable us to use a smaller number of equalizer taps, resulting in reduced hardware complexity.

Figure 3.10 shows the delay spread as the distance between transmitter and receiver is varied. At a horizontal range less than 2 km, the signal delay spread due to multipath is 100 ms, which corresponds to 500 symbols duration at 5 ksymbols/s. Figure 3.11 shows largest arriving angle vs. distance between transmitter and receiver. At shorter transmission ranges, the arrival angles of signal paths are larger which allows us to use a directional receiver effectively to remove reflected signal paths with a larger angular spread. At large horizontal ranges, the largest arrival angle decreases, requiring a high resolution directional receiver, but signal delay spread is also reduced to an amount relatively easy to equalize. This indicates that using a directional receiver is better suited for channels with small RDR and equalization methods are better suited for a channel with large RDR.

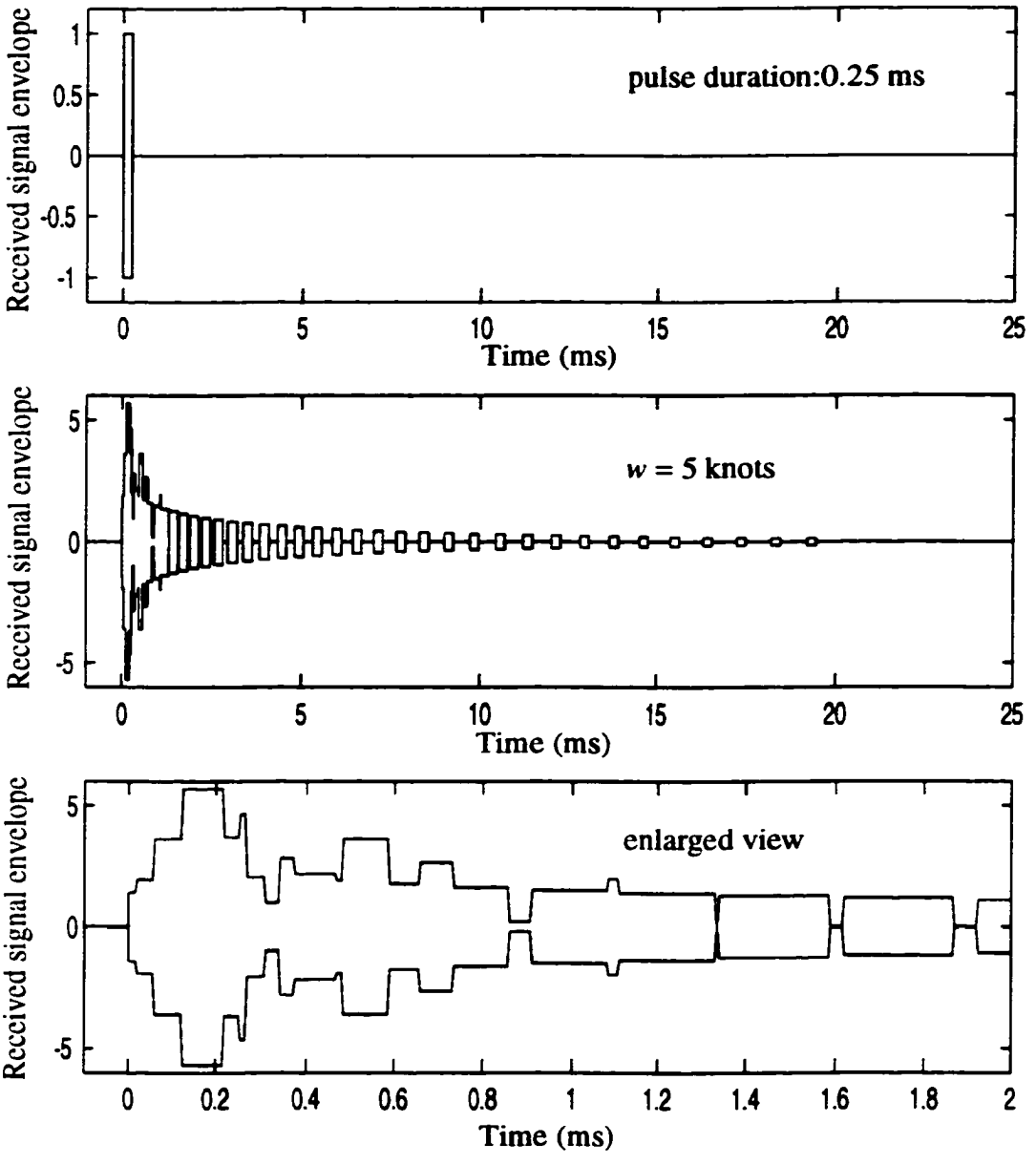

Figure 3.5: Received signal envelope when a pulse is transmitted

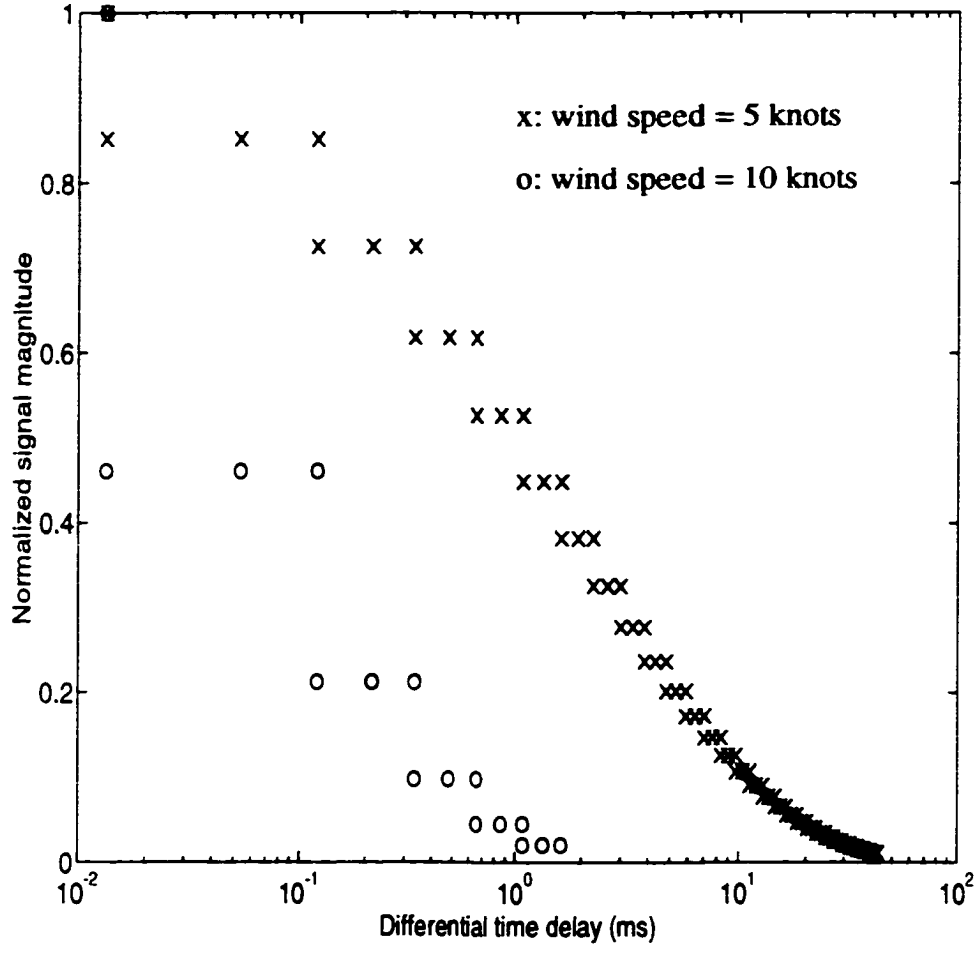

Figure 3.6: Differential time delay and normalized signal amplitude

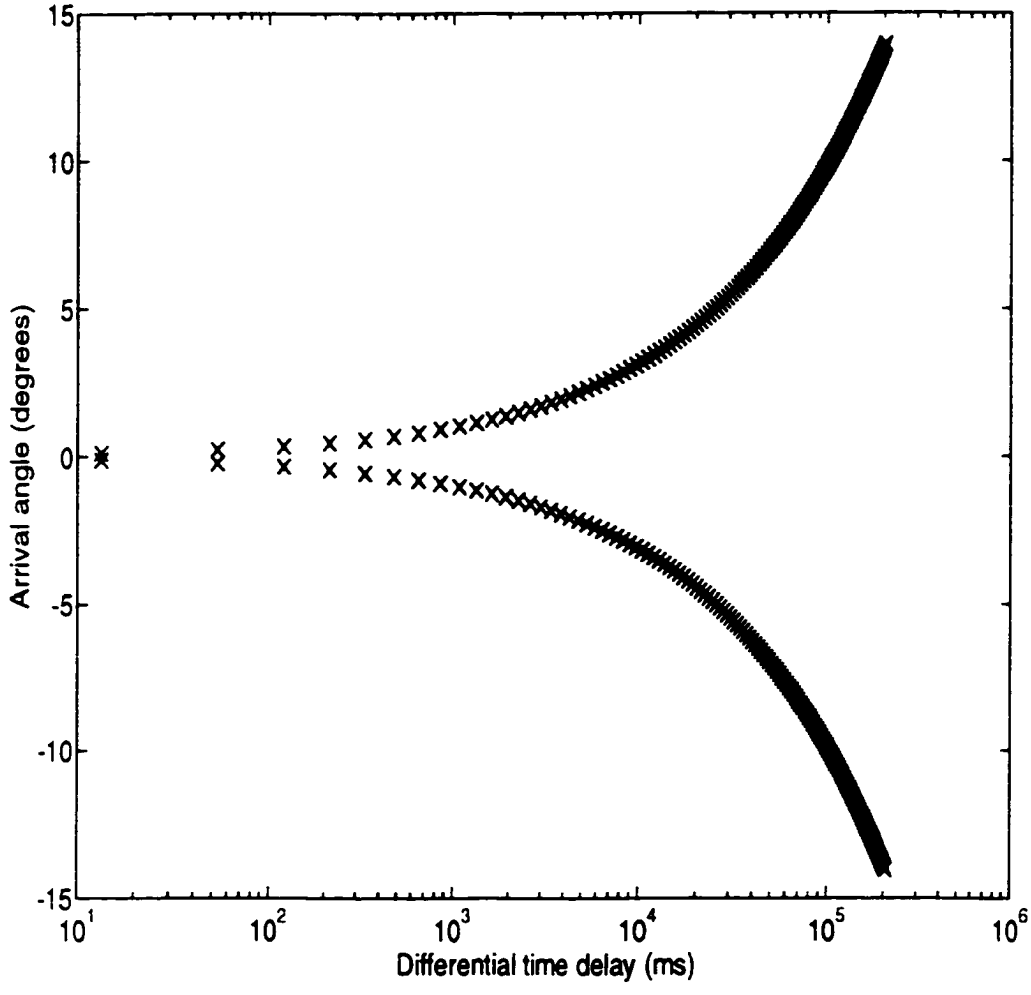

Figure 3.7: Arrival angles vs. differential time delay

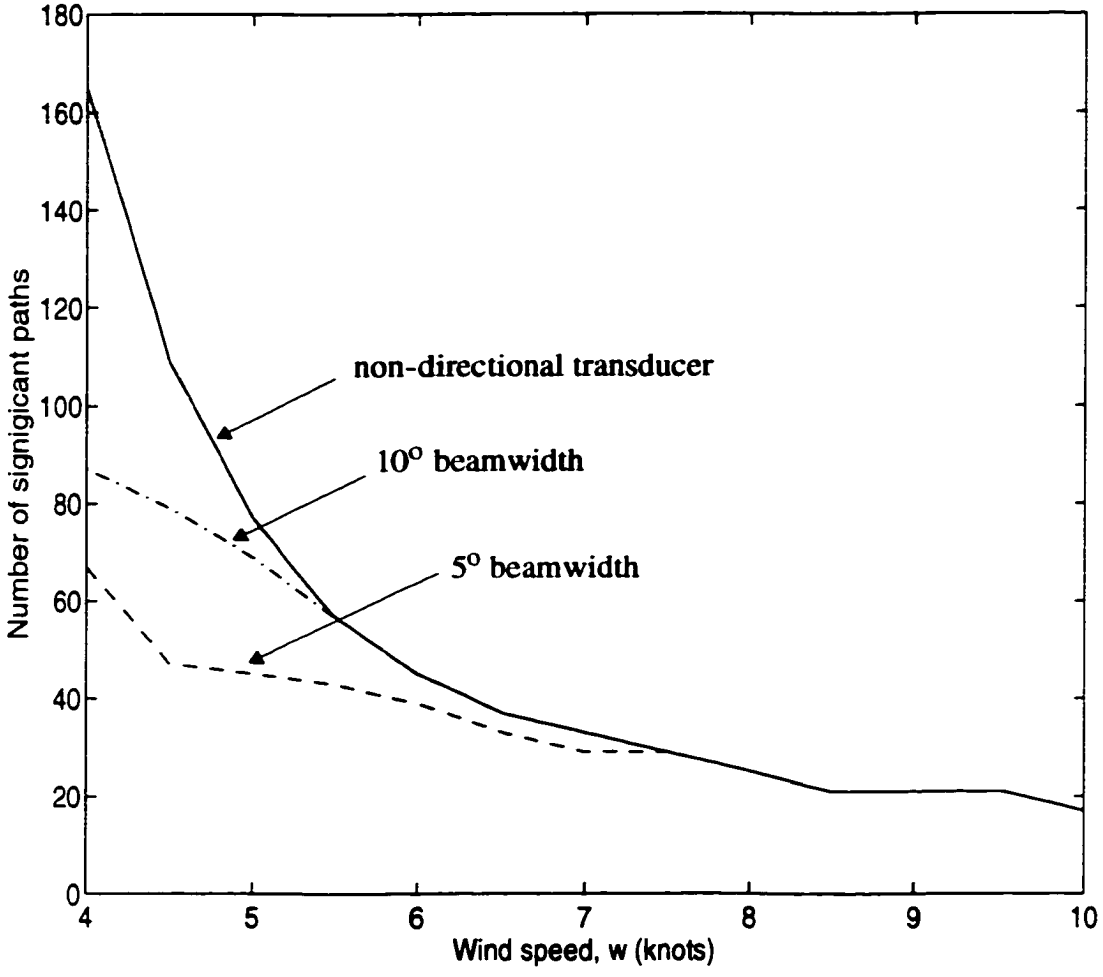

Figure 3.8: Number of significant paths vs. wind speed

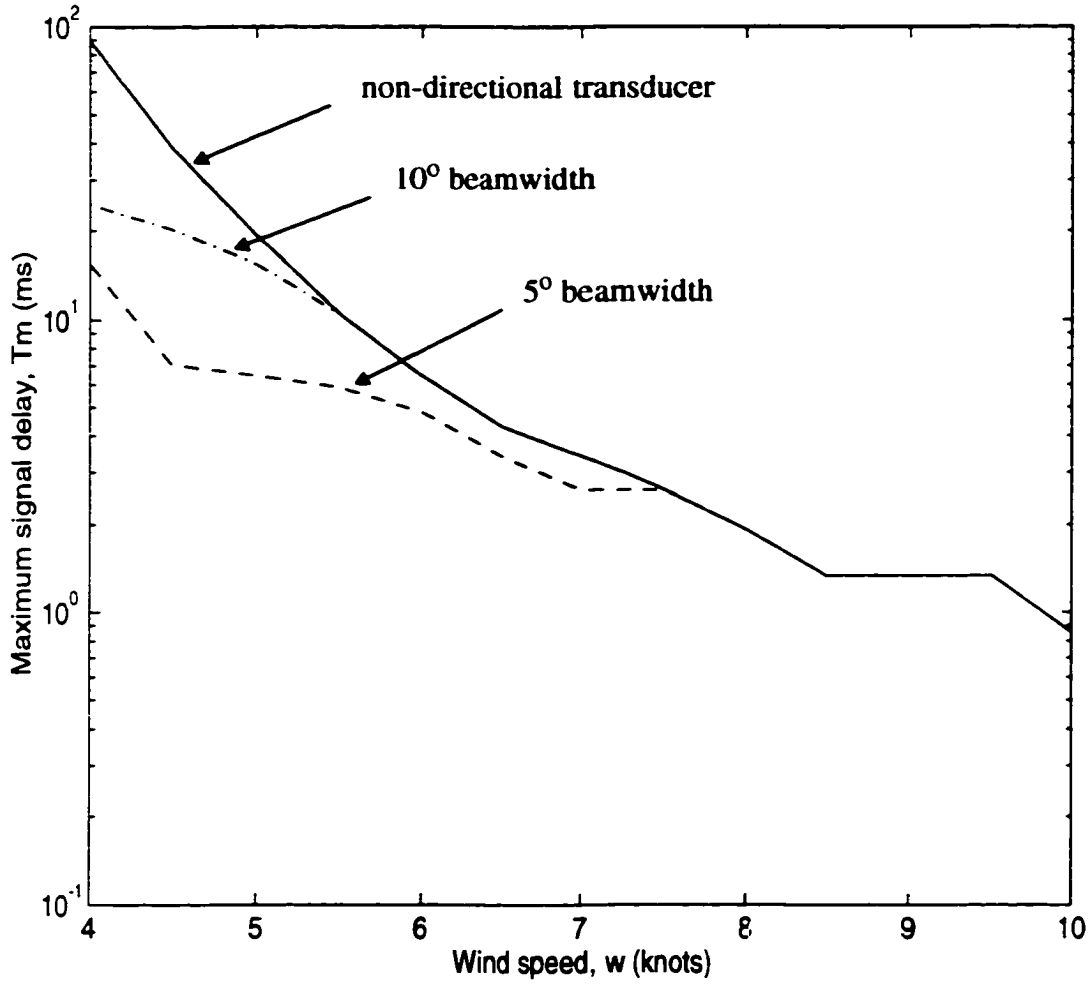

Figure 3.9: Signal delay spread vs. wind speed

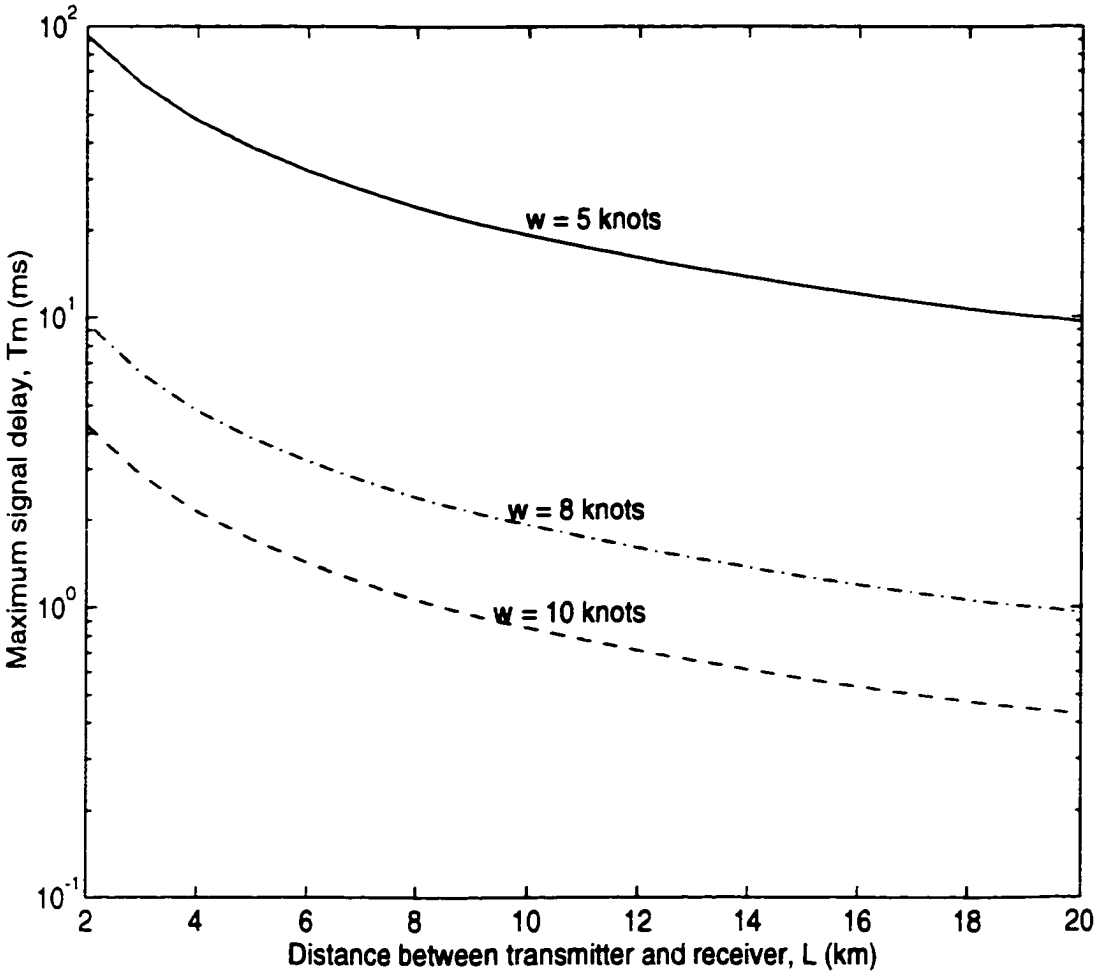

Figure 3.10: Distance between transmitter and receiver vs. delay spread

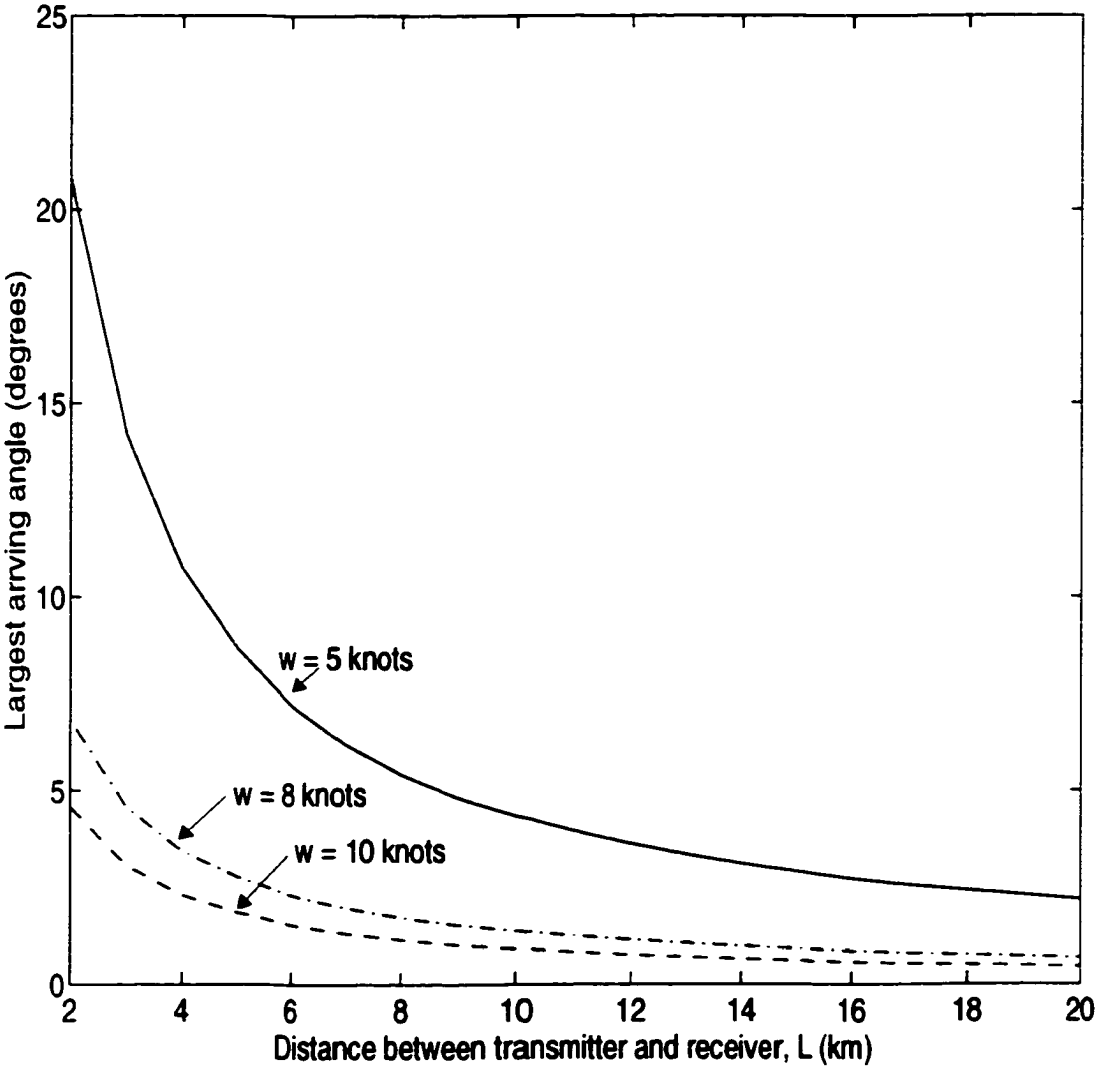

Figure 3.11: Distance between transmitter and receiver vs. largest arriving angle

3.3 The Dynamic Time-Variant Channel Model

We will broaden the time-invariant static channel model by incorporating a Doppler effect caused by relative motion of the transmitter and the receiver. This takes into consideration the time-variant channel characteristics.

Here, we assume that our multipath consists of discrete uncorrelated rays. The time-variant impulse response for a channel containing discrete multipath components can be described as [7, 69]:

$$\begin{aligned} h(t) &= \sum_{i=1}^{N_{path}} a_i(t) e^{-j2\pi f_c \tau_i(t)} \delta(t - \tau_i(t)) \\ &= \sum_{i=1}^{N_{path}} a_i(t) e^{-j\phi_i(t)} \delta(t - \tau_i(t)) \end{aligned} \tag{3.42}$$

where N_{path} is the number of multipath signals, a_i is the complex amplitude of the signal received along the i-th path, τ_i and $\phi_i(t)$ are the corresponding delay and associated phase shifts. The complex nature of the signal amplitude takes into consideration of the phase shift introduced by surface/bottom reflections, that is,

$$a_i(t) = A_i(t) e^{j\varphi_i(t)} \tag{3.43}$$

where $A_i(t)$ and $\varphi_i(t)$ represent the magnitude of real amplitude and phase shift for each path.

Combining Eq. (3.42) and Eq. (3.43), we can get

$$h(t) = \sum_{i=1}^{N_{path}} A_i(t) e^{-j(\phi_i(t) + \varphi_i(t))} \delta(t - \tau_i(t)) = \sum_{i=1}^{N_{path}} A_i(t) e^{-j\theta_i(t)} \delta(t - \tau_i(t)) \tag{3.44}$$

where $\theta_i(t)$ is a sum of $\phi_i(t)$ and $\varphi_i(t)$.

Thus, the received signal consists of the sum of a number of time-varying phasors with amplitude $A_i(t)$ and phase $\theta_i(t)$. If a signal amplitude and the time delay do not change with time, the impulse response will result in the static case of the channel model where parameters can be calculated from the method described in Section 3.2.

The phase variations of each path due to the movements of the transmitter-receiver can be calculated as follows:

$$\Delta\phi_i(t) = 2\pi\Delta f_i t \tag{3.45}$$

with

$$\Delta f_i = f_c \beta_i(t) \text{ and } \beta_i(t) = \frac{v}{c}\cos(\psi_t - \Psi_{ti}) \tag{3.46}$$

where v is the relative velocity between the transmitter and receiver, c is the sound velocity in water, ψ_t denotes the angle between the direction of movement and the direct path, and Ψ_{ti} denotes the angle between the direct and actual path for each of the reflected paths.

As an example, for an autonomous underwater vehicle traveling at a maximum speed of $v = 5$ m/s (10 knots), the Doppler frequency shift is $\Delta f_i = 33.3$ Hz for a carrier frequency of 10 kHz.

3.4 Summary

In this chapter, the underwater acoustic channel model suitable for computer analysis was introduced. To find the deterministic propagation paths, the method of computation of signal attenuation and delay has been described based on the consideration of channel geometry, environmental conditions and system parameters. A case of the channel model was studied to investigate signal attenuation and arriving angles with respect to time delay and wind speed. As the differential time delay increases, the inter-arrival angle between reflected signals becomes larger, allowing us to limit the number of multipath signals using a directional receiver.

The time-variability of the channel response was accounted for by considering the Doppler effect due to the transmitter/receiver motion.

Chapter 4

Performance Analysis of Digital Acoustic Communication

4.1 Introduction

In the deep ocean, multi-path signals are attenuated by spreading and reflection losses at relatively large grazing angles. The effects of multi-path interference can be reduced by using a directional transmitter and/or receiver. However, spatial discrimination of direct path and multi-path signals by directional arrays in shallow water is virtually impossible. On the other hand, under certain conditions multi-path signals can add constructively to increase the strength of a received signal. Therefore, it is anticipated that high rate, coherent communication might be possible for a certain range of channel geometries and parameters.

In this chapter, the concept of effective signal strength and corruptive multi-path signal strength are introduced. Then, as a performance measure applicable to the shallow water channel, the signal-to-corruptive-multi-path-signal ratio (SMR) is proposed. The data rate of the achievable error-free transmission at a given SMR is studied while

the effect of Gaussian noise is assumed negligible. The results of computer analyses indicate that transmission rates in excess of 8 kbits/s are possible over a distance of 10.3 km and in a water depth of only 20 metres using a four-phase phase-shift-keying system (4-PSK). In Section 4.2, several measures to assess the degree of intersymbol interference are reviewed. A new performance measure for a shallow water channel based on the SMR is described Section 4.3. The condition of error-free transmission is described in Section 4.4. In Section 4.5, a sample system is analyzed and results are explained.

4.2 Performance Measure for Intersymbol Interference

In mobile communication studies, extensive research has been undertaken on how to assess the degree of intersymbol interference. We will briefly summarize their contributions and weak points. In [34], the definition of "significant multipath" was introduced for gigabits/s indoor wireless systems which is useful for modulation schemes such as phase-shift-keying (PSK) and quadrature-amplitude-modulation (QAM). The presence or absence of "significant multipath" is determined based on a criterion $\sum_{k=1}^{\infty} |\alpha_k| > x_0$ or $\sum_{k=1}^{\infty} |\alpha_k| < x_0$, where α_k is a real attenuation factor with α_o normalized to 1 and x_o is a threshold value with typical values of $20\log(x_o)$ in the range of -20 to -6 dB. The underlying assumption of this definition is that at high data rates where the symbol duration T_s is much less than the time delay of the first multipath signal, the multipath will arise from data bits other than the current symbol [34]. Therefore, the multipath components may add so as to reduce the data eye opening. However, in a shallow water channel, there exists a reflected signal arising from current symbols as well as symbols with delays larger than a symbol period. This prevents us from using

the definition of "significant multipath" introduced in [34].

As another performance measure to assess the degree of intersymbol interference, a signal-to-intersymbol interference ratio (SIR) has been frequently used [2]. When a data symbol waveform $u(t)$ is transmitted, the resulting received baseband signal is given by

$$r(t) = \sum_{n=1}^{N} A_n u(t-\tau_n) e^{-j(\theta_n + \Delta\theta_n)} + n(t) \tag{4.1}$$

where A_n, τ_n, θ_n and $\Delta\theta_n$ are signal amplitude, delay, phase shift and phase offset, respectively. The summation of the signals from all delayed pulses at sampling time t_k can be written as:

$$b(t_k) = \sum_{m=-\infty}^{\infty} r(t_k - mT_s). \tag{4.2}$$

From Eq. (4.2), the interference power and the signal power can be computed when $m \neq 0$ and $m = 0$, respectively. Then, SIR is the ratio of the signal power and the interference power. However, the computation of the interference and signal power using Eq. (4.2) is highly dependent on the sampling times t_k.

Here, we propose a simpler but effective method to evaluate performance suitable for underwater communications.

4.3 Signal-to-Multipath Ratio (SMR)

We postulate that digital information is transmitted by means of signalling elements (symbols), each of duration T_s. We assume that the data stream is transmitted

for a period much longer than the duration of the channel impulse response such that a steady state is achieved at the receiver. We further postulate that at the receiver the signal is analyzed within an observation window of duration equal to the signalling element width, T_s. This observation window is coincident with the "current" direct path symbol. We encounter, within the window, two forms of multi-path interference which have distinctly different effects on the direct path symbol. The first form, which we will call self-multipath, is a consistent form of multipath interference corresponding to symbols arriving with delays less than T_s, as shown in Figure 4.1. In this case the interference derives from delayed replicas of the current direct path symbol. We seek an estimate of the signal strength, S, resulting from the combination of direct path and self-multipath signals.

The second type of multipath, which we call cross-multipath, is an inconsistent, corruptive form of multipath interference. Cross-multipath interference derives from symbols transmitted prior to the current direct path signal. We also seek an estimate of the corruption strength, M, resulting from the cross-multipath interference. The estimation of S and M allows us to define a signal-to-corruptive-multipath ratio, SMR, which is used in a similar manner to the signal-to-noise ratio in a noise-limited channel.

These aspects can be explored in more detail by assuming that a differential phase modulation based on a carrier frequency f has been used for data transmission. Suppose for a moment that only the self-multipath is present in the observation window T_s.

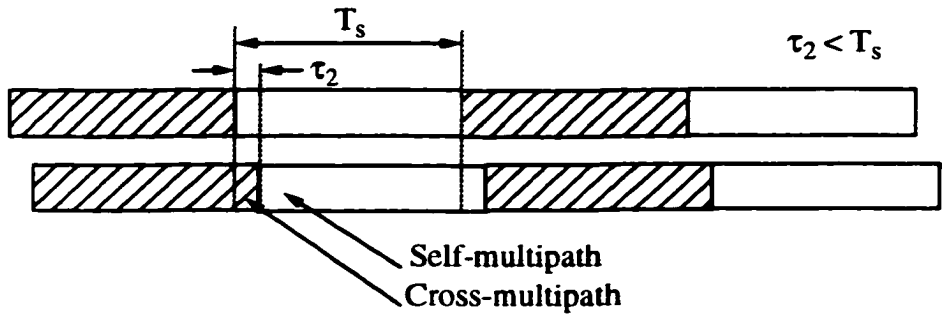

Figure 4.1: Signal structure for calculation of SMR.

At the very beginning of the observation window there is only a direct path signal, followed by multipath signals arriving at delays $\tau_i < T_s$. This causes modulation of the phase and the envelope of the resulting signal. At this point it is convenient to represent these self-multipath signals as phasors:

$$S_i = \alpha_i e^{-j2\pi f \tau_i} = \alpha_i e^{-j\Phi_i}. \tag{4.3}$$

We postulate that the phase detector employed to demodulate the phase modulated sequence reacts to the weighted average phasor within the window T_s. The conventional in-phase and quadrature demodulator followed by an integrator is an example of such a detector. In our study, for simplicity, we assume that rectangular pulse shapes are used. That is, a signalling waveform $u(t)$ is a rectangular pulse with symbol duration T_s as:

$$u(t) = \begin{cases} 1 & -T_s/2 \le t \le T_s/2 \\ 0 & \text{otherwise} \end{cases}. \tag{4.4}$$

Then, the weights are products of the amplitude of the multipath signals and the proportion of time they occupy the observation window. From the above definition, the effective signal strength S is:

$$S = \left| \sum_{i=1}^{r} \left(1 - \frac{\tau_i}{T_s}\right) S_i \right| \tag{4.5}$$

where r indicates the number of self-multipath interferers. From now on we call the direct path signal combined with self-multipath interferers within the observation window T_s simply *the signal*. Similarly, the multi-path signal strength M_s is:

$$M_s = \left| \sum_{i=2}^{r} \frac{\tau_i}{T_s} S_i \right| + \sum_{i=r+1}^{\infty} |S_i|. \tag{4.6}$$

In Eq. (4.6), the first term arises from the presence of the multi-path signal at tails of duration τ_i in the beginning of the observation window. The second term arises from all other previously transmitted signaling elements with delays larger than the signal width T_s, such that $\tau_i > T_s$. We assume that the phases of previous symbols are unknown and random. Therefore, the upper bound of the strength of the interfering cross-multipath signals arriving randomly can be expressed by:

$$M = \left[\sum_{i=2}^{r} \frac{\tau_i}{T_s} |S_i| + \sum_{i=r+1}^{\infty} |S_i| \right] \geq M_s. \tag{4.7}$$

From now on we call the combined cross-multipath interferers within the observation window T_s, as given by Eq. (4.7), simply *the multipath*.

4.4 The Condition of Error-Free Transmission

In this research we assume that the dominant source of error is multipath interference and neglect the effects of ambient noise. We will see that the condition of error-free transmission for a digital communication system can be determined by the value of the SMR as defined in the previous section. The maximum possible error-free data rate for a system using N-ary PSK modulation is derived.

We represent the signal and the multi-path as phasors **S** and **M** as shown in Figure 4.2. Suppose now that we analyze the 4-PSK system. The signal phasor can assume four phases separated by 90°. In Figure 4.2 these phases are selected for convenience as 0°, 90°, 180° and 270°, and the corresponding decision regions are indicated as 1, 2, 3 and 4.

The decision regarding the transmitting symbol is based on the position of the resultant phasor $\mathbf{R} = \mathbf{S} + \mathbf{M}$ at the end of the observation window. Since **M** can assume any phase, the expected phase-scatter diagram will have an envelope with radius **M** centered at distance **S** from the origin. We see in Figure 4.2 that the worst case condition for error-free transmission using 4-PSK is:

$$\text{SMR} = \frac{|\mathbf{S}|}{|\mathbf{M}|} = \frac{S}{M} > \sqrt{2}. \tag{4.8}$$

Once the condition Eq. (4.8) is satisfied, the SMR can be used as a measure of system robustness against ambient noise and interfering signals. Note that even for $\text{SMR} < \sqrt{2}$ the channel can still be used for transmission, but with a certain probability of error. This error performance can be improved by using suitable error correcting coding [71]. It is also evident from Figure 4.2 that the condition for error-free detection in the case of N-ary PSK is:

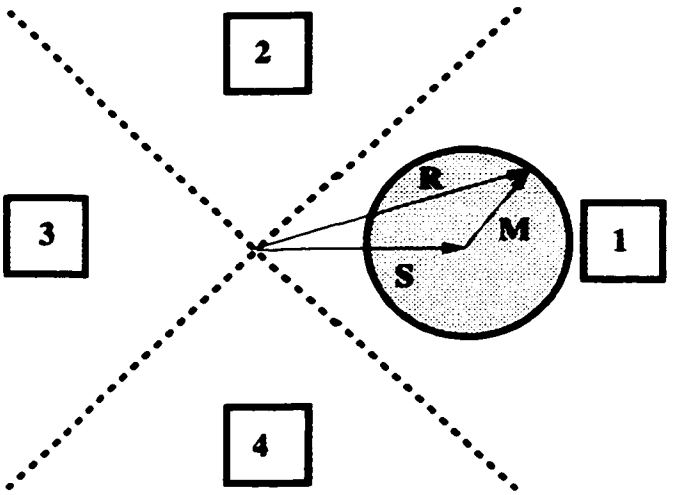

Figure 4.2: Signal space and decision regions for a 4-PSK system.

$$\text{SMR} > \frac{1}{\sin\left(\frac{180^{\circ}}{N}\right)}. \tag{4.9}$$

Eq. (4.9) can be used to determine, for a given SMR, the maximum N that will allow error-free transmission.

4.5 Results of the Analysis of a Sample System

To investigate the performance of a sample system under various conditions, we performed a computer analysis using the parameters given in Table 4.1.

Table 4.1: Characteristic parameters of a sample system and channel.

(a) System parameters	
carrier frequency	10 kHz
channel bandwidth	2.0 kHz
signalling rate	4.0 ksymbols/s
(b) Channel parameters	
channel depth	20 m
sound speed	1500 m/s

In order to compute signal attenuations and delays, the channel model and the method of signal computations described in Chapter 3 are employed.

Table 4.2 shows computed values of different paths for an assumed wind speed of 10 knots (corresponding reflection coefficient $|r_s| = 0.461$) and transmitter depth and receiver depth of 10 m. For a given channel condition, the strength of reflected signals after several bounces at the surface and bottom becomes negligibly small. Signals for $i = 19$ and higher, which have amplitudes below the threshold as defined in Chapter 3, are neglected in the computation of the signal strength.We find severe cancellation of signals due to the phase change at the surface and bottom. For instance, a direct path signal adds destructively to the BB_1 path; the SS_1 and BB_2 signals are cancelled by the SB_1 and BS_1 signals, and so on. Therefore, we expect that the signal strength S becomes zero when L becomes large enough to cause negligibly small differences in time between successive, adjacent path signals.

Table 4.2: The parametric values of direct and multipath signals.

	delay (τ_i)	amplitude ($\|\alpha_i\|$)	arriving angle	type
i=1	0	1	0	D
i=2	0.13/L	-1	-atan(20/L)	BB_1
i=3	0.13/L	-0.4610	atan(20/L)	SS_1
i=4	0.53/L	0.4610	-atan(40/L)	SB_1
i=5	0.53/L	0.4610	atan(40/L)	BS_1
i=6	1.20/L	-0.4610	-atan(60/L)	BB_2
i=7	1.20/L	-0.2125	atan(60/L)	SS_2
i=8	2.13/L	0.2125	-atan(80/L)	SB_2
i=9	2.13/L	0.2125	atan(80/L)	BS_2
i=10	3.33/L	-0.2125	-atan(100/L)	BB_3
i=11	3.33/L	-0.0980	atan(100/L)	SS_3
i=12	4.80/L	0.0980	-atan(120/L)	SB_3
i=13	4.80/L	0.0980	atan(120/L)	BS_3
i=14	6.53/L	-0.0980	-atan(140/L)	BB_4
i=15	6.53/L	-0.0452	atan(140/L)	SS_4
i=16	8.53/L	0.0452	-atan(160/L)	SB_4
i=17	8.53/L	0.0452	atan(160/L)	BS_4
i=18	10.80/L	-0.0452	-atan(180/L)	BB_5

SMR versus transmitter depth at three different receiver depths is plotted in Figure 4.3(a). We see that the maximum SMR occurs when the transmitter and receiver are situated in the middle of the channel, that is, when $h_a = h_b = 10.0$ m. The signal and multipath strength versus transmitter depth is shown in Figure 4.3(b) and Figure 4.3(c), respectively. The SMR value is dominantly dependent on the variation of signal strength with transmitter depth.

Figure 4.4(a) shows SMR as a function of wind speed w. We see that error-free transmission (SMR > 1) is possible with binary PSK even in a relatively moderate sea

(sea state-2) with wind speed of approximately 8.5 knots. For higher wind speeds, the SMR increases so that a larger N-ary PSK system can be employed as given by Eq. (4.9). The SMR increase with higher wind speed is due to the rapid decrease of multipath signals as we can see from Figure 4.4(b). For a wind speed of w = 10 knots, we obtain an SMR of 1.5, which enables us to employ a 8-PSK system corresponding to 8 k-bits/s transmission rate at a range of 10 km.

Figure 4.5(a) shows SMR values as a function of distance between transmitter and receiver for a wind speed of 10 knots. We note that the SMR is larger than 1.0 over ranges from L = 5.4 km to L = 11.9 km and from L = 13.4 km to L = 14.9 km. This allows N = 2 and yields an error-free transmission rate of 4 k-bits/s for these ranges. For ranges between L = 9.0 km and L = 10.3 km, the SMR is larger than $\sqrt{2}$ which allows N = 4 and the corresponding transmission rate of 8 k-bits/s. Figure 4.5(b) shows the effective signal strength S and the multipath signal strength M as distance between transmitter and receiver is varied. Both S and M shows the trend of decreases as L increases.

Figure 4.6(a) shows SMR variations when a directional receiver is employed. SMR improves at low wind speed, but still with unacceptable values for error-free communication. Figure 4.6(b) shows that a directional receiver effectively rejects multipath signals at low wind speed which eventually enables us to reduce the hardware complexity at the receiver.

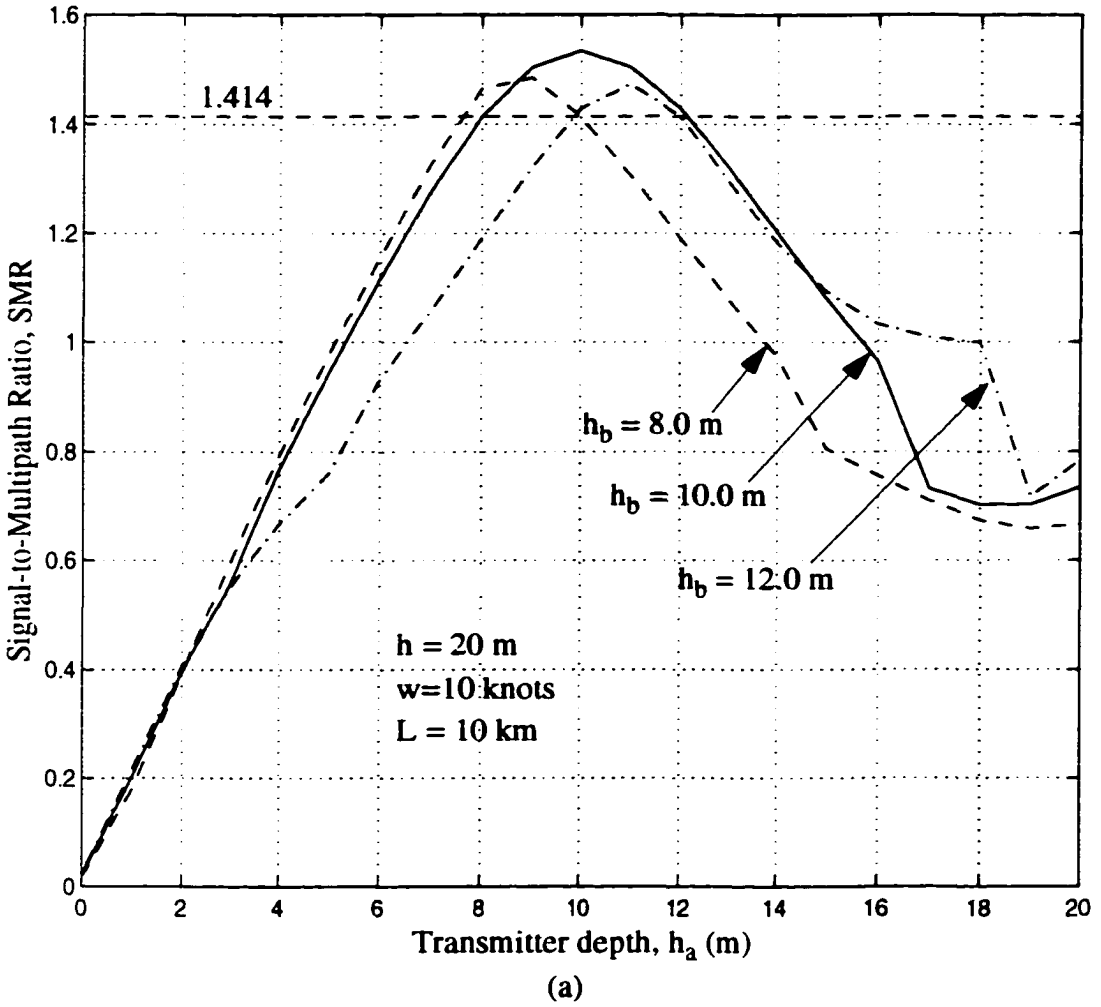

Figure 4.3: SMR vs. transmitter depth. (a) Depth at three different receiver depths (b) Effective signal strength versus transmitter depth. (c) Multipath strength versus transmitter depth.

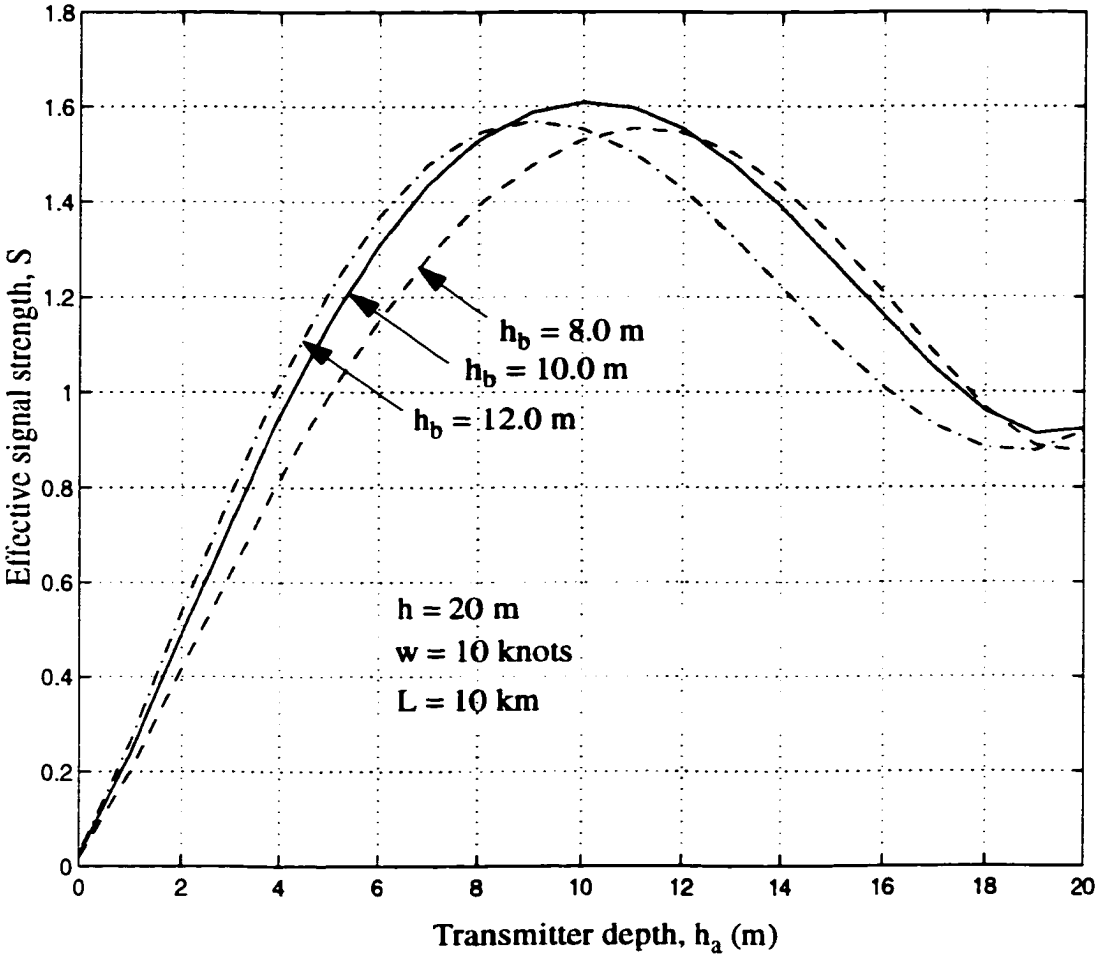

(b)

Figure 4.3: (Continued)

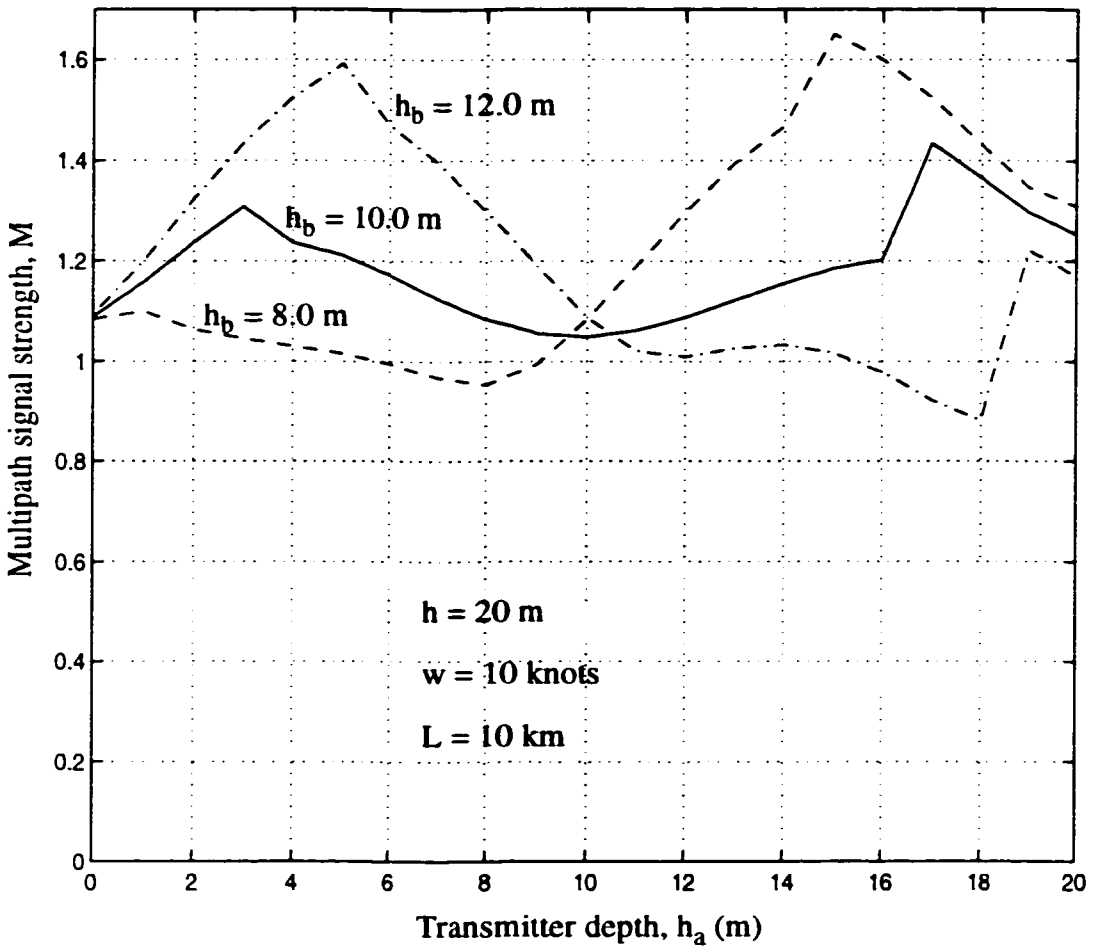

(c)

Figure 4.3: (Continued)

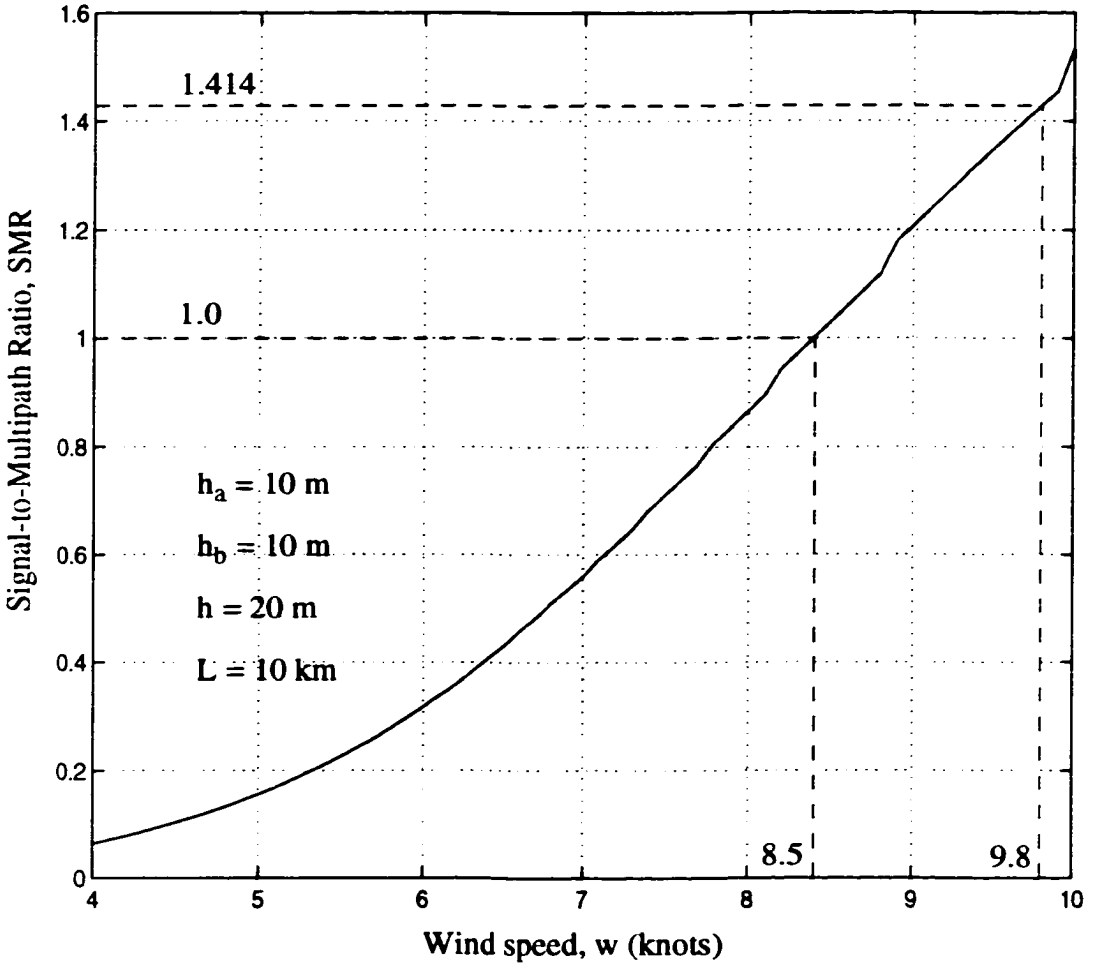

(a)

Figure 4.4: SMR vs. wind speed.

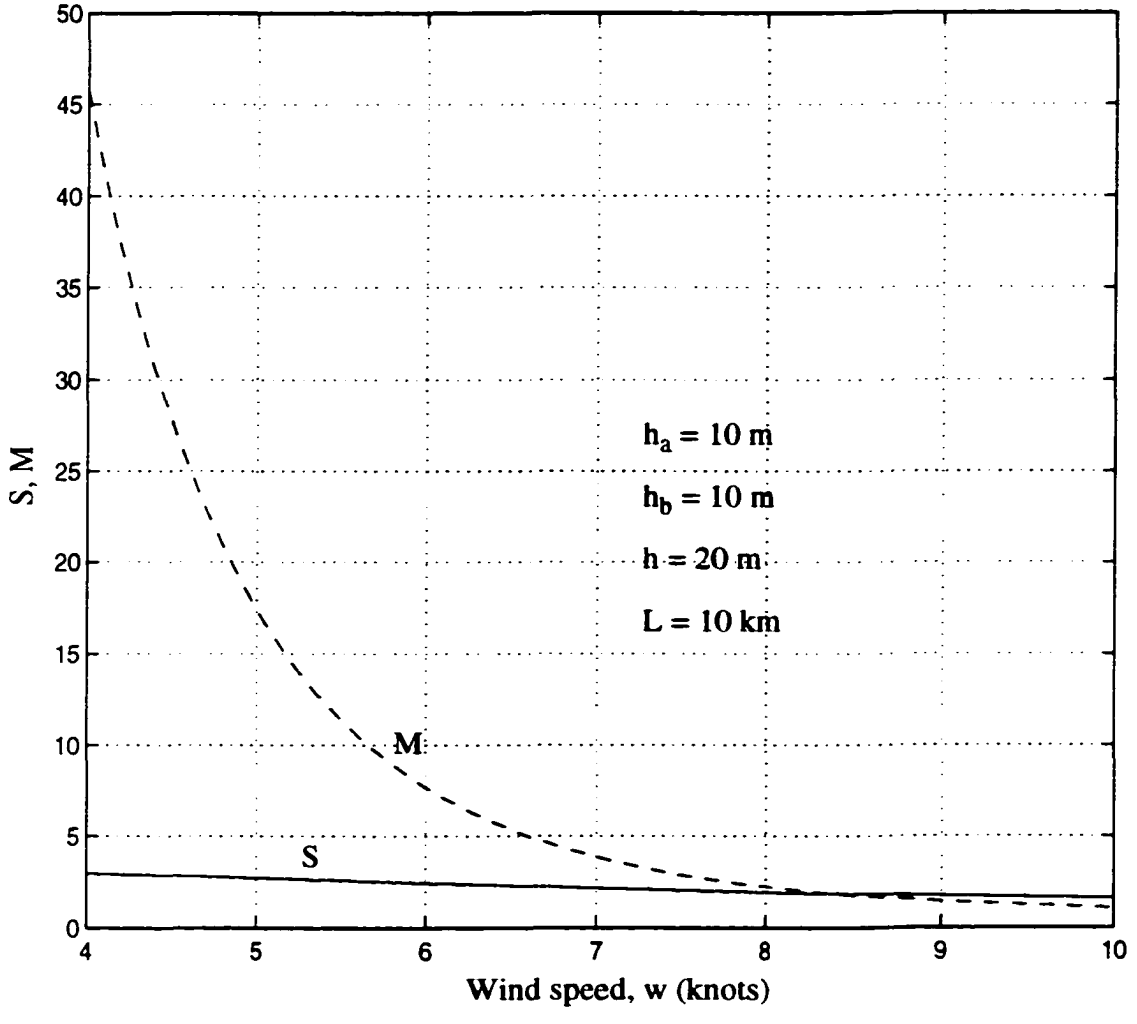

(b)

Figure 4.4: (Continued)

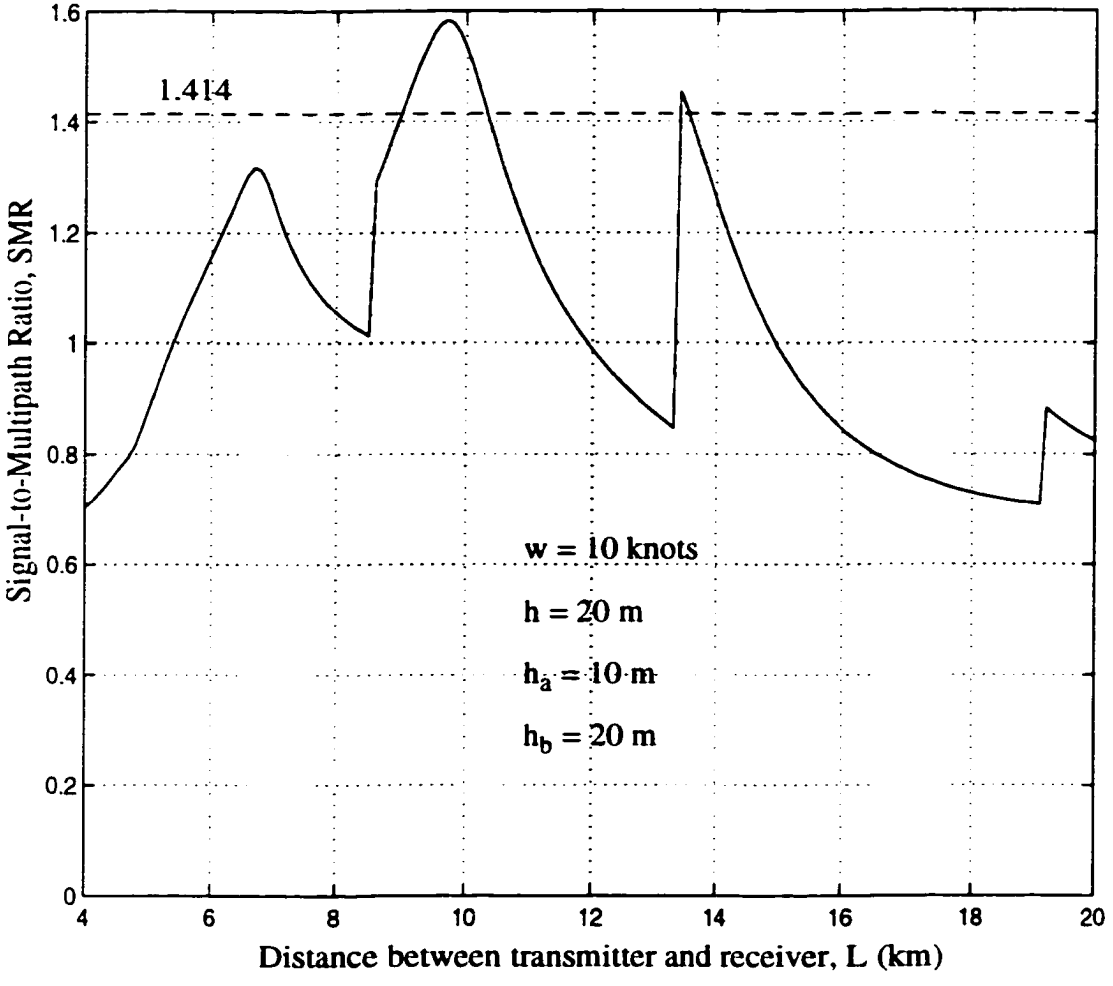

(a)

Figure 4.5: (a) SMR vs. range (L) (b) S,M vs. range

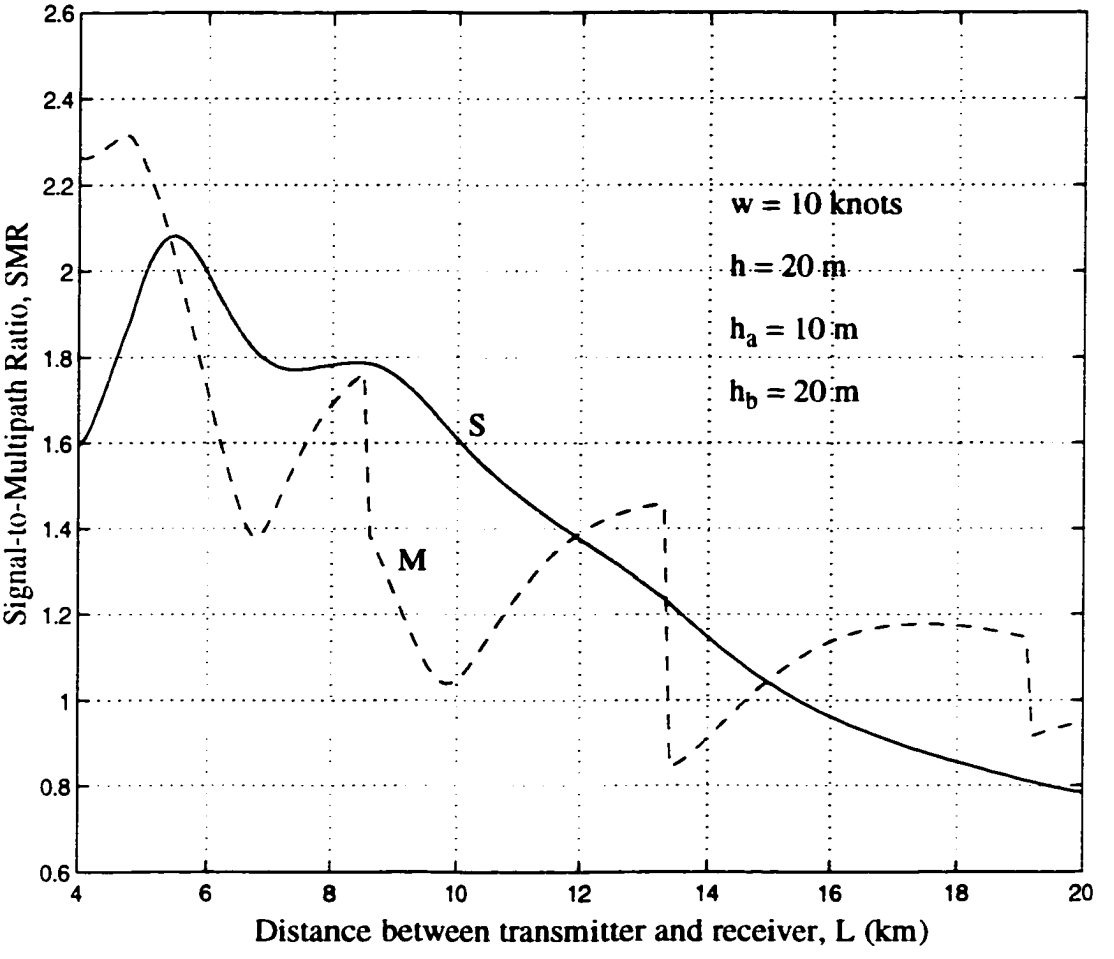

(b)

Figure 4.5: (continued)

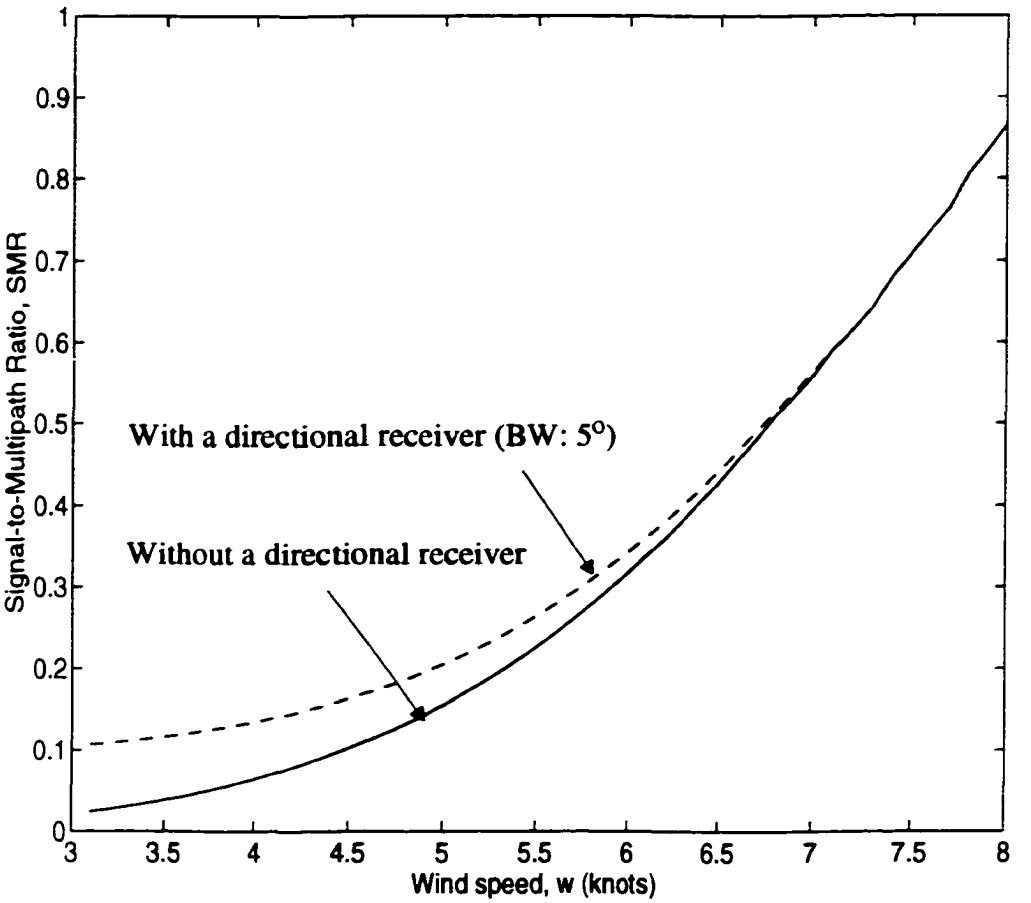

(a)

Figure 4.6: SMR when a directional receiver is employed

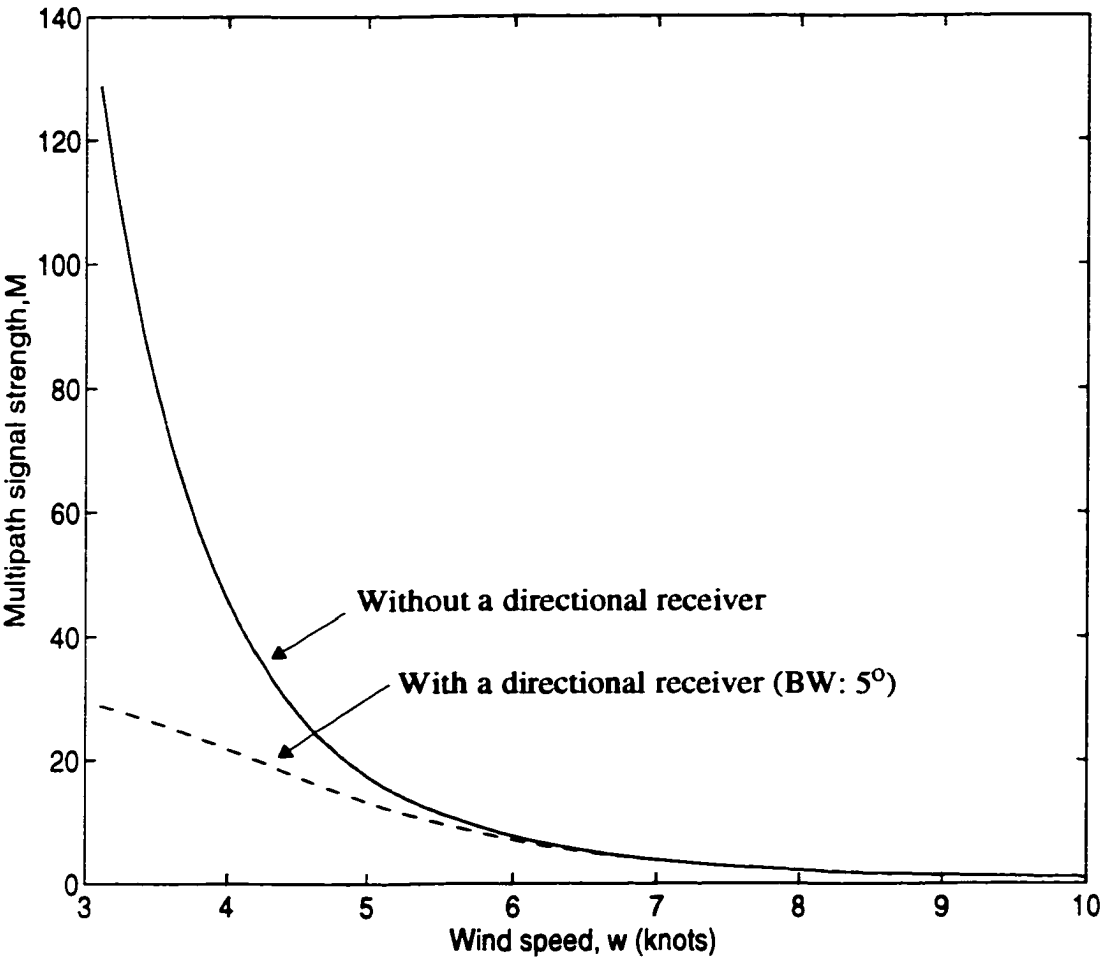

(b)

Figure 4.6: (Continued)

4.6 Summary

We have developed a performance measure for high data rate acoustic communication in a shallow water channel.We then performed analyses for a test acoustic system. The analyses results suggest that a high transmission rate may be possible over a very shallow water channel using digital differential phase modulation. Such transmission is possible in the presence of constructive interference between the direct and multi-path signals. The robustness of the transmission depends on sea state; it improves with rough sea conditions. Alternatively, higher transmission rates can be achieved by using a larger number of phases to modulate the signal. The SMR was studied when a directional receiver is employed. While a directional receiver is effective in removing multipath signals, the improvement in performance is not enough to achieve error-free communication, even under the assumption of the absence of ambient noise.

Chapter 5

Simulation of the Equalizer for Shallow Water Acoustic Communication

5.1 Introduction

Acoustic signals transmitted in shallow water are corrupted by interference from signals reflected and scattered at both the water surface and bottom [22]. This causes time spreading of a transmitted signalling impulse. This spreading may amount to hundreds of signalling intervals, causing intersymbol interference (ISI). The shorter the signalling interval (higher transmission rate), the larger the number of interfering symbols at the receiver. Several anti-multipath techniques have been developed [4, 22, 66, 81].

In many situations, the direct-path signal and multipath signals arrive from distinctively different angular directions. In these circumstances, the multipath can be effectively reduced by a directional receiver [51]. However, spatial discrimination in a long range shallow channel is virtually impossible due to the relatively small differenc-

es in arrival angles. This results in significant corruption due to large amplitude multi-path signals [22, 81]. In such a case, adaptive equalization can be effectively used [4, 74, 78]. Since the underwater acoustic channel characteristics change due to fluctuations of the sea state and transmitter/receiver position changes, any equalizer also should be able to track these changes adaptively.

In this chapter, we analyze the performance of a communication system in a static time-invariant underwater channel using adaptive equalization and test it by computer simulation. The case of time-variant channel will be studied in the next chapter. In simulations we utilized the channel model described in Section 3.2.

The equalizer structure and algorithms employed for simulation are described in Section 5.2 and the simulation results are presented in Section 5.3.

5.2 Equalizer Structure and Algorithms

The selection of an equalizer should take into consideration the convergence rate of adaptation algorithms, its processing complexity and its ability to track changes in the channel characteristics. In this section, the equalizer structure and its algorithm are described. The hardware complexity associated with an equalizer is also investigated.

5.2.1 Equalizer structure

A variety of structures and associated algorithms have been proposed for use in underwater acoustic communication. Among them, the stochastic gradient least mean square (LMS) [74], the recursive least squares (RLS) [72] and the stochastic gradient lattice [66] algorithms seem to be the most popular. The equalizers can be classified as linear or non-linear [72, 73]. The decision feedback equalizer [72] is an example of a non-linear class of equalizer. Another classification is based on the tap spacing, namely, a symbol-spaced or fractionally-spaced equalizer (FSE) [70]. We select a decision feed-

back equalizer where the forward filter is fractionally spaced with spacing $T/2$. For the adaptation algorithm we have chosen the stochastic gradient LMS algorithm [72, 73] due to its numerical stability and computational advantage.

Figure 5.1 shows the structure of the selected equalizer. The equalizer consists of the adaptive feed-forward and feedback transversal filters. For notational simplicity, let us represent the input and output of the equalizer at time $t = kT$ as $y(kT) = y_k$ and $z(kT) = z_k$, respectively. The complex signal y_k is passed through the adaptive transversal filter, that is, y_k at the n-th forward tap is

$$y_{k,n} = y\left(t_o + kT - n\frac{T}{2}\right) \tag{5.1}$$

where t_o is the sampler delay (for simplicity we assume that $t_o = 0$).

This filter is intended to minimize the intersymbol interference. Before normal operation, the equalizer is subject to training mode (switch S in Figure 5.1 is in position 2). During training mode, a block of data, d_k, known to the receiver is transmitted and used to adjust the equalizer tap coefficients. After completion of the training period the switch S in Figure 5.1 is changed to position 1 and the receiver does not know the actual transmitted data so that the adjustment of the equalizer coefficients (tap gains) is performed using the decisions at the output of the detector (decision-directed). For symbol error rates less than 10^{-2}, the occasional errors made by the decision device have a negligible effect on the performance of the equalizer [73].

Let the number of taps of the feed-forward and feedback transversal filters be N_1 and N_2, respectively. Then the total number of tap coefficients is $N_{eq} = N_1 + N_2$. The output of a complex transversal equalizer z_k is given by [73]

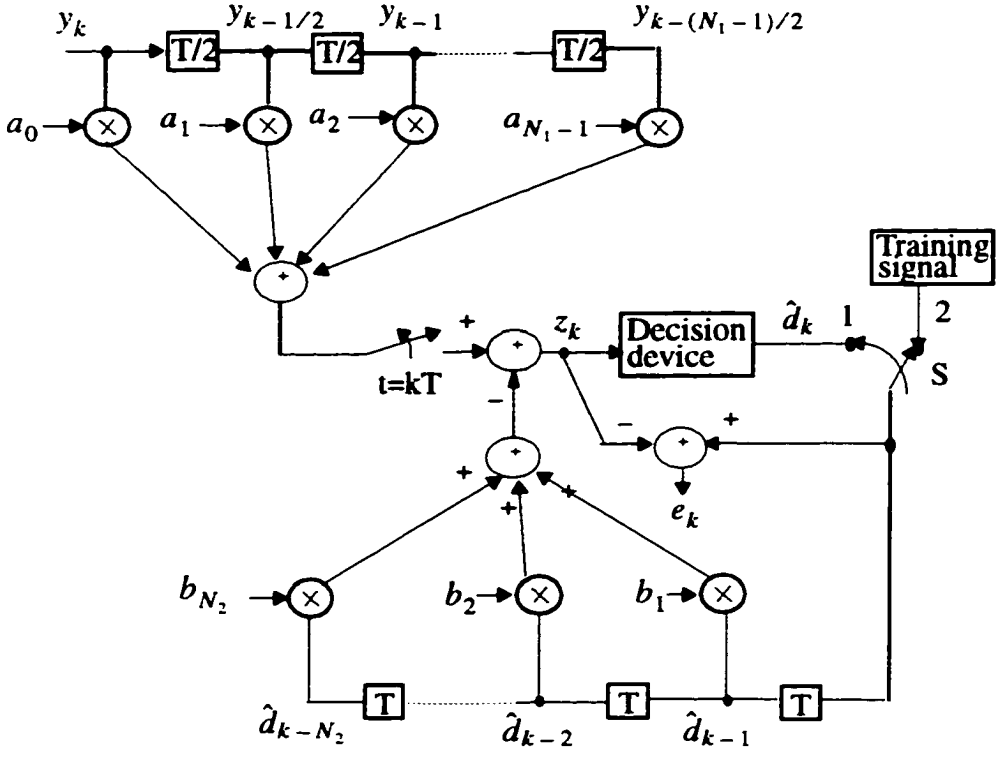

Figure 5.1: Structure of the Decision Feedback Equalizer (DFE)

$$z_k = \sum_{i=0}^{N_1 - 1} a_{k-1,i} y_{k,i} - \sum_{j=1}^{N_2} b_{k-1,j} \hat{d}_{k,j} \tag{5.2}$$

where $a_{k,i}$, $b_{k,j}$ and $\hat{d}_{k,j}$ are the i-th forward tap gain, the j-th feedback tap gain and the detected symbol at time kT, respectively.

Define the tap weight vector as

$$\begin{aligned} \boldsymbol{C}_{k-1} &= [\boldsymbol{A}_{k-1}^T, \boldsymbol{B}_{k-1}^T]^T \\ &= [a_{k-1,0}, \ldots, a_{k-1,N_1-1}, b_{k-1,1}, \ldots, b_{k-1,N_2}]^T, \end{aligned} \tag{5.3}$$

where $\mathbf{A}_{k-1}$ and $\mathbf{B}_{k-1}$ are the weight vector of the forward and feedback section, respectively. The observed data vector is

$$\boldsymbol{X}_k = [\boldsymbol{Y}_k^T, -\boldsymbol{D}_k^T]^T, \tag{5.4}$$

where

$$\boldsymbol{Y}_k = [y(kT + (N_1/2)\Delta), \ldots, y(kT), \ldots, y(kT-(N_1/2)\Delta)]^T, \tag{5.5}$$

$$\boldsymbol{D}_k = \begin{cases} [d_{k-1} \ldots, d_{k-N_2}]^T \text{ in training mode, or} \\ [\hat{d}_{k-1} \ldots, \hat{d}_{k-N_2}]^T \text{ in decision directed mode,} \end{cases} \tag{5.6}$$

where d_k is the training sequence and $\hat{d}_k$ is the detected symbol at time kT, respectively.

With these notations, Eq. (5.2) can be conveniently written as

$$z_k = \boldsymbol{C}_{k-1}^T \boldsymbol{X}_k. \tag{5.7}$$

5.2.2 Optimization algorithm

In this section, adaptive algorithms for the calculations of the equalizer parameters are described. The most commonly used criterion in the optimization of the equalizer coefficients is the minimization of the mean square error (MSE), that is,

$$J = \min([E|e_k|^2]), \tag{5.8}$$

where e_k is the error signal:

$$e_k = d_k - z_k = d_k - \boldsymbol{C}_{k-1}^T \boldsymbol{X}_k \tag{5.9}$$

while d_k and z_k are the actual transmitted data and the equalizer output at $t = kT$, respectively. For an ideal channel, $d_k = z_k$.

The minimization of the MSE is accomplished recursively by the use of the stochastic gradient algorithm, called the least mean square (LMS) algorithm [70]. A new set of coefficients is obtained iteratively as

$$\boldsymbol{C}_k = \boldsymbol{C}_{k-1} - \frac{\mu}{2} \nabla_C \left[E\left\{ \left| d_k - \boldsymbol{C}^T \boldsymbol{X}_k \right|^2 \right\} \right] \Bigg|_{\boldsymbol{C} = \boldsymbol{C}_{k-1}}. \tag{5.10}$$

where $\nabla_C = \dfrac{\partial}{\partial \boldsymbol{C}_k}$ is the gradient with respect to the coefficients.

Instead of the true gradient of the MSE

$$\nabla_C \left[E\left\{ \left| d_k - \boldsymbol{C}_{k-1}^T \boldsymbol{X}_k \right|^2 \right\} \right], \tag{5.11}$$

we will use its estimate

$$\nabla_C[|d_k - C_{k-1}^T X_k|^2]. \tag{5.12}$$

Eq. (5.10) with this estimate becomes:

$$C_k = C_{k-1} + \mu X^*_k[d_k - z_k]. \tag{5.13}$$

Rewriting Eq. (5.13) using Eq. (5.3) and Eq. (5.4), we obtain

$$\begin{aligned} A_k &= A_{k-1} + \mu e_k Y^*_k \\ B_k &= B_{k-1} - \mu e_k \hat{D}^*_k \end{aligned} \tag{5.14}$$

where μ is a positive adaptation constant (step size) and * denotes the complex conjugate of the vector.

The step-size parameter μ controls the rate of adaptation of the equalizer and stability of the stochastic gradient algorithm. Larger step-size μ leads to more rapid convergence, but also leads to larger fluctuations in the equalizer coefficients during steady state operation. The selection of step-size μ is therefore a compromise between rapid convergence and small variance of self noise.

The degrees of freedom of the equalizer can be increased if the selection of step size μ is made self-adaptive [11, 20].

The iterative procedure to update a step size μ can be obtained using gradient-search procedure:

$$\mu_k = \mu_{k-1} - \frac{\alpha}{2}\frac{\partial J_k}{\partial \mu_k} \tag{5.15}$$

where $J_k = |e_k|^2 = |d_k - z_k|^2$ is the squared error at time k and α is an arbitrary positive small constant.

Let $\boldsymbol{G}_k = \dfrac{\partial \boldsymbol{C}_k}{\partial \mu}$ be the gradient of the tap-weight vector $\boldsymbol{C}_k$ with respect to the step-size parameter μ.

Differentiating the cost function J_k with respect to the step-size parameter μ yields the scalar gradient

$$\begin{aligned} \nabla_{\mu, k} &= \frac{\partial J_k}{\partial \mu} \\ &= \frac{1}{2} E\left[\frac{\partial}{\partial \mu} e_k e_k^* + \frac{\partial}{\partial \mu} e_k^* e_k\right]. \end{aligned} \tag{5.16}$$

From Eq. (5.9) and the definition of $\boldsymbol{G}_k$, we find that

$$\frac{\partial \boldsymbol{e}_k}{\partial \mu} = -\boldsymbol{G}_k^H \boldsymbol{X}_k \tag{5.17}$$

Then, Eq. (5.16) may be expressed as

$$\nabla_{\mu, k} = -\frac{1}{2} E[\boldsymbol{G}_k^T \boldsymbol{X}_k e^*{}_k + \boldsymbol{G}_k^H \boldsymbol{X}^*{}_k e_k] \tag{5.18}$$

Let μ_k and $\hat{\boldsymbol{C}}_k$ denote the actual sequences of step sizes and estimates of $\boldsymbol{C}_k$, respectively, resulting from the adaptive scheme.

The iterative procedure to update the step size μ_k may be formulated as

$$\mu_{k+1} = \mu_k - \frac{\alpha}{2} \hat{\nabla}_{\mu, k}, \tag{5.19}$$

where α is a small, positive learning-rate parameter and $\hat{\nabla}_{\mu, k}$ is an estimate of the scalar gradient $\nabla_{\mu, k}$.

Let us define $\hat{G}_k = \dfrac{\partial \hat{C}_k}{\partial \mu}$ as the estimates of the derivative G_k. Then, the instantaneous estimate can be formulated from Eq. (5.18) as

$$\begin{aligned} \nabla_{\mu,k} &= -\frac{1}{2}E[G_k^T X_k e^*_k + G_k^H X^*_k e_k] \\ &= -\frac{1}{2}\mathrm{Re}[G_k^H X_k e^*_k] \end{aligned} \tag{5.20}$$

where Re signifies the real-part operator. Summarizing the derivations, we have the LMS algorithm with adaptive step size:

$$\begin{aligned} e_k &= d_k - C_{k-1}^T X_k \\ C_k &= C_{k-1} + \mu_k X^*_k [d_k - z_k] \\ \mu_{k+1} &= \mu_k + \alpha \mathrm{Re}[G_k^H X_k e^*_k] \\ \hat{G}_{k+1} &= \hat{G}_k + X_k e^*_k - \mu_k X_k X^{*T}_k \hat{G}_k \end{aligned} \tag{5.21}$$

The LMS algorithm with adaptive step size described above is usually called a fast self-optimized LMS algorithm (FOLMS) [11, 20].

A faster converging algorithm can be obtained from the minimization of the sum of exponentially weighted squared errors, that is,

$$\begin{aligned} J_k &= \sum_{n=0}^{k} \omega^{k-n} |d_n - z_n| \\ &= \sum_{n=0}^{k} \omega^{k-n} \left| d_n - C_{k-1}^T X_n \right|. \end{aligned} \tag{5.22}$$

where ω is a value slightly less than unity.

The recursive least square (RLS) and its variations are based on Eq. (5.22);they have fast convergence but high computational complexity [72]. Comparative study be-

tween square-root RLS and LMS algorithms will be performed regarding the convergence characteristics and hardware complexities.

5.2.3 Hardware complexity

In this section, we will investigate the hardware complexity associated with equalizers. LMS, FOLMS and square-root RLS algorithms, frequently employed for the update of an equalizer's coefficients, are investigated. The computational load of the equalizer, expressed by floating point operations per second (FLOPS), is approximately given as:

$$FLOPS \approx f(N_{eq}) \times updates/s, \tag{5.23}$$

where $f(N_{eq})$ is the computational load per the iteration of the adaptive algorithm and $updates/s$ is the number of iterations per second of the adaptation algorithm [54]. Using FLOPS to estimate the computational load of the equalizer is an approximate approach. However, it gives us good general understanding of relation between the computational load and selected adaptation algorithm, the number of equalizer taps and the number of updates/second. For an implementation of the LMS, $f(N_{eq}) = 8N_{eq}$ while $f(N_{eq}) = 24N_{eq}$ and $9N_{eq}^{2}$ for a FOLMS and a square-root RLS algorithm, respectively [20, 44, 54]. Observing Eq. (5.23), we see that the computational requirements of the equalizer can be reduced by reducing N_{eq}, by using a more efficient adaptation algorithm with smaller $f(N_{eq})$ for a given N_{eq} or by updating the parameters less frequently. Less frequent update of the parameters is possible for a channel with slow variations with time. In such a case, the equalizer parameters can be sporadically updated whenever the equalizer performance falls below a predefined threshold. This approach of reducing the iteration rate of the adaptation algorithm is usually called the sparse updating method. In this study, we will consider the first two approaches, that is,

reducing N_{eq} using a directional receiver and reducing $f(N_{eq})$ by using a less computationally intensive algorithm.

In order to investigate the effect on the computational complexity associated with different selection of adaptation algorithm, let us roughly determine how many digital signal processing (DSP) chips are needed to deal with the computational load of an equalizer for a shallow water channel. The currently popular DSP chip TMS320C50 has a capability of 50 MFLOPS. For the computation, a decision feedback equalizer in which the forward filter is fractionally spaced (T/2 spaced where T is a symbol duration) is used. We assume that the number of total taps including forward and feedback filters is three times that of delay spread associated with the channel. Channel and system parameters used for this study are shown in Table 5.1.

Table 5.1: Channel and system parameters

signalling rate	5.0 ksymbols/s
carrier frequency	10 kHz
transmission range	10 km
channel depth	20 m
transmitter/receiver depth	10 m

Table 5.2 shows the computational load of a sample system with channel conditions shown in Table 5.1 at a wind speed of $w = 4$ knots. When an LMS and FOLMS algorithm are used, a few TMS320C50 DSP chips can handle the computations required for the update of equalizer taps, even without a directional receiver. For a directional receiver with LMS algorithm, only 18% of their full capability are needed, respectively, while for FOLMS, 54% are needed. This allows us to use a DSP chip with less capability. However, when a square-root RLS algorithm is used, 46 DSP chips are required with a directional receiver and 1641 DSP chips with a non-directional receiver. The latter is impractical to implement.

Table 5.2: Computational loads of an equalizer.

		Delay spread (symbols)	Computational load (MFLOPS)	# of TMS320C 50
LMS	non-directional receiver	450	54	~1
	directional receiver (BW=5°)	75	9	1 (18%)
FOLMS	non-directional receiver	450	162	~3
	directional receiver (BW=5°)	75	27	1 (54%)
square-root RLS	non-directional receiver	450	82000	1641
	directional receiver (BW=5°)	75	2280	46

5.3 Simulation Results

In this section, using a sample channel geometry, the effectiveness of an equalizer for shallow water acoustic communication is demonstrated. Here, we assume perfect synchronization. The channel characterization by the impulse response will be performed. The impulse response gives us information regarding the degree of multipath present. The scatter diagram shows the signal distortion caused by intersymbol interference. The scatter diagram of an N-ary PSK system with N = 4 and 8 is investigated by transmitting a random data sequence through a shallow water channel.

5.3.1 Channel characterization

Table 5.3 shows the channel and system parameters selected for simulation. Figure 5.2 shows SMR values for a given channel. We can see that SMR values tend to increase as distance between the transmitter and receiver is increased. SMR values for

all distance ranges are below the condition of error-free transmission for QPSK (and 8-PSK). An overlap of received signal clusters would prevent error-free transmission, even in the absence of ambient noise if no further signal processing were applied. However, one should remember that the SMR values as calculated represent the lower bound (worst case values) and the actual SMR will be larger than the lower bound.

Table 5.3: Simulation parameters.

range	10, 15, 20 km
ocean depth	50 m
wind speed	10 knots
transmitter depth	25 m
receiver depth	25 m
carrier frequency	10 kHz
system bandwidth	2 kHz
transmission rate	4 kbaud
modulation	QPSK, 8-PSK

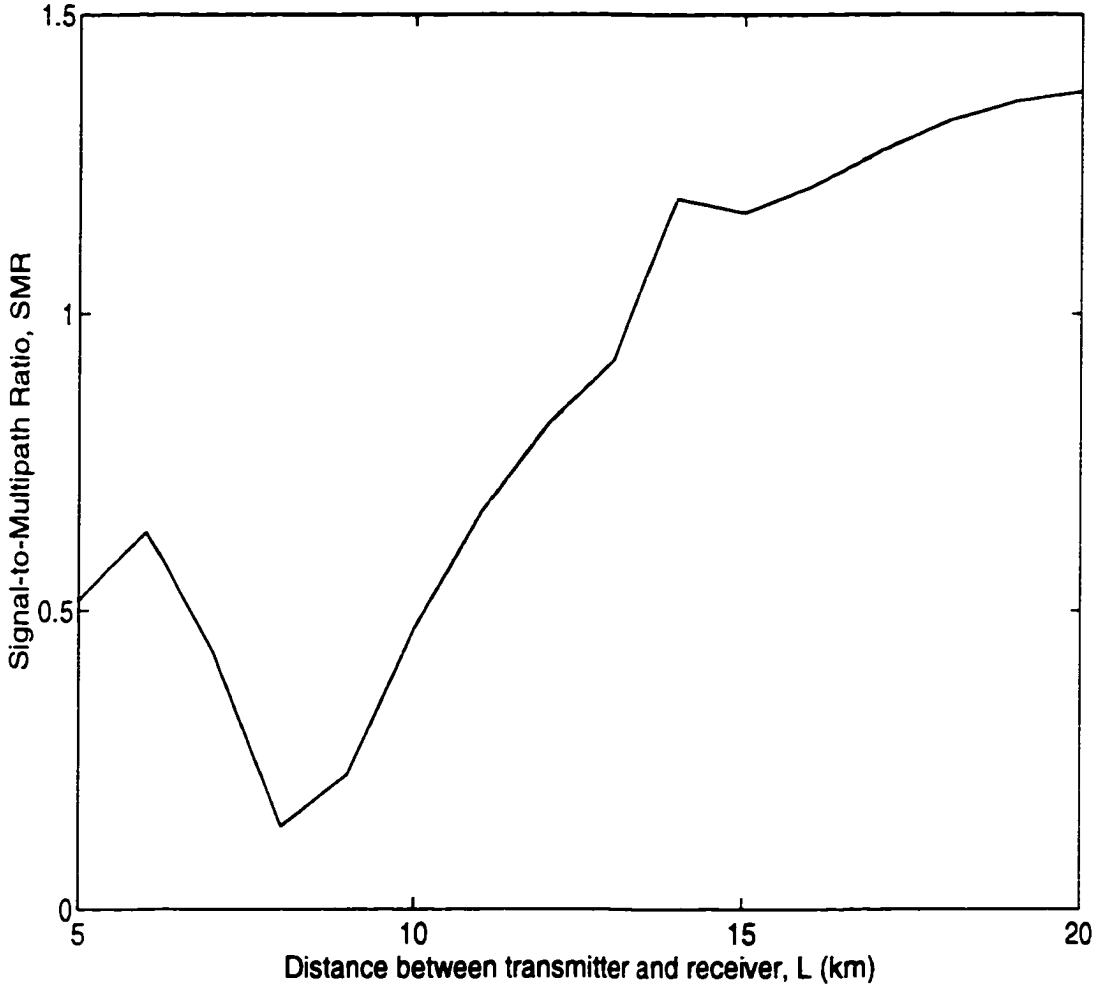

Figure 5.2: SMR vs. distance between transmitter and receiver for a given channel

Figure 5.3 shows the block diagram of the simulator which was programmed in the C/C++ language. This simulator allows us to evaluate the performance of a digital communication system under different channel conditions. It is very effective in comparing performances when the effects of channel geometry and the location of transducers on the received signal are investigated. Digital finite impulse response (FIR) filters are used to simulate both the transmitting and receiving filters. Channel parameters employed for simulations such as time delay and signal attenuation are pre-computed based on the procedure described in Section 3.2. In simulations, a double precision of floating point was used to compute signal values. This is accurate enough to guarantee the proper evaluation of equalizer as studied in [69].

Figure 5.4 shows the resultant impulse responses for a given channel condition. We observe that the duration of the impulse response is approximately 50T, 35T, and 27T for L = 10, 15 and 20 km, respectively.

Figure 5.5 shows the received signal waveform and its eye pattern when the signal is transmitted through a shallow water channel. The comparison with the received signal through an ideal channel which is presented in Figure 2.8 clearly shows the distorted waveform and closed eye pattern caused by multipath propagation through a shallow channel. These distorted waveform and closed eye pattern indicate the impossibility of correct detection of a signal at the receiver without further signal processing such as an equalization.

Figure 5.6 depicts scatter diagrams of a QPSK system for a given channel condition. We see that for L = 10 km no distinct phase constellations are present (no opening is present in the eye pattern). This indicates that even in the absence of other sources of noise, error-free transmission is impossible in this case. For L = 15 and 20 km, scatters form distinct constellations, but the equalization reduces the scatter and assures a better transmission performance in the presence of noise.

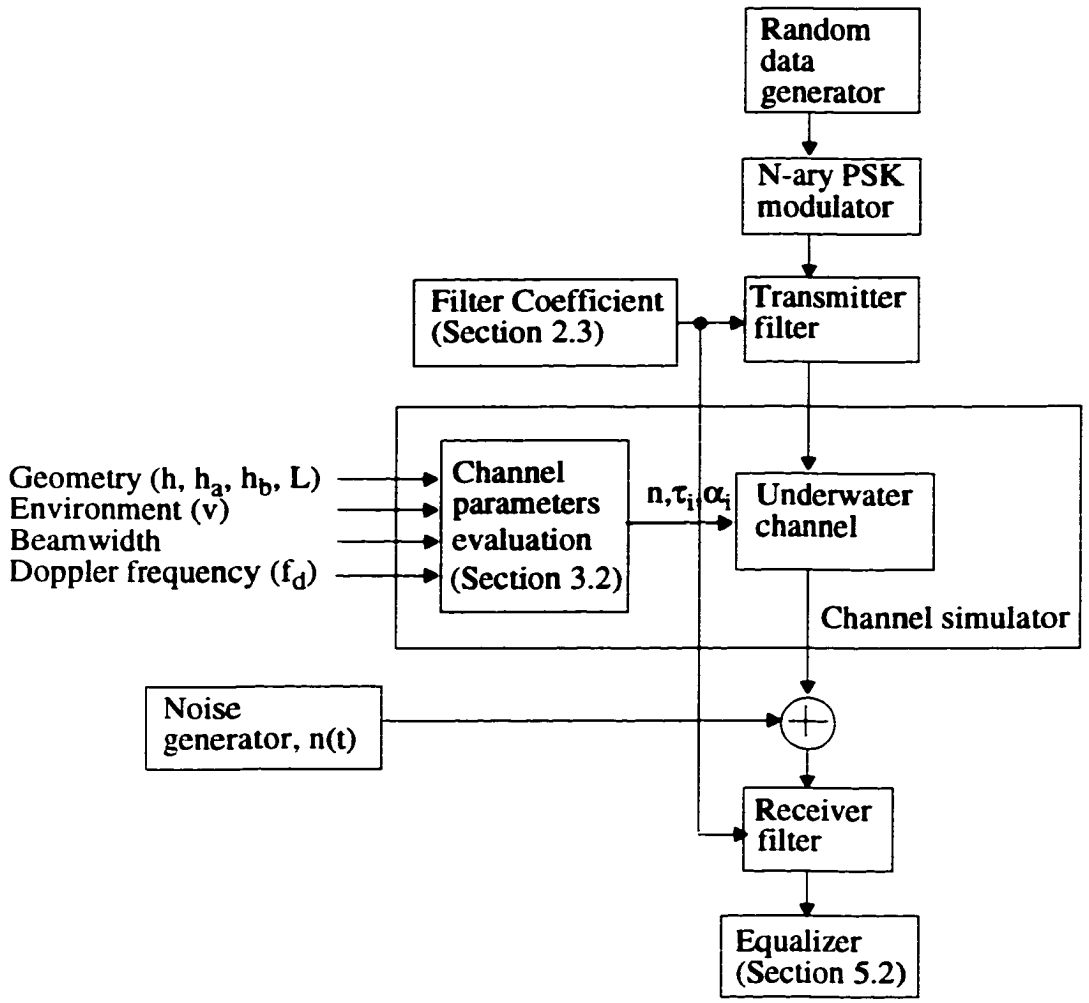

Figure 5.3: Simulator block diagram

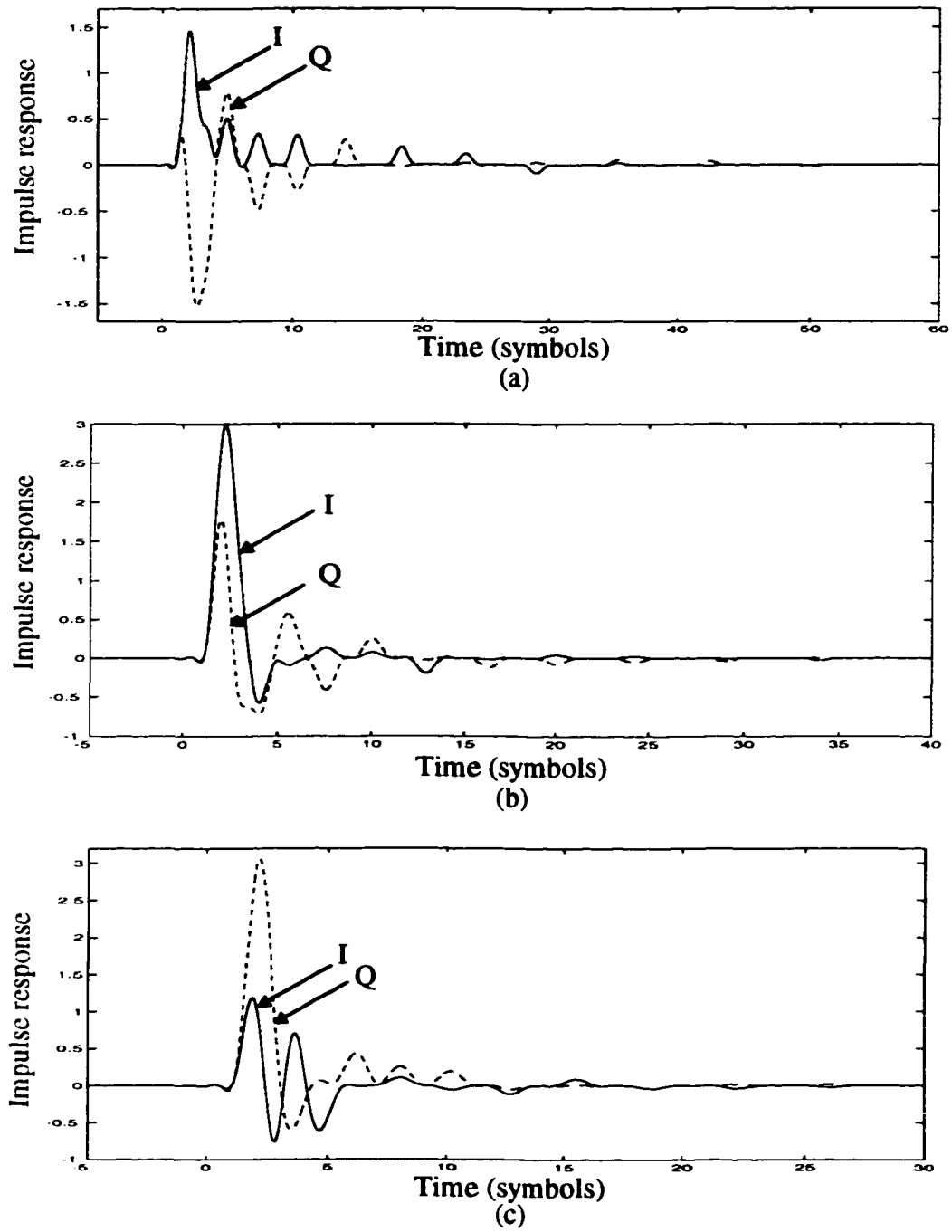

Figure 5.4: Impulse response of channel (a) L = 10 km, (b) L = 15 km, (c) L = 20 km.

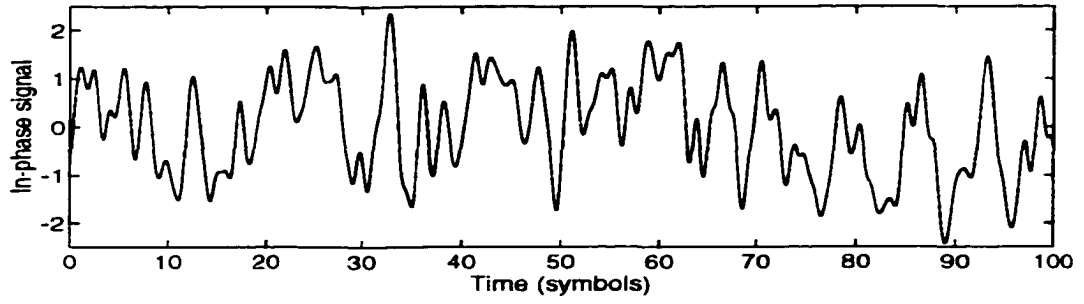

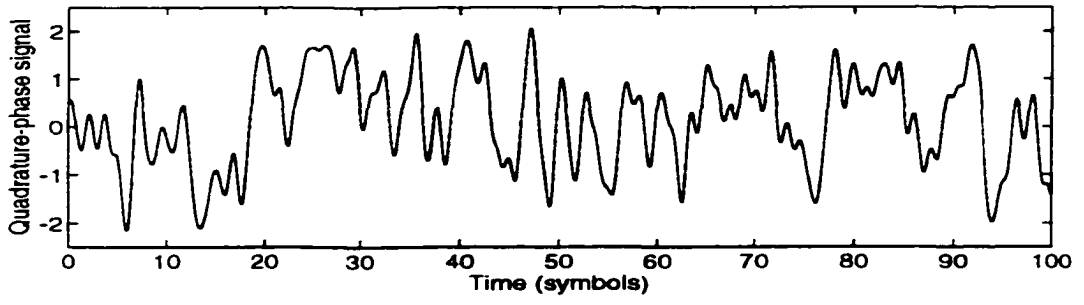

(a)

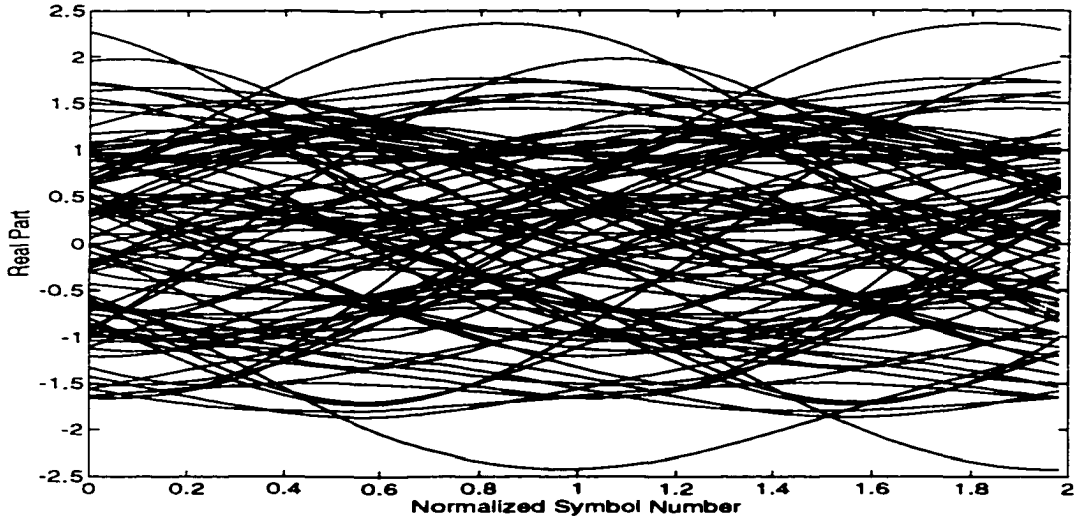

(b)

Figure 5.5: Received signal and eye diagram (L = 10 km)

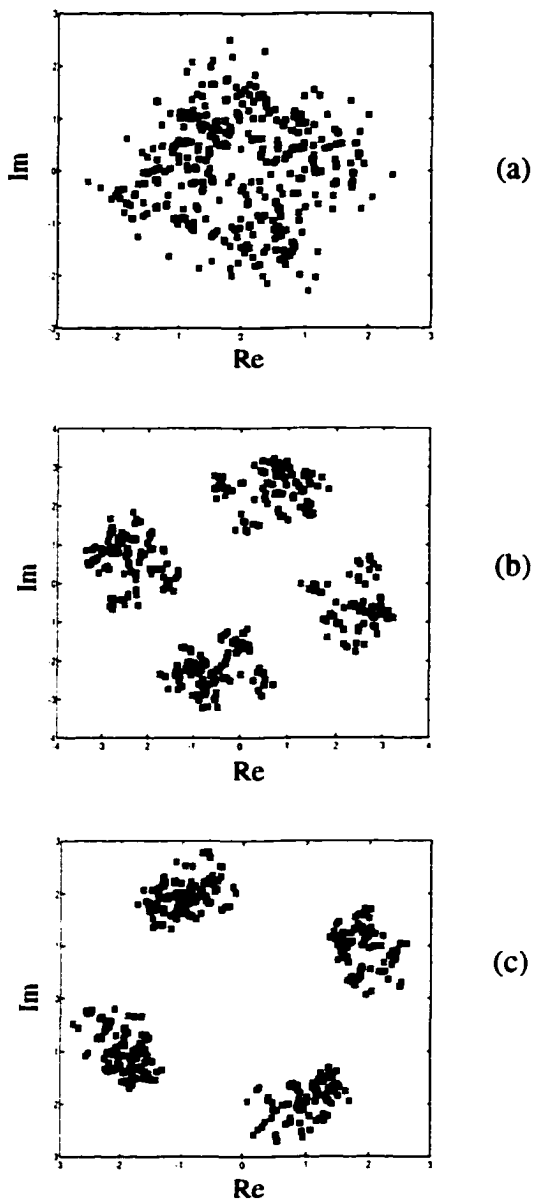

Figure 5.6: Scatter diagrams before equalization

(a) L = 10 km, (b) L = 15 km, (c) L = 20 km.

5.3.2 Performance results of an equalizer

To investigate the convergence rate of the equalizer, we plot the estimated magnitude of mean squared error $E[e_k^2]$ vs. number of iterations. The estimated mean squared error $E[e_k^2]$ is obtained by averaging over 100 independent simulation runs. We selected N_{eq} = 100 and $M_{eq} = N_{eq}/2$ = 50 as the number of forward and feedback equalizer taps, which approximately equals the channel delay spread divided by the symbol duration. During the training period, the training sequence of 1000 random symbols known to the receiver is transmitted. After the training period, the adjustment of the equalizer coefficients is performed by the iterative procedure using the receiver estimates $\{\hat{d}\}$ of the transmitted sequence $\{d\}$. We expect that after the training sequence, most decisions are correct [72]. The result of the LMS algorithm is shown in Figure 5.7 for an adaptation step $\mu = 0.002$. The step size μ was chosen to be approximately one-tenth of the inverse of the product of the received signal power and the number of equalizer coefficients [66]. As can be seen in Figure 5.7, for convergence the equalizer requires over 2300, 700 and 500 iterations for L = 10, 15 and 20 km, respectively. The shorter convergence time at longer transmission range can be accounted for by the fact that at longer range SMR values are larger and impulse responses are shorter as shown in Figure 5.2 and Figure 5.4.

Figure 5.8 shows the scatter diagram at the output of the equalizer after approximately 2400, 800 and 600 iterations for L = 10, 15 and 20 km, respectively. The scatter plot shows that the ISI caused by multipath transmission is dramatically reduced. This result indicates that error-free data transmission over a distance of 20 km at a transmission rate of 8 k-bits/s might be possible if an equalizer is employed.

Figure 5.9 shows the convergence characteristics of the square-root RLS algorithm. It shows that the convergence occurs in less than 250 iterations, 1/10 that of the LMS algorithm for L = 10 km. In other words, a square-root RLS algorithm has a much faster convergence characteristic compared with LMS algorithm, even though it is very

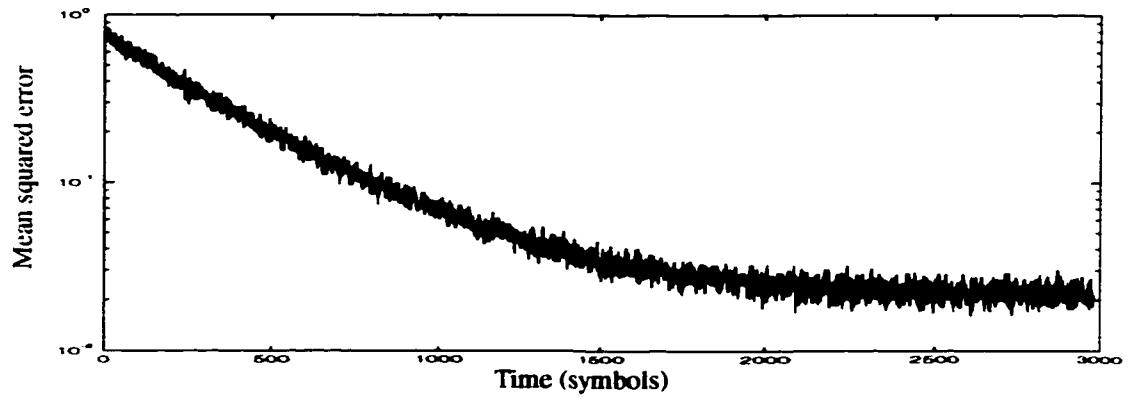

(a) L = 10 km

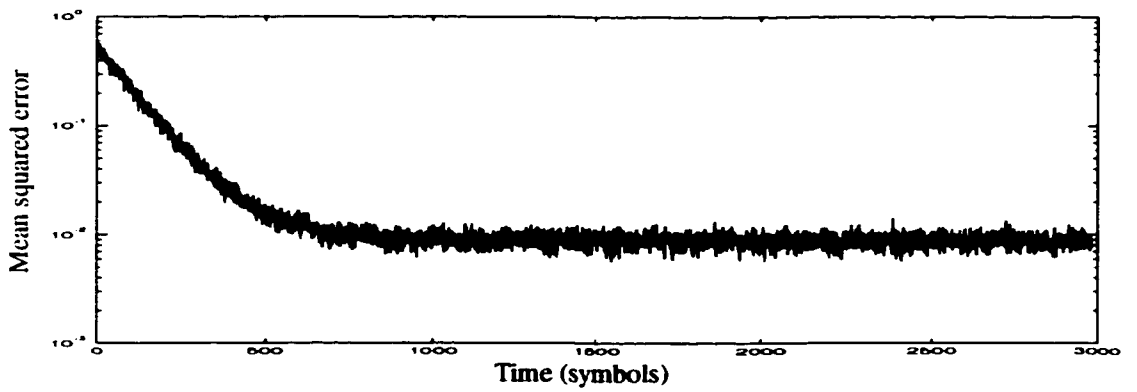

(b) L= 15 km

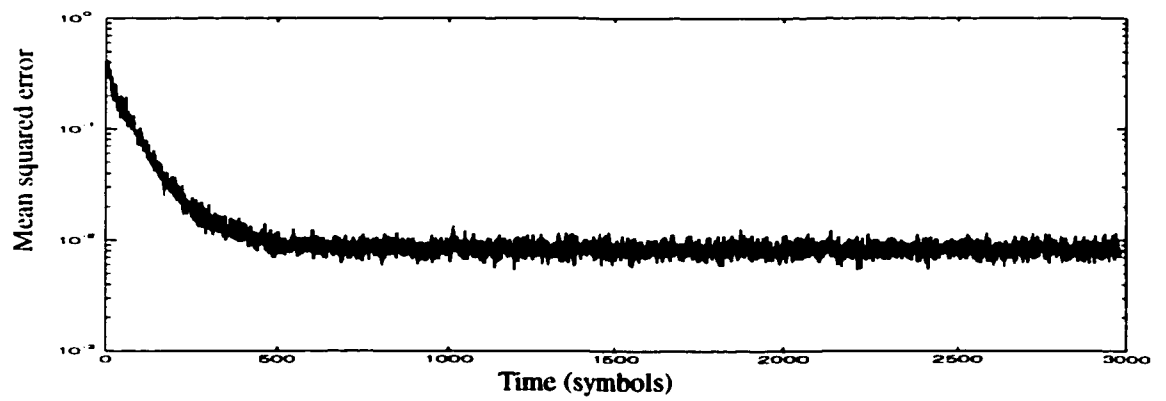

(c) L = 20 km

Figure 5.7: The variation of mean squared error with time (LMS, $\mu = 0.002$)

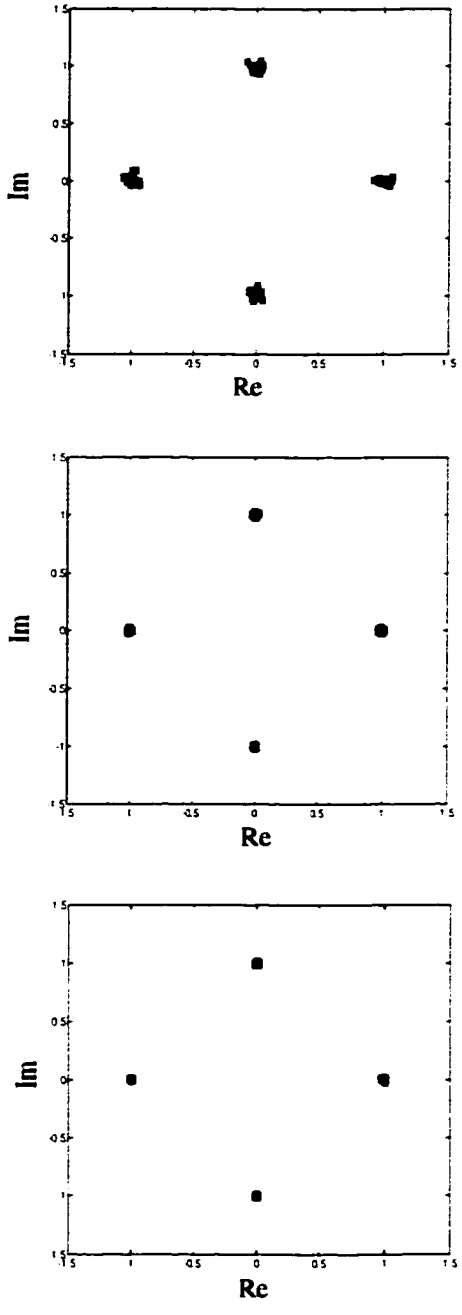

Figure 5.8: Scatter diagram after equalization (LMS)

(a) L = 10 km, (b) L = 15 km, (c) L = 20 km

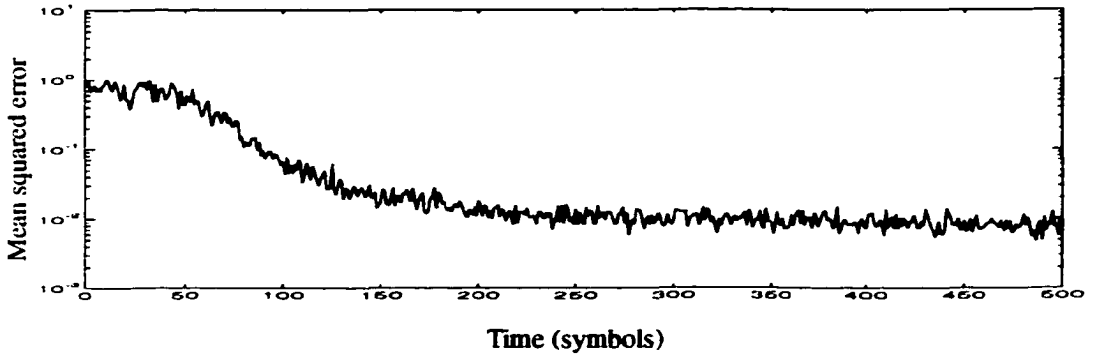

(a)

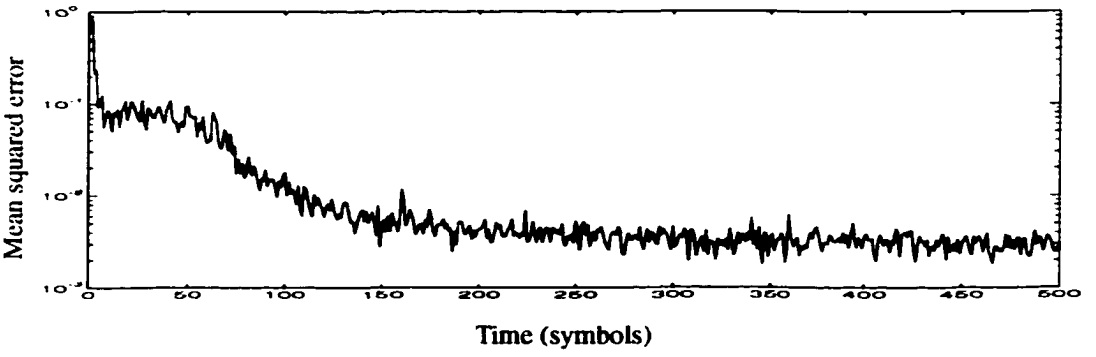

(b)

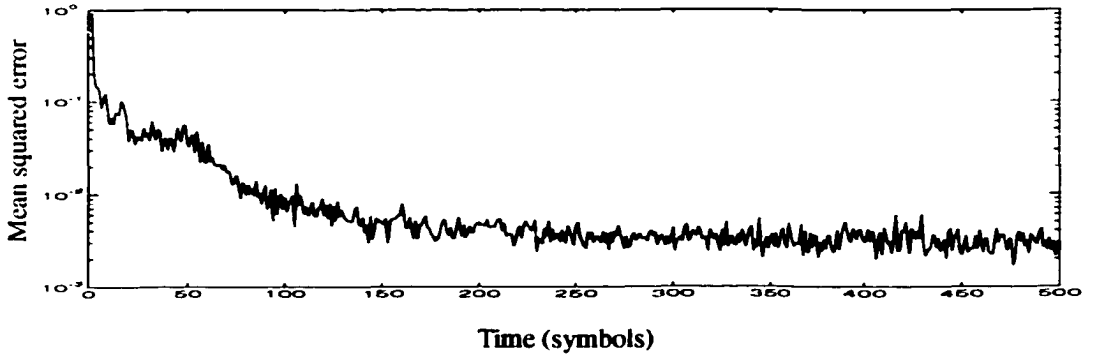

(c)

Figure 5.9: Mean squared errors (square-root RLS, $\omega = 0.99$)

(a) L = 10 km, (b) L = 15 km, (c) L = 20 km

complex to compute (see Table 5.2).

The phase scatter diagrams before and after equalization when 8-PSK system is employed are shown in Figure 5.10. An LMS algorithm was used for the equalizer coefficient update. We see that no distinct phase constellations are present in any case when an equalizer is not employed. This indicates that for all cases, even in the absence of other sources of noise, error-free transmission is impossible without an equalizer. The scatter plots after equalization show that the ISI caused by multipath transmission is dramatically reduced. Since an 8-PSK system allows transmission of 3 bits per symbol, simulation results indicate that, neglecting ambient noise, error-free data transmission at a data rate of 12 kbit/s might be possible over a distance of 20 km if an equalizer is employed.

Figure 5.11 shows the effect of step size μ on equalizer performance. It shows that larger step-size μ result in more rapid convergence, but also produces larger fluctuations in the equalizer coefficients during steady state operation.

Figure 5.12 shows the performance comparison between a LMS and a FOLMS algorithms. A FOLMS algorithm shows the improved convergence while achieving the same value of steady state MSE.

Figure 5.13 shows the variation of step size with a FOLMS algorithm as a function of time. In the beginning, large step size enables an equalizer to converge at a fast rate. As a squared error becomes smaller, the step size of an equalizer becomes smaller which is needed for a small steady state MSE.

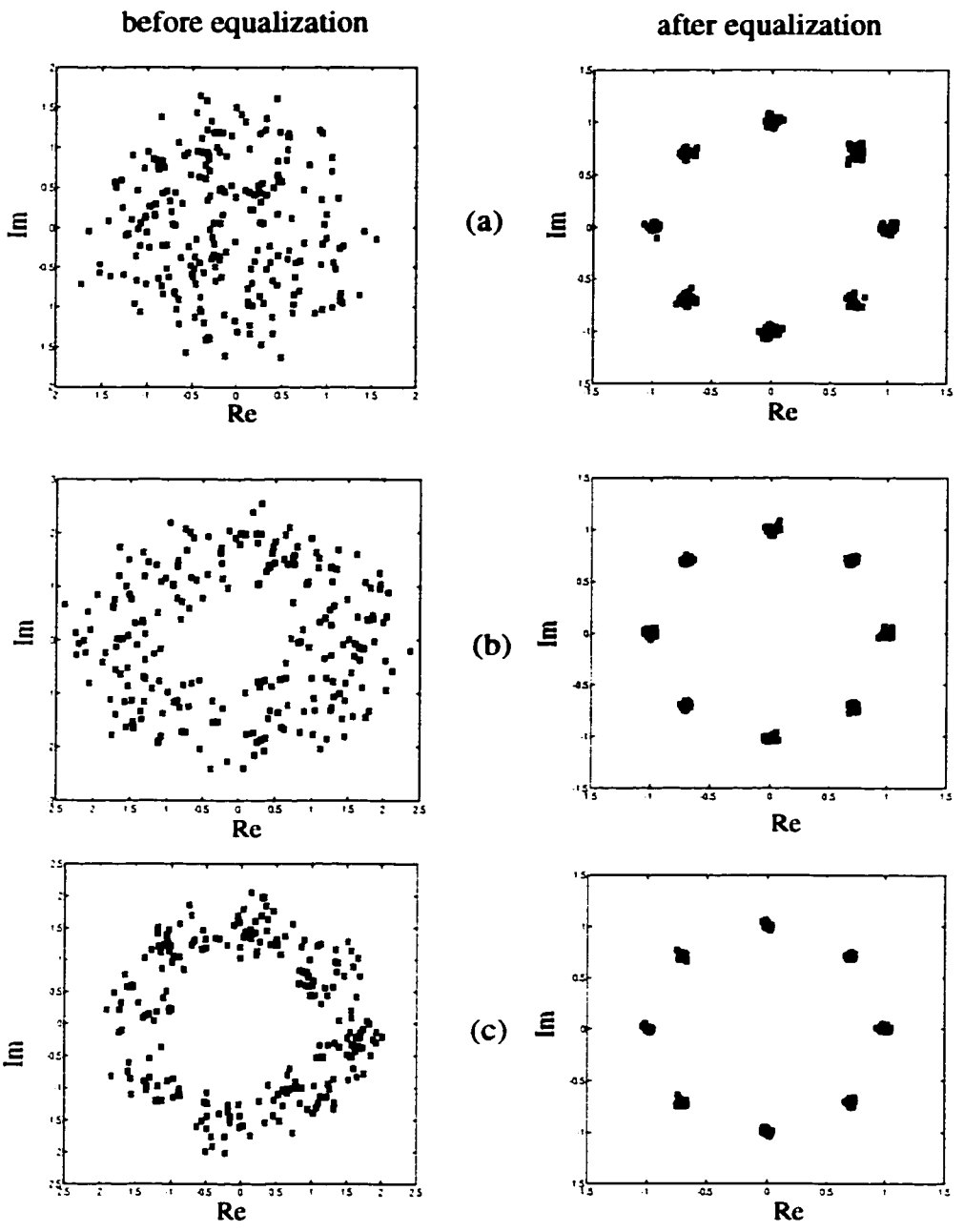

Figure 5.10: Scatter diagrams before/after equalization for 8-PSK transmission

(a) L = 10 km, (b) L = 15 km, (c) L = 20 km.

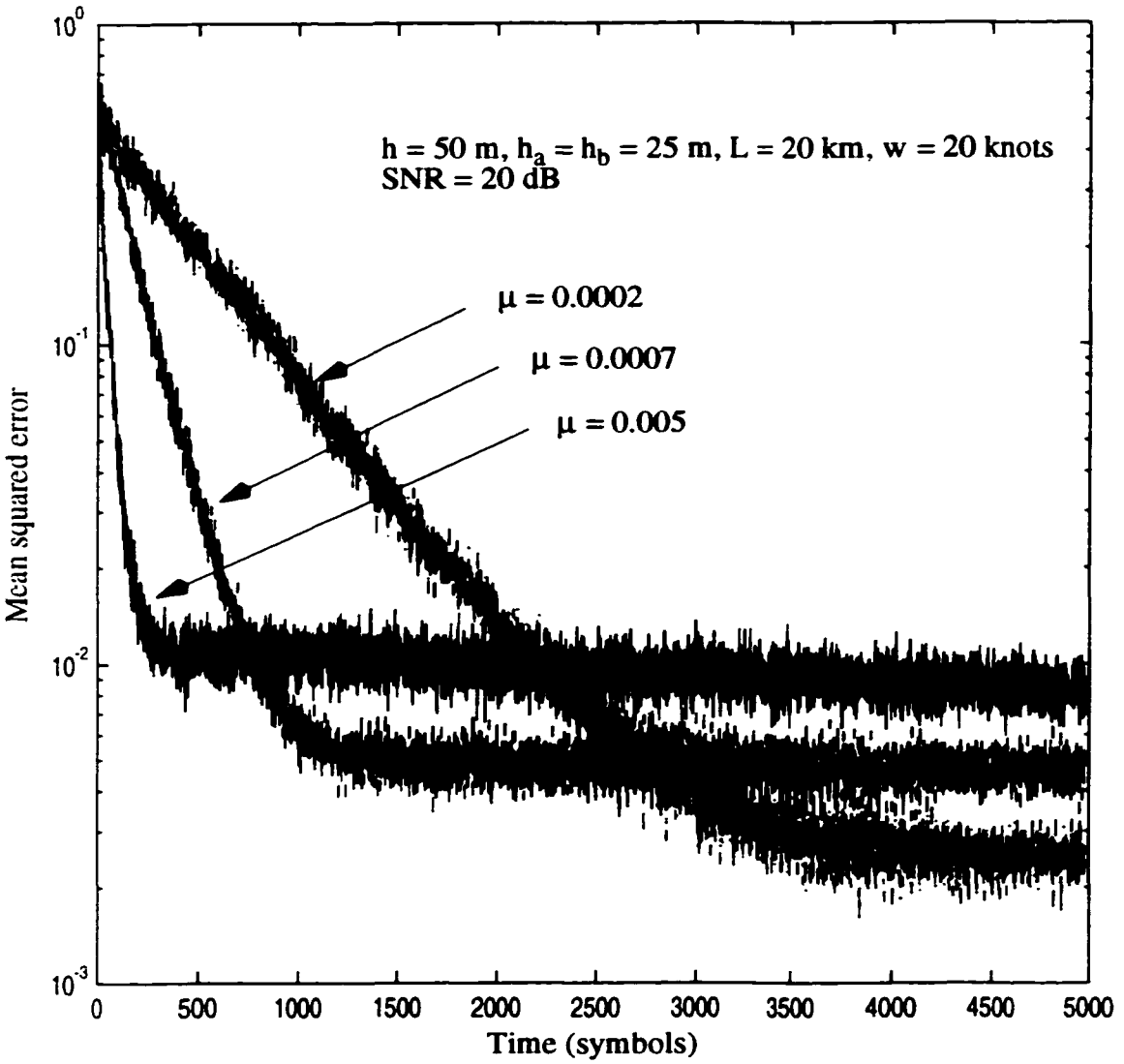

Figure 5.11: Effect of step size(μ) with LMS algorithm

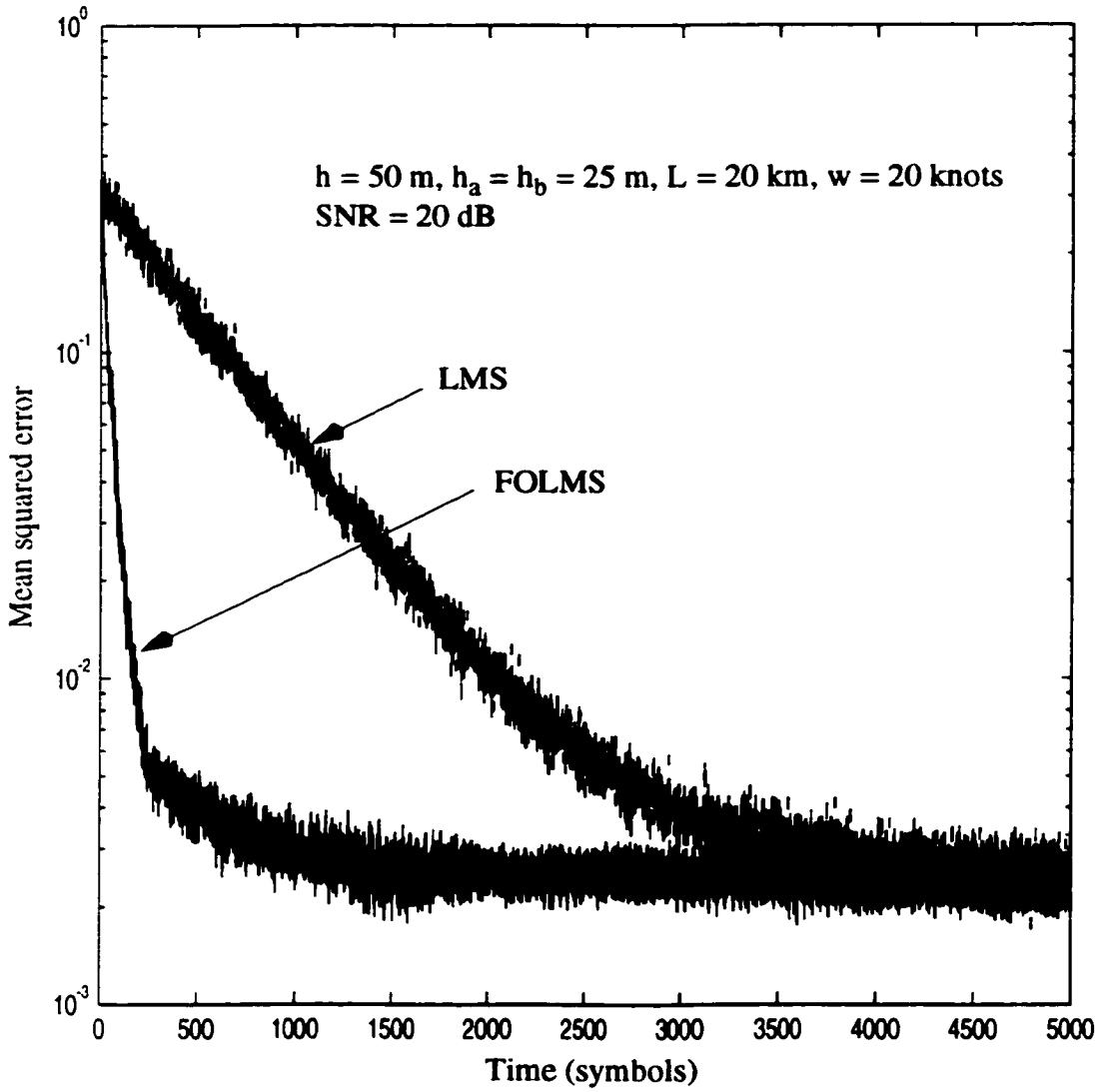

Figure 5.12: Comparison of convergence characteristic

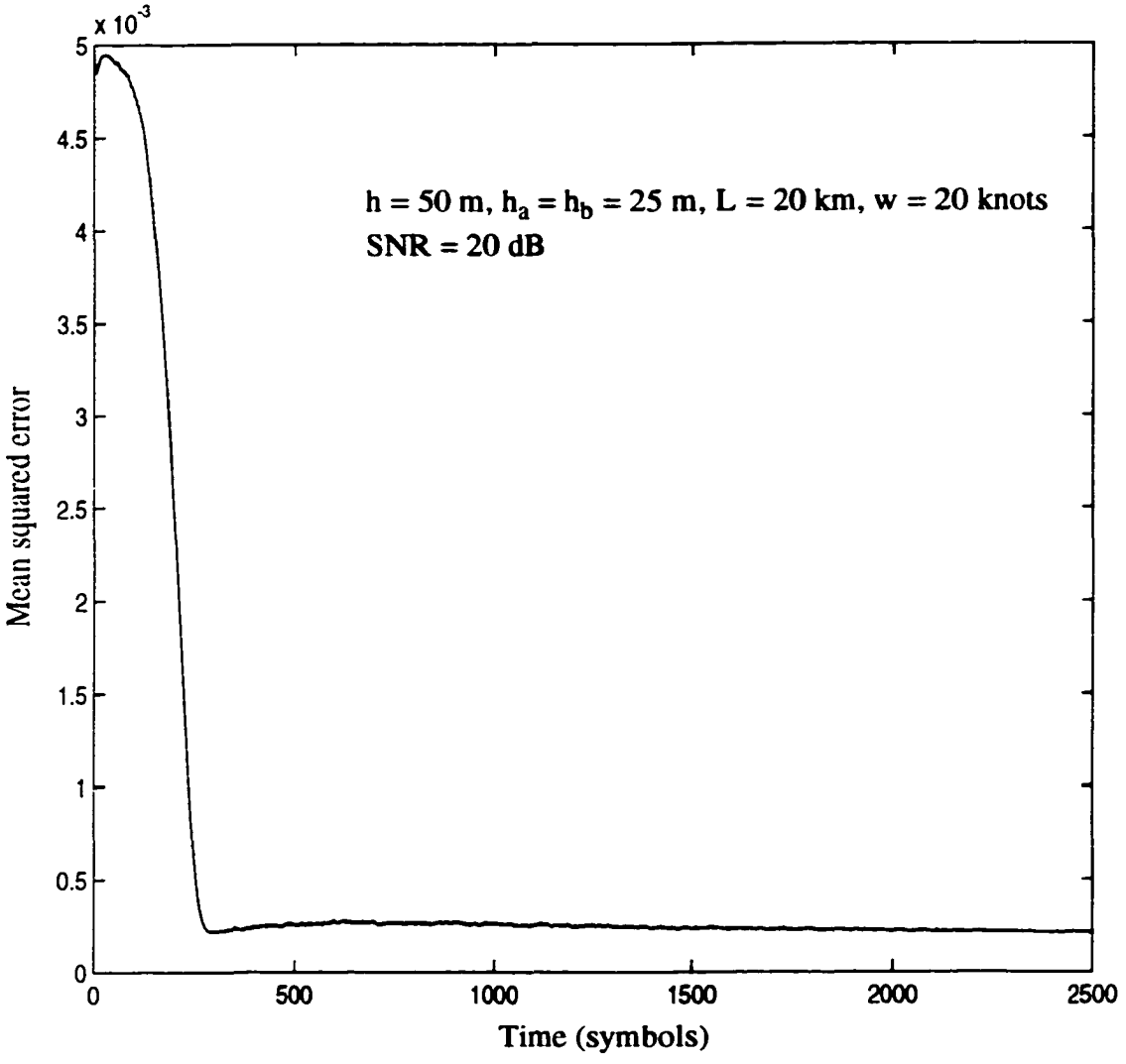

Figure 5.13: Variation of step size(μ) with FOLMS algorithm

For a large SNR, ISI is a limiting factor in shallow water transmission. However, for small SNR, both ISI and ambient noise must be considered. We will investigate the effect of ambient noise on transmission performance assuming that the ambient noise is Gaussian distributed. Channel and system parameters described in Table 5.3 are used for analysis.

Figure 5.14 shows variations of the bit error rate (BER) with time for different SNR values when a DFE with a LMS algorithm is utilized. These plots provide information about the time needed for an equalizer to achieve a certain error rate for a given channel condition. For instance, to achieve BER better than 10^{-3} at SNR = 10 dB, the time duration needed is1500 symbols.

Figure 5.15 shows BER at the steady state (after an equalizer has converged) vs. SNR. For instance, we can see that if an application requires a BER better than 10^{-3}, a channel should have SNR larger than 9.5 dB.

Figure 5.16 compares convergence characteristics of LMS and FOLMS algorithms. For the case considered, FOLMS requires a time duration of about 500 symbols to achieve a bit error rate of 10^{-3}, while LMS needs a time of approximately 1500 symbols. The result indicates that a FOLMS algorithm has three times faster convergence speed compared with a LMS algorithm for this case.

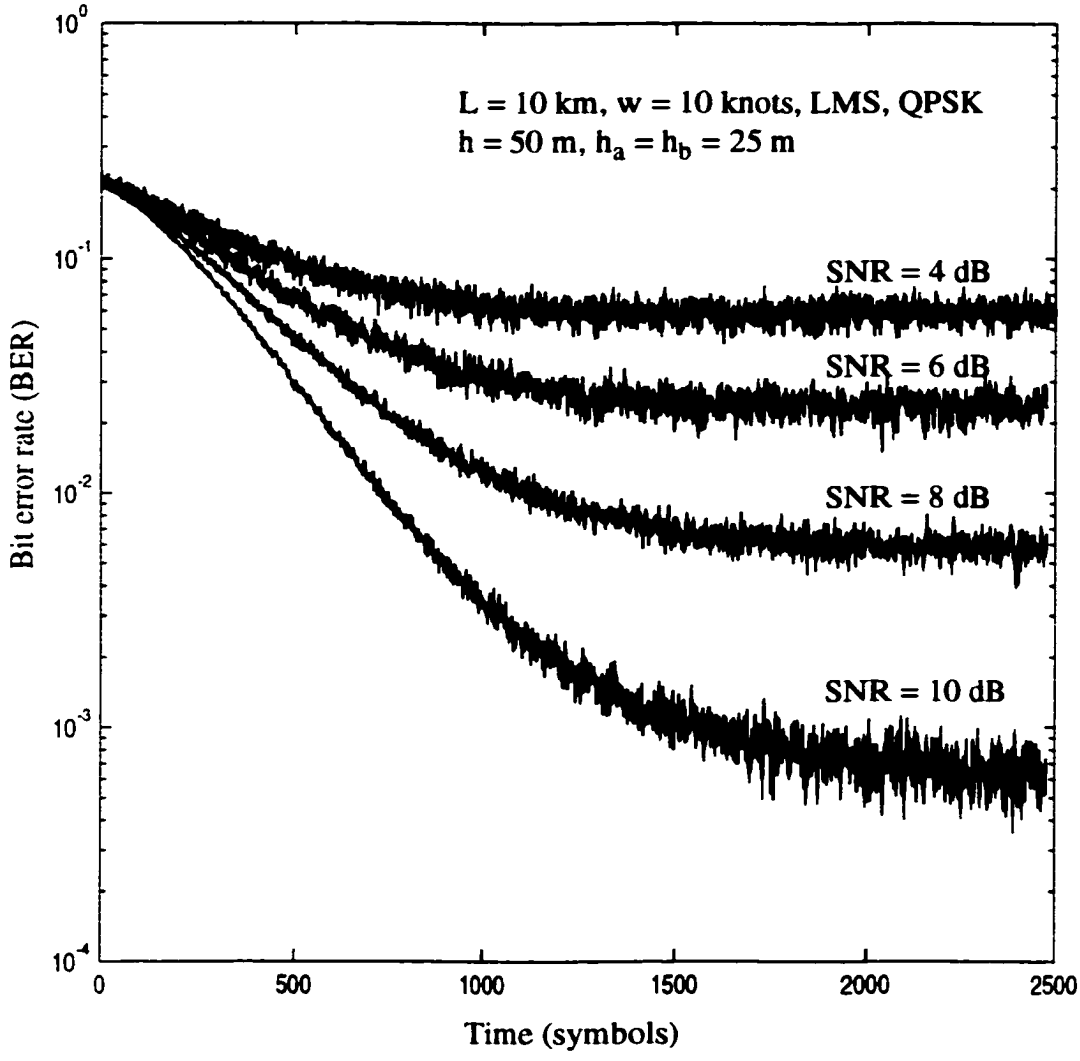

Figure 5.14: Variation of bit error rate with time

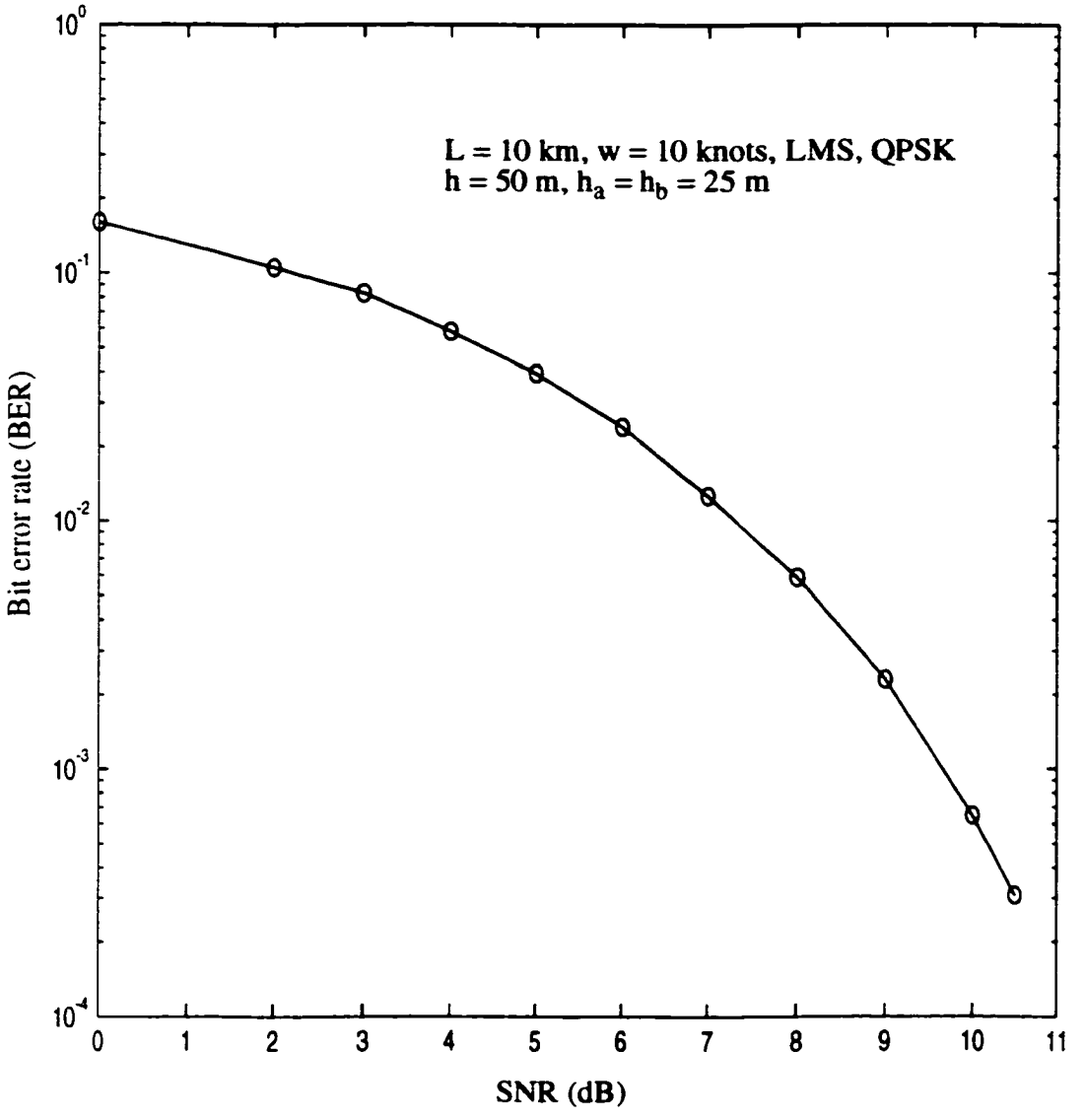

Figure 5.15: Bit error rate vs. SNR

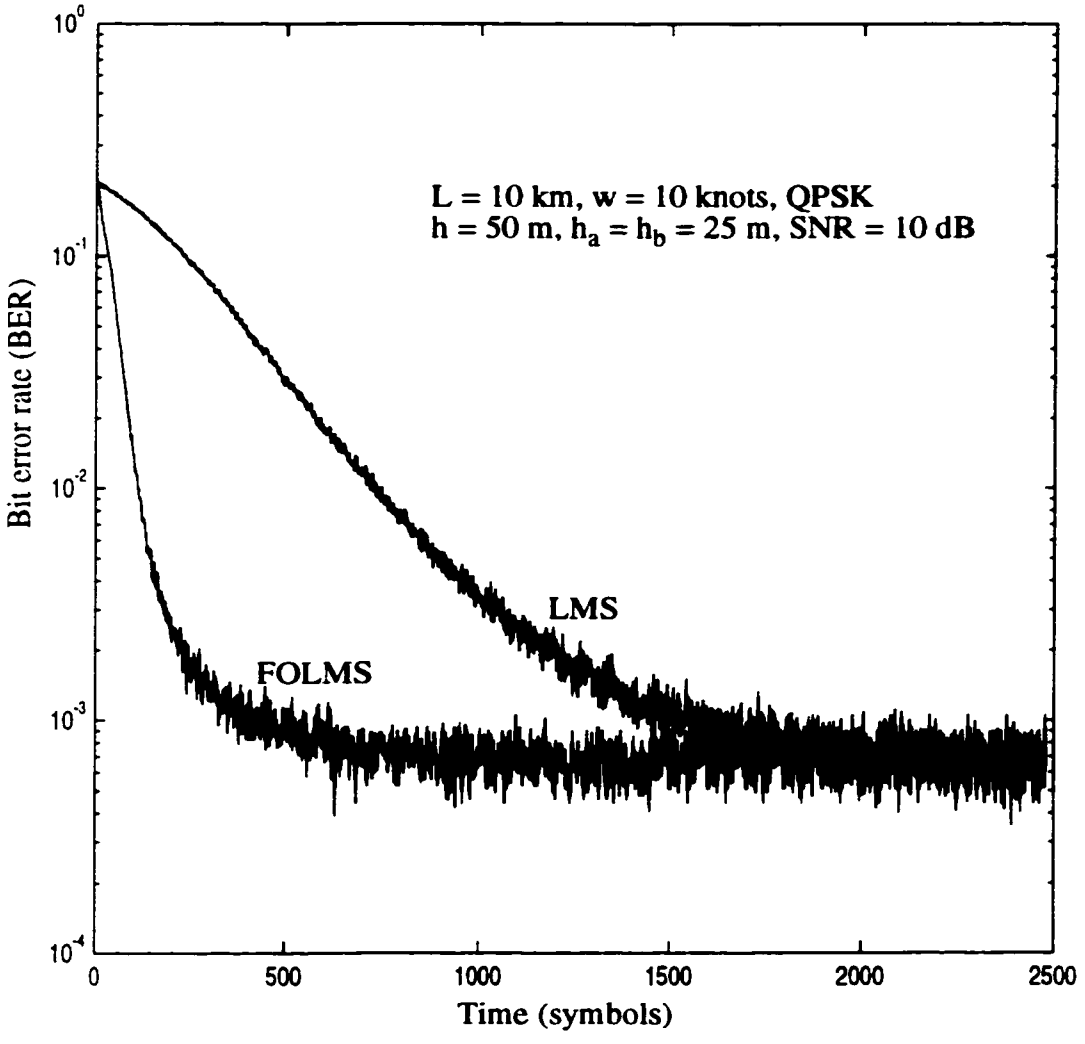

Figure 5.16: Comparison of convergence characteristics between FOLMS and LMS algorithms

5.4 Summary

In this chapter, an adaptive equalizer to cope with intersymbol interference was studied. To demonstrate the effectiveness of equalization, we chose a channel condition which has severe intersymbol interference. Simulation results for a chosen channel show that adaptive equalization for digital acoustic communication in a long range shallow water channel is feasible. Data rates in excess of 12 kbits/s are possible over a 20 km distance. Here, we assume that the channel is time invariant and the synchronization is perfect.

Adaptation algorithms, LMS, FOLMS and square-root RLS were studied. While an LMS algorithm has the advantage of a smaller computational load compared with square-root RLS, it has slower convergence characteristics. By adaptively adjusting the step size of an equalizer with FOLMS algorithm, we demonstrate by simulations that the faster convergence and a small steady state error can be obtained. In some cases where the channel impulse response is changing faster than an equalizer tracking ability, the performance of LMS in adaptive equalizers is unacceptable. Consideration of channel variation and the study of a corresponding technique is the subject of the next chapter.

Chapter 6

Anti-multipath Technique for Time-varying Underwater Channel

6.1 Introduction

In this chapter, the time variation within an underwater acoustic channel is considered. The time variation of a channel is caused by changes of the sea state and other factors. In addition, relative motion between the transmitter and the receiver introduces Doppler phase shifts.

Both the time varying multipath and Doppler shift effects can be overcome by means of jointly optimized adaptive equalization and synchronization. More specifically, a receiver structure which employs decision-feedback equalizer (DFE) combined with a digital phase-locked loop (DPLL) has been shown to be effective [38, 77]. While adaptive equalization is effective in compensating for the distortions introduced by multipath propagation, a DPLL provides a solution to the problem of acquiring a carrier reference needed for coherent demodulation.

When the sea state is changing due to changes in wind speed, the extent of the signal delay spread varies greatly. This large variation of signal delay spread translates into inefficient operation of an equalizer if the number of equalizer taps is fixed. In oth-

er words, if an equalizer is designed with a large number of taps to cope with the worst case of signal delay spread, the equalizer will perform more computations than is necessary and consume more power with redundant taps whenever the extent of a signal delay spread is reduced as the channel conditions become favorable.

In this study, a novel equalizer structure with an adaptive number of taps is proposed. The structure will adjust the number of equalizer taps adaptively depending on the sea state. A smaller number of taps at favorable channel conditions results in less computation in updating coefficients. This allows for less power consumption, desirable for prolonged battery life of a remotely operated system [35]. It also potentially enables a faster transmission rate or larger number of phases for N-ary PSK modulated signals. The performance of the proposed structure in a time-varying underwater acoustic channel is investigated by computer simulations in which the channel model described in Chapter 3 was used.

In Section 6.2, the effects of the variation of wind speed and directionality of the receiver on the received acoustic signal are investigated. In Section 6.3, the structure of the DFE/synchronizer is described and the optimization algorithm for equalizer and synchronizer is explained. The method of an adaptive adjustment of the number of equalizer taps is described in Section 6.3.3 while simulation results for the proposed structure are presented in Section 6.4.

6.2 The effect of variation of wind speed

In this section, the effect of time variation of wind speed on the system impulse response is investigated. Table 6.1 shows parameters of the channel and system used for this analysis. The system with transmitter and receiver filter as described in Section 2.3 is used. For computation of the received signal, the method described in Section 3.2 is utilized. In order to limit the number of terms used in computations, the truncation method described in Section 3.2 is applied. To investigate the effect of a di-

rectional receiver, a simplified beam pattern as described in Section 3.2 is postulated.

Table 6.1 Channel and system parameters

range	10 km
ocean depth	50 m
transmitter depth	25 m
receiver depth	25 m
carrier frequency	10 kHz
system bandwidth	2 kHz
transmission rate	4 kbaud

Figure 6.1 shows the received signal power (envelope) at three different wind speeds. The signal delay spread at the wind speed of $w = 5$ knots may reach a duration of 500 symbols while the signal delay spread decreases to a duration of less than 25 symbols as the wind speed increases beyond 10 knots. The shorter signal delay spread at higher wind speeds is due to the increased signal attenuation at the water surface. This indicates that the extent of variation of signal delay spread can be as large as 20 times as the wind speed varies between 5 and 10 knots. Figure 6.2 shows an enlarged view of Figure 6.1 with a same time (x-axis) scale to compare shapes of signal envelopes at the same time instant.

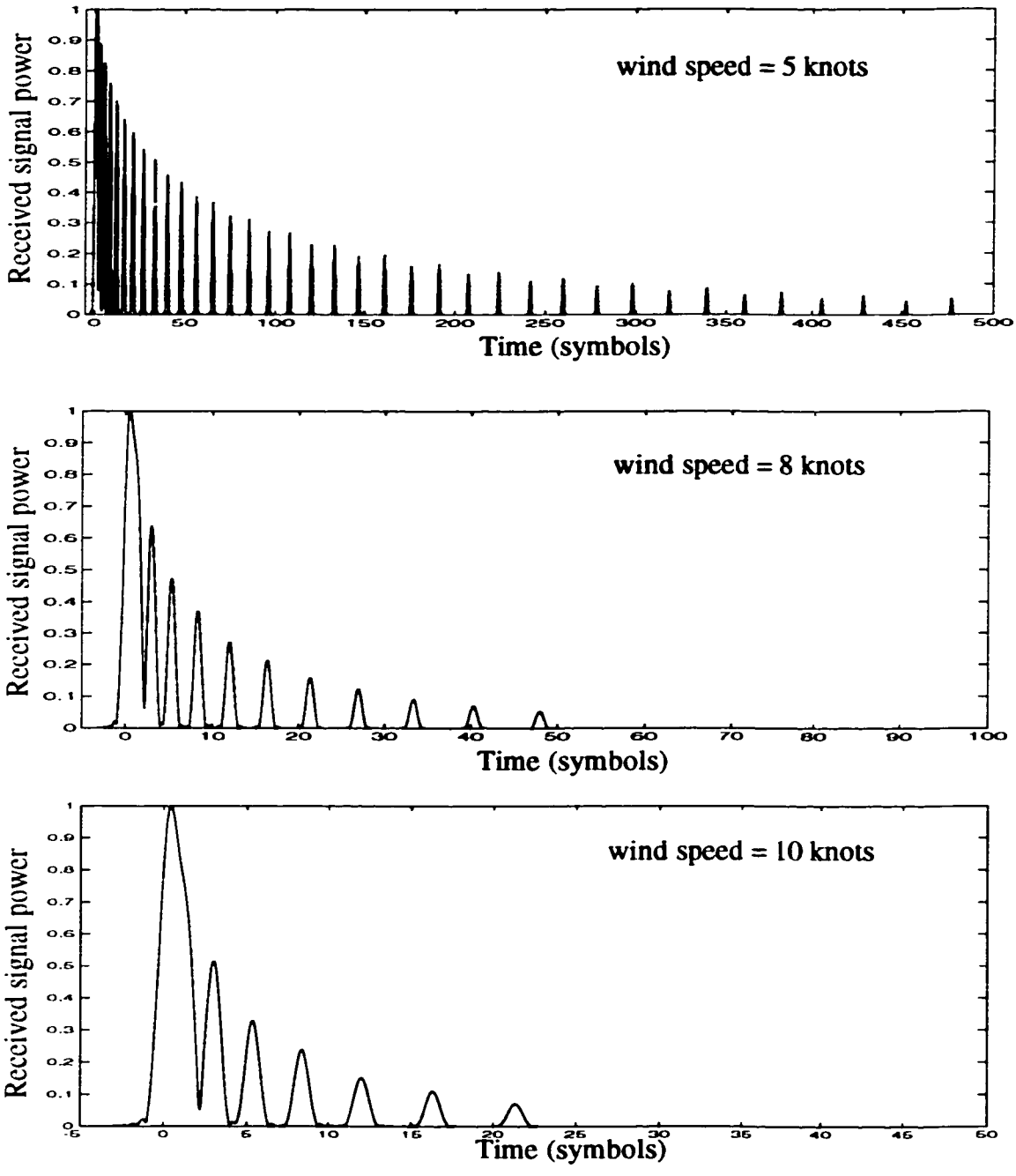

Figure 6.1: Received signal power at different wind speeds

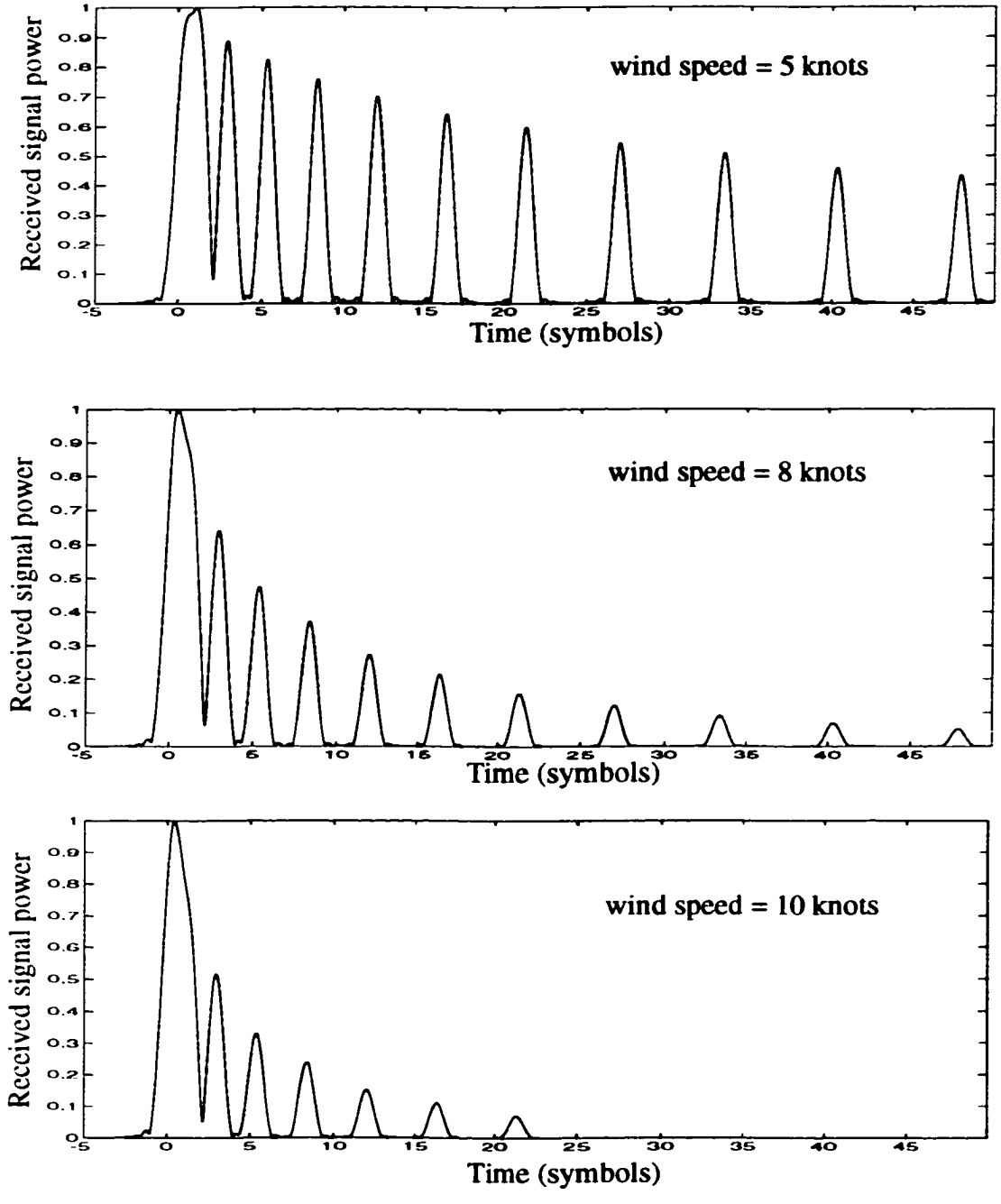

Figure 6.2: Enlarged view of Figure 6.1 for comparison

Let us investigate the effectiveness of utilization of a directional receiver as described in Section 3.2. We assume that signals arriving outside of the main lobe are subject to equal 20 dB suppression. Figure 6.3 shows the received signal envelope with different beamwidths when a directional receiver is employed. At wind speed $w = 5$ knots, the duration of received signal is effectively reduced to less than 130 symbols with beamwidth of 10°, and further to 100 symbols with a beamwidth of 5°.

Figure 6.4 and Figure 6.5 show the received signal power at different wind speeds with beamwidth of 10° and 5°, respectively. By employing a directional receiver with a beamwidth of 10°, the signal delay spread varies between 130 and 23 symbols (1:5.65 times) when wind speed changes from 5 knots to 10 knots. When the beamwidth is further reduced to 5°, the signal duration is reduced to a 23 to 80 symbol range(1:3.48) times) given the same channel conditions.

To summarize the above results, even though a directional receiver can reduce the extent of signal delay spread, a change of wind speed causes a large variation in the signal delay spread with both a non-directional receiver and directional receiver. This fact suggests that a conventional equalizer with constant (fixed) number of taps will operate inefficiently in performing complicated computations with a large number of redundant taps at favorable channel conditions. To improve the efficiency of an equalizer, a method of adaptively adjusting the number of taps is proposed in the next section.

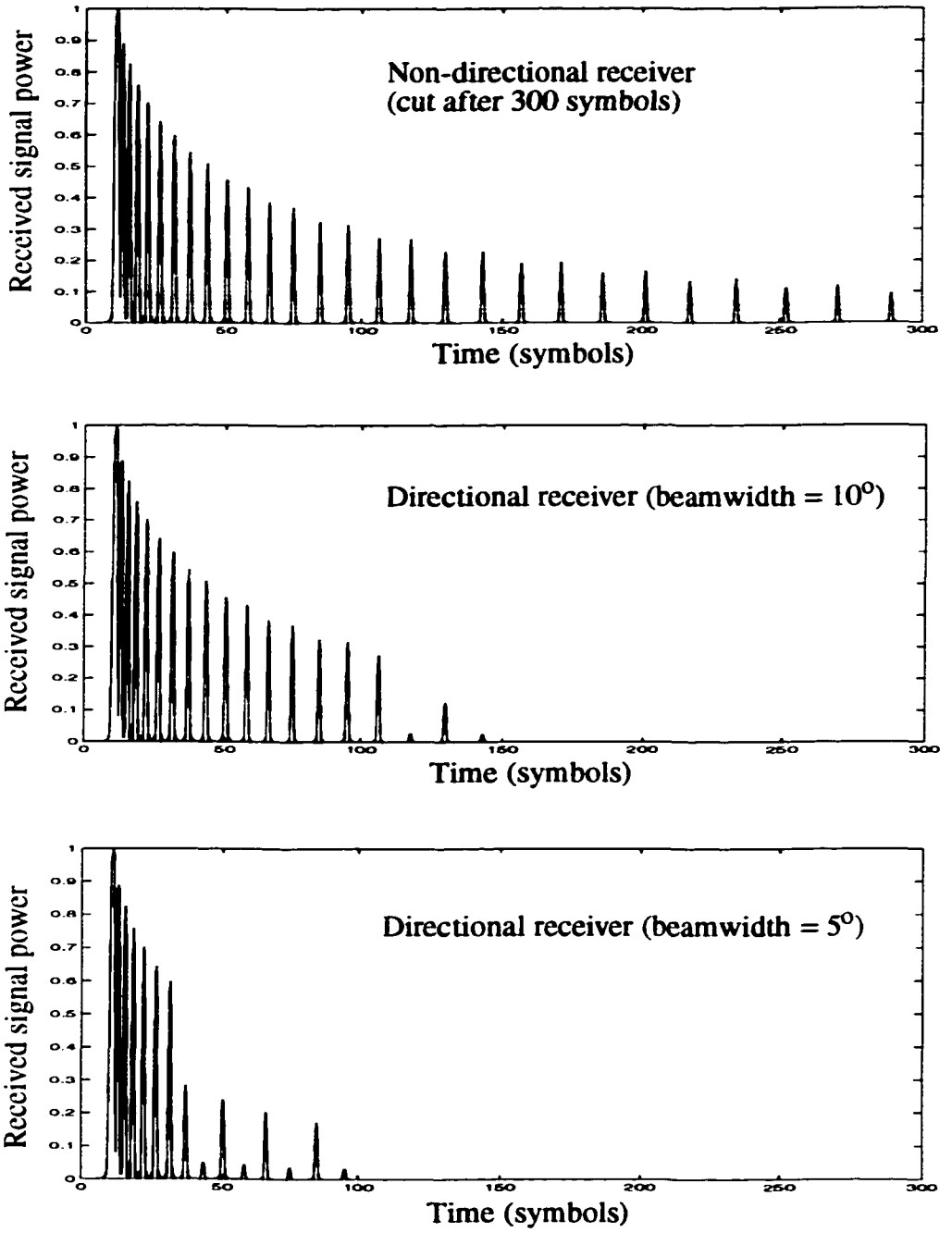

Figure 6.3: Received signal envelope when a directional receiver is employed (wind speed = 5 knots)

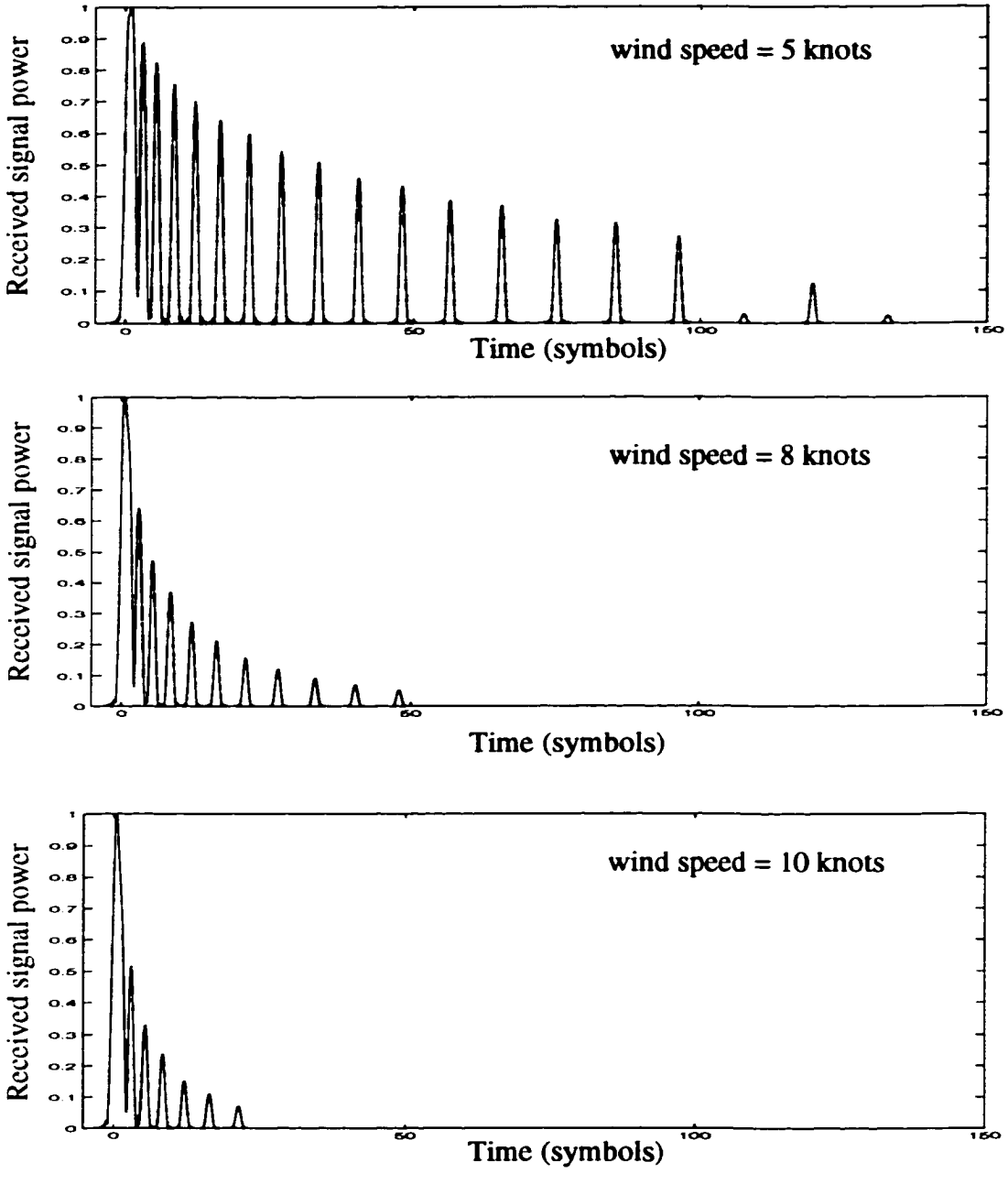

Figure 6.4: Received signal envelope at different wind speed when a directional receiver with beamwidth = 10° is employed

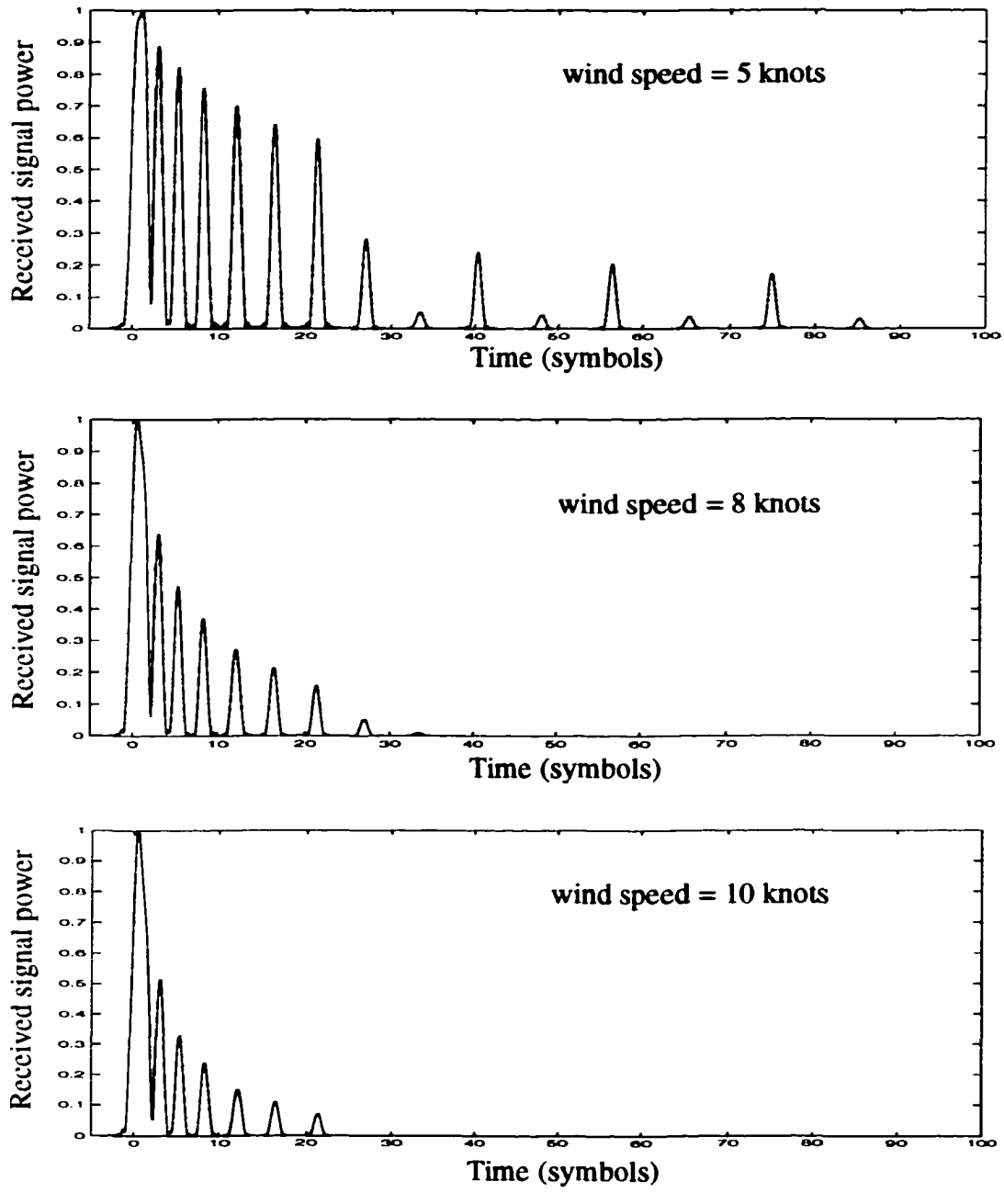

Figure 6.5: Received signal envelope at different wind speeds when a directional receiver with beamwidth = 5° is employed

6.3 Structure of the DFE/synchronizer

6.3.1 Equalizer optimization algorithm

The structure of a receiver suitable for joint equalization and synchronization proposed by Falconer [38] and further studied for the underwater channel by Stojanovic *et al.* [77] has been generalized by the author to include a variable number of equalizer taps as shown in Figure 6.6. In Figure 6.6, the block with a variable number of equalizer taps is indicated by a shaded box.

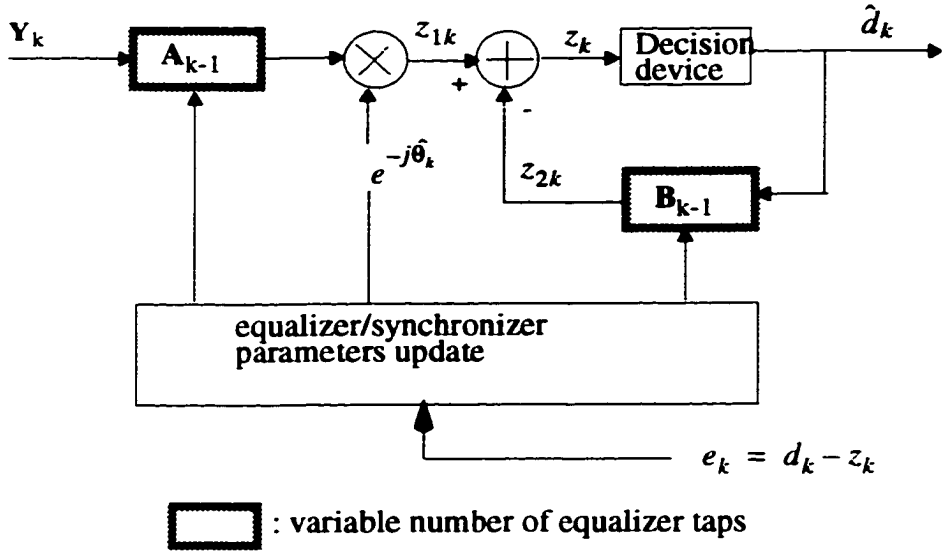

Figure 6.6: Structure of the DFE/synchronizer.

The algorithm for updating equalizer coefficients is the same as the coefficient update algorithm described in Chapter 5 for the time-invariant channel with the exception of the routine for phase correction. To include the phase correction for this structure, the coefficient update algorithm described in Chapter 5 requires a slight

modification. That is, Y_k must be replaced by $Y_k(n)e^{-j\hat{\theta}_k}$ where $\hat{\theta}_k$ denotes the estimated phase error.

Since the structure includes a module to track the phase shift, the algorithm must estimate the phase error for a synchronizer. This algorithm is described in the next section. The novel feature of this structure is that the number of equalizer taps ($\mathbf{A}_{k-1}$, $\mathbf{B}_{k-1}$) can be made variable depending on the sea-state. The algorithm to implement the proposed feature is described in Section 6.3.3.

6.3.2 Algorithm for adaptive carrier synchronization

The task of the carrier synchronization is to estimate the residual phase error due to frequency offsets between a local oscillator and Doppler shifts. An estimate can be made using the steepest descent (gradient) approach:

$$\hat{\theta}_k = \hat{\theta}_{k-1} - \frac{\mu_\theta}{2}\nabla_{\hat{\theta}}[MSE] \tag{6.1}$$

where μ_θ is an arbitrary constant and $\nabla_{\hat{\theta}}$ is a scalar gradient with respect to phase.

Denote the output of feedforward and feedback equalizer as z_{1k} and z_{2k}, respectively. The signal at the input of the decision device is denoted as $z_k = z_{1k} - z_{2k}$. Those signals are indicated in Figure 6.6.

We can replace $\nabla_{\hat{\theta}}[MSE]$ by its estimate $\hat{\nabla}_{\hat{\theta}}[MSE]$ defined as

$$\hat{\nabla}_{\hat{\theta}}[MSE] \approx \hat{\nabla}_{\hat{\theta}}[|d_k - z_k|^2]. \tag{6.2}$$

After some manipulation, we obtain:

$$\hat{\nabla}_{\hat{\theta}}[MSE] = -2\mathrm{Im}\{z_{1k}[d_k + z_{2k}]^*\} \tag{6.3}$$

or

$$\hat{\nabla}_{\hat{\theta}}[MSE] = -2\mathrm{Im}\{z_{1k}[d_k - z_k]^*\}. \tag{6.4}$$

With Eq. (6.1) and Eq. (6.4), the update algorithm of a synchronizer becomes:

$$\hat{\theta}_k = \hat{\theta}_{k-1} + \mu_\theta \mathrm{Im}\{z_{1k}[d_k - z_k]^*\}. \tag{6.5}$$

This is the algorithm corresponding to a first order Costas loop [65]. In Eq. (6.5), the term $\Phi_k = \mathrm{Im}\{z_{1k}[d_k - z_k]^*\}$ expresses the phase error signal. In order to avoid the steady state error caused by an offset frequency, we should use the second or higher order phase locked loop. The second order loop can be obtained simply by filtering the error signal:

$$s_{\theta,k} = \mathrm{Filter}\{\Phi_k\} = G_{1,\theta} + G_{2,\theta}/[1 - z^{-1}], \tag{6.6}$$

where Filter{ } is a filtering operator, $G_{1,\theta k}$ and $G_{2,\theta k}$ are loop gains which determine the tracking characteristics of the loop. Combining Eq. (6.5) and Eq. (6.6), the second order PLL loop becomes

$$\begin{aligned} \hat{\theta}_k &= \hat{\theta}_{k-1} + s_{\theta,k} \\ \hat{\theta}_{k+1} &= \hat{\theta}_k + G_{1,\theta k} + \sum_{i=0}^{k} G_{2,\theta i}\Phi_i \ . \end{aligned} \tag{6.7}$$

6.3.3 Adaptive adjustment of number of equalizer taps

In this section, the method of adjusting the number of equalizer taps is described. Figure 6.7 shows the algorithm to adjust number of equalizer taps adaptively. Let us define "the performance penalty" as the difference in the squared errors between the output with a larger number of taps and the output with a reduced number of taps. The number of equalizer taps are decreased whenever two conditions are simultaneously met:

- the squared error at the output of an equalizer is below the predefined value; and
- the performance penalty is below a certain specified value.

The first condition guarantees the operation of the equalizer with a performance better than a certain minimum allowable level. The second condition controls the performance degradation due to a reduced number of taps as a result the number of taps will be varied, as we will see from results of computer simulations. This approach is possible because the values of equalizer taps which are longer than the system response have very small values. In other words, taps longer than system impulse responses have quite small effects on the computation of the equalizer output. This allows us to reduce the number of taps. When the number of taps becomes smaller than needed to cover the system impulse response, the performance penalty rapidly increases. This is because taps with significant contributions start to be truncated. To increase the safety of the proposed equalizer operation, we can limit the number of taps operating in some ranges to a certain maximum and minimum number of taps.

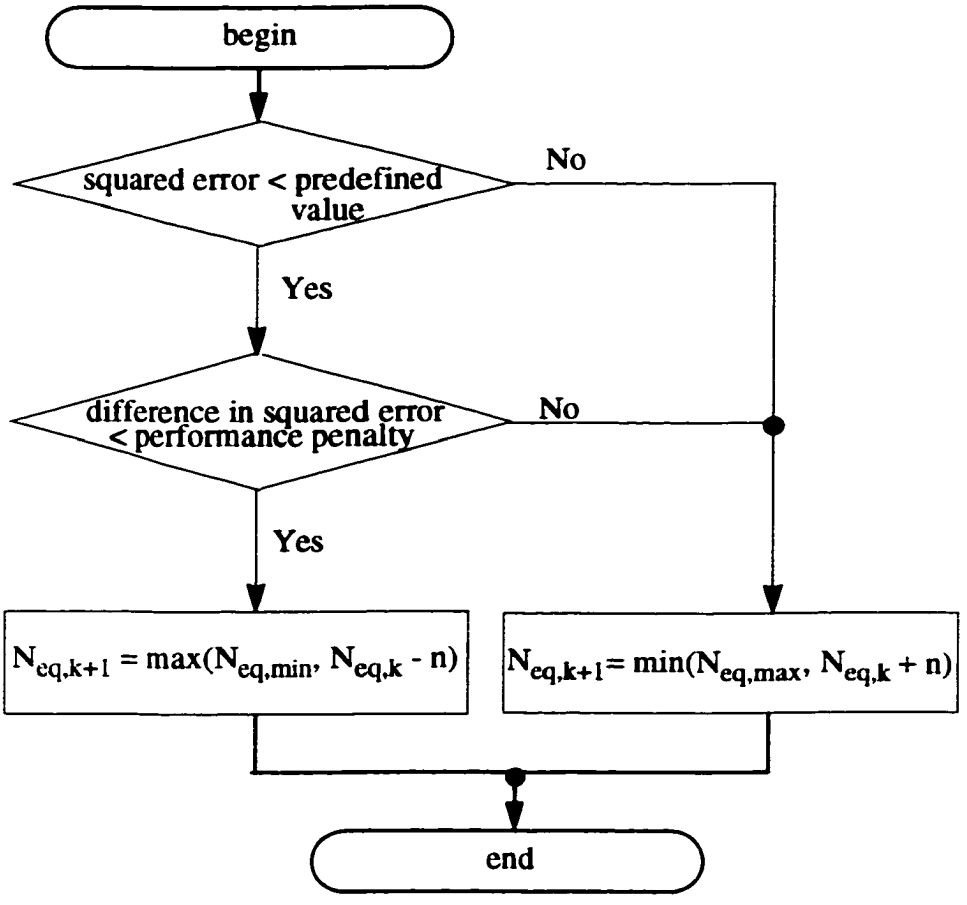

n; the number of taps of increase/decrease

$N_{eq,min}$, $N_{eq,max}$; minimum and maximum number of equalizer taps

Figure 6.7: The algorithm to adjust number of equalizer taps adaptively

6.4 Simulation Results

In this section, simulation results for a proposed structure using parameters of the channel and system as shown in Table 6.1 are presented. We assume a Doppler frequency shift $f_d = 3.33$ Hz.

Figure 6.8 shows the effect of equalizer output when the wind speed is abruptly changed at some time instant. It shows that the equalizer adjusts adaptively to the new environment. It also shows that a fast optimized least mean square (FOLMS) algorithm has better convergence characteristics than that of a least mean square (LMS) algorithm. Figure 6.9 shows the variation of step size μ with a FOLMS algorithm when wind speed is abruptly changed. The step size μ of the equalizer is adaptively changed from large values desirable for fast convergence in the beginning and transition time, to small values desirable for a better steady state performance as time passed.

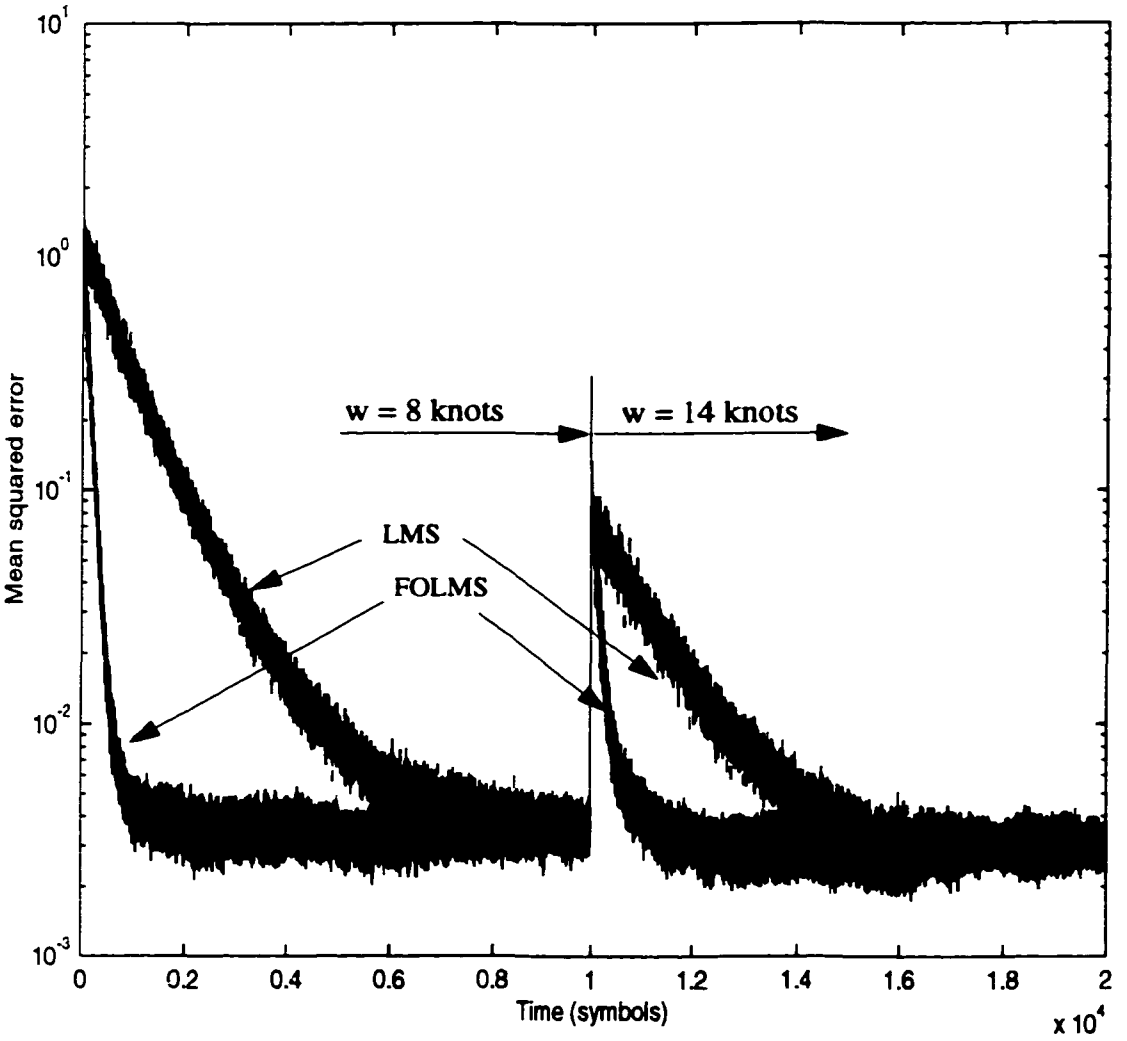

Figure 6.8: The effect of abrupt change of wind speed

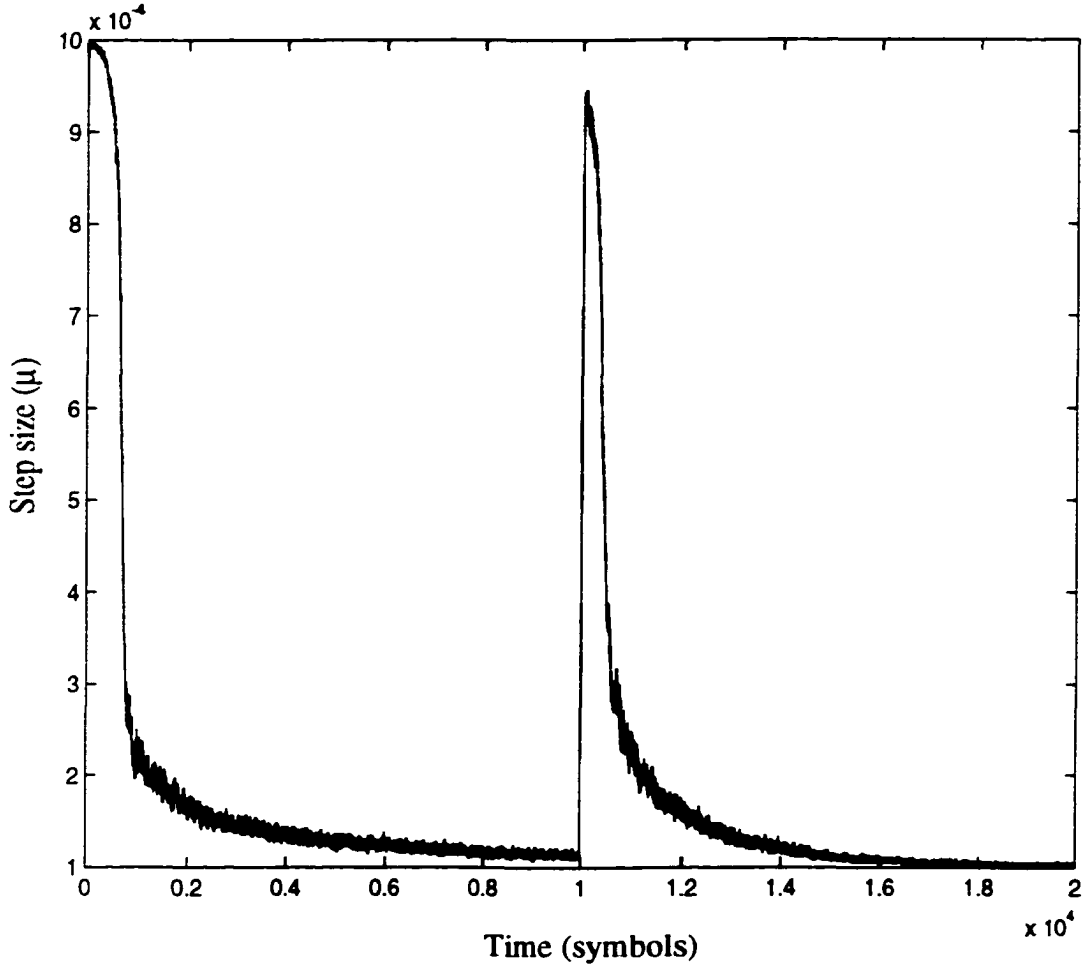

Figure 6.9: Variation of step size (μ) when wind speed is changed at time of 10000 symbols

Figure 6.10 shows the variation of number of equalizer taps when wind speed is changed. This result proves that the proposed method works effectively depending on the wind speed.

Figure 6.11 and Figure 6.12 show the effect of the number of equalizer taps on different values of the performance penalty. With a larger performance penalty, we can achieve an equalizer with a smaller number of taps at the expense of performance. As the performance penalty is changed from 1% to 5%, the number of equalizer taps is reduced from 82 to 38.

Figure 6.13 shows the bit error rate as a function of the performance penalty. The larger the performance penalty, the larger the bit error rate (the worse performance).

Figure 6.14 shows the number of equalizer taps as a function of wind speed when a directional receiver is used with the proposed structure. A directional receiver with the proposed structure is much more effective at low wind speeds. If we assume that wind speed varies between w =7 knots and w = 14 knots with equal probability over time, the saving in computational load up to 60% with a non-directional receiver and up to 30% with directional receiver can be obtained.

Figure 6.15 shows the number of equalizer taps as a function of iterations for different value of tap increase/decrease per iteration, n. With a larger n, a slightly improved convergence property results at the cost of larger number of equalizer taps after convergence. Also, simulation results on bit error rates after convergence indicated less than 1% difference with step size n between 1 and 3. These results suggest that n=1 would be the best choice for the proposed method.

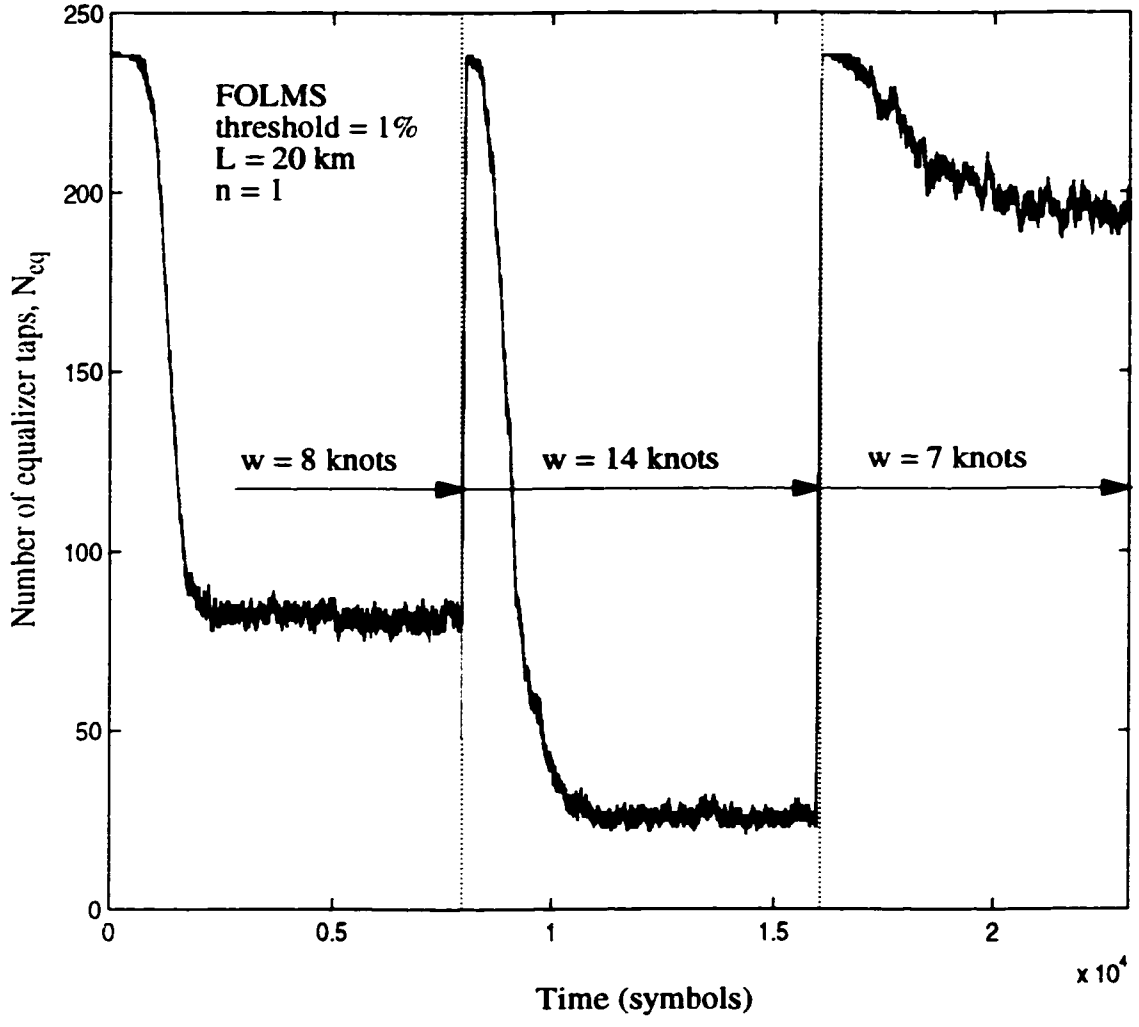

Figure 6.10: The variation of number of equalizer taps when wind speeds are changed

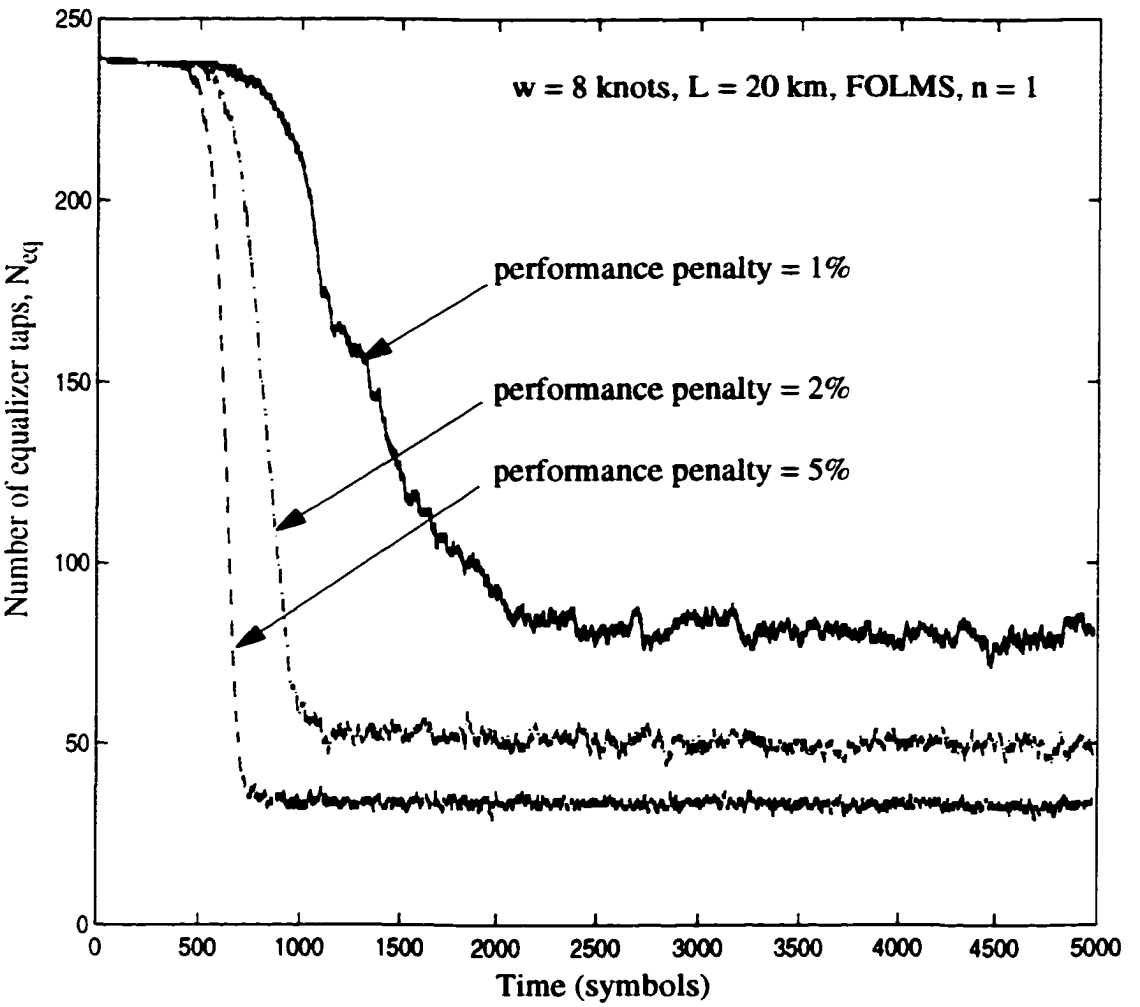

Figure 6.11: The effect of number of equalizer taps on different values of the performance penalty

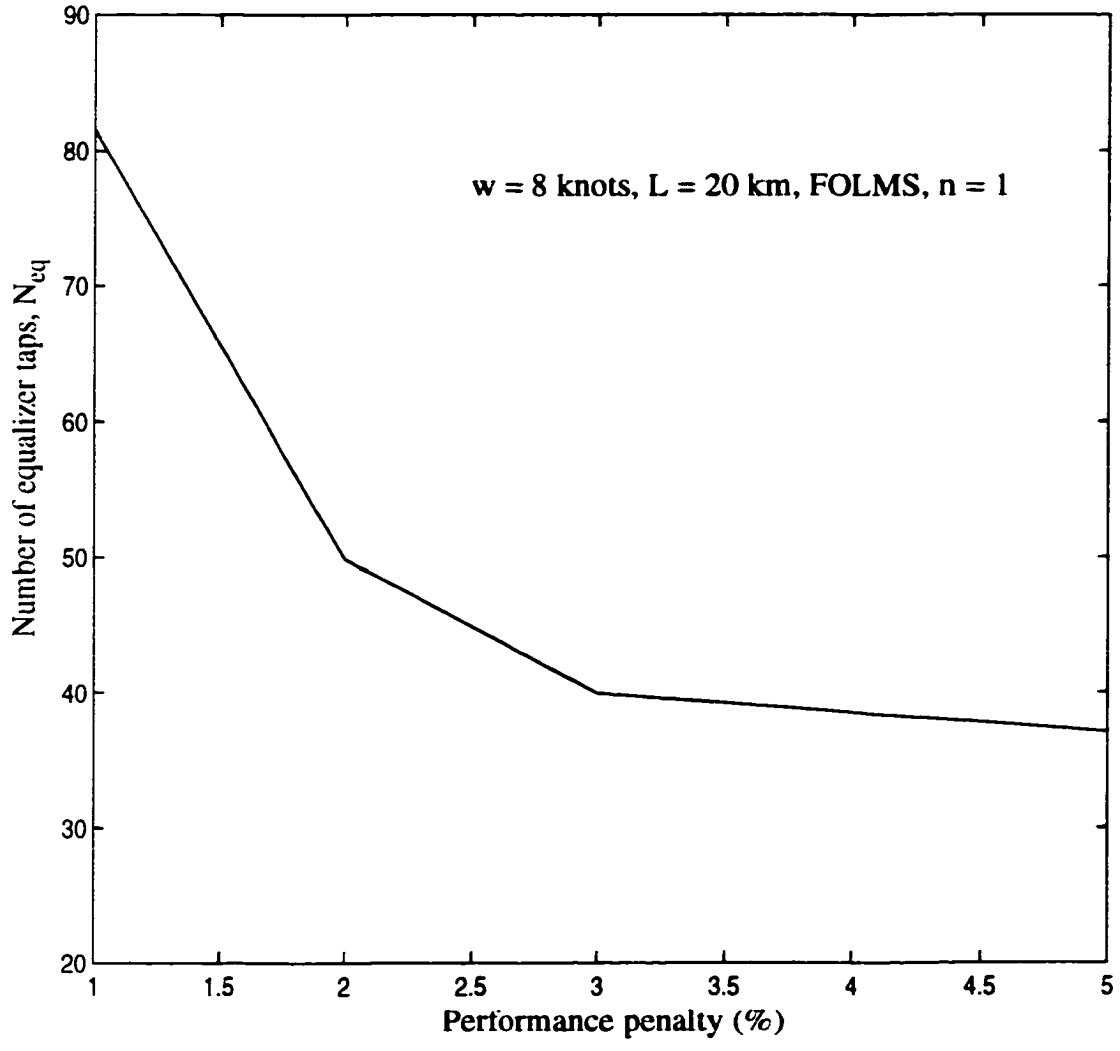

Figure 6.12: Number of equalizer taps vs. performance penalty

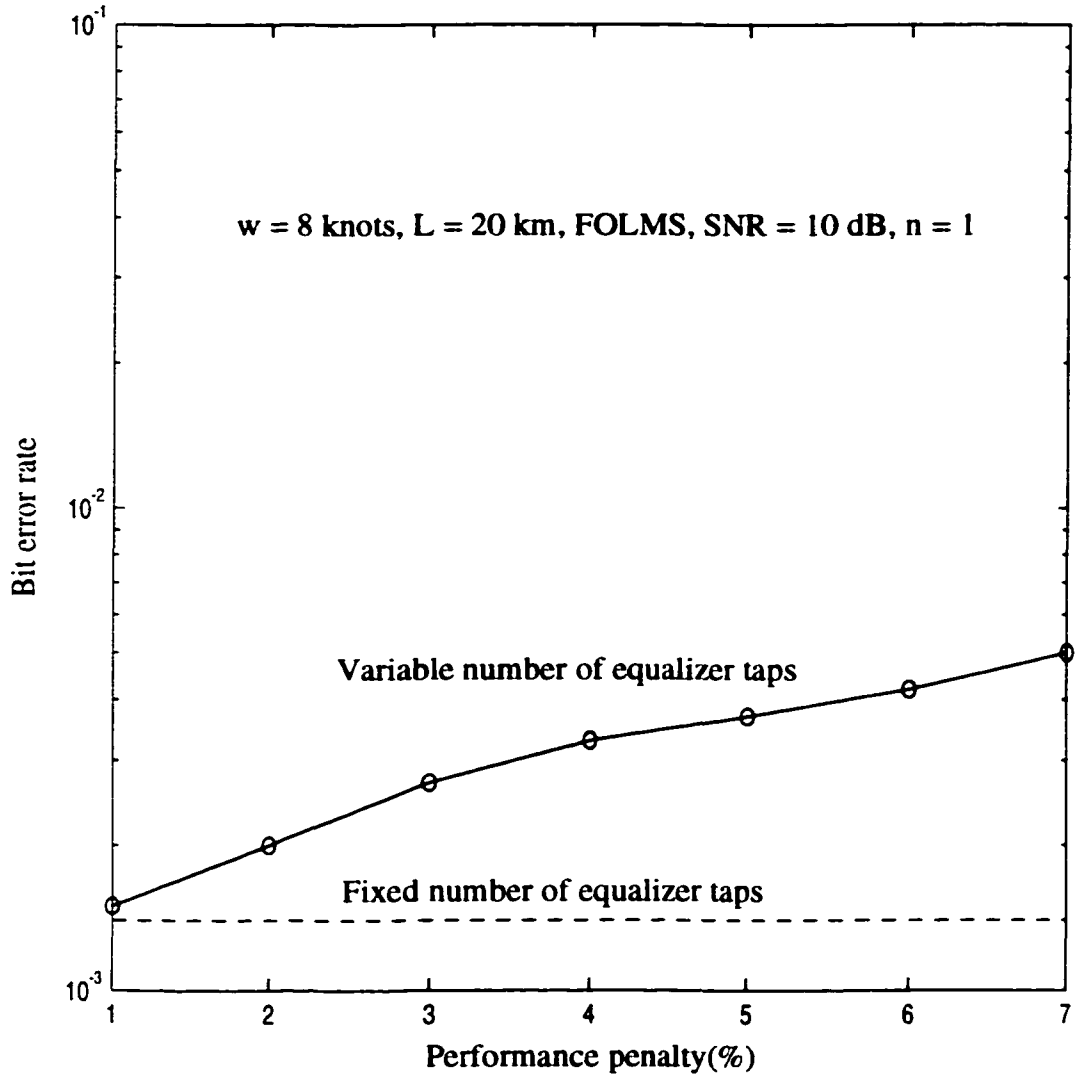

Figure 6.13: Bit error rate at steady state

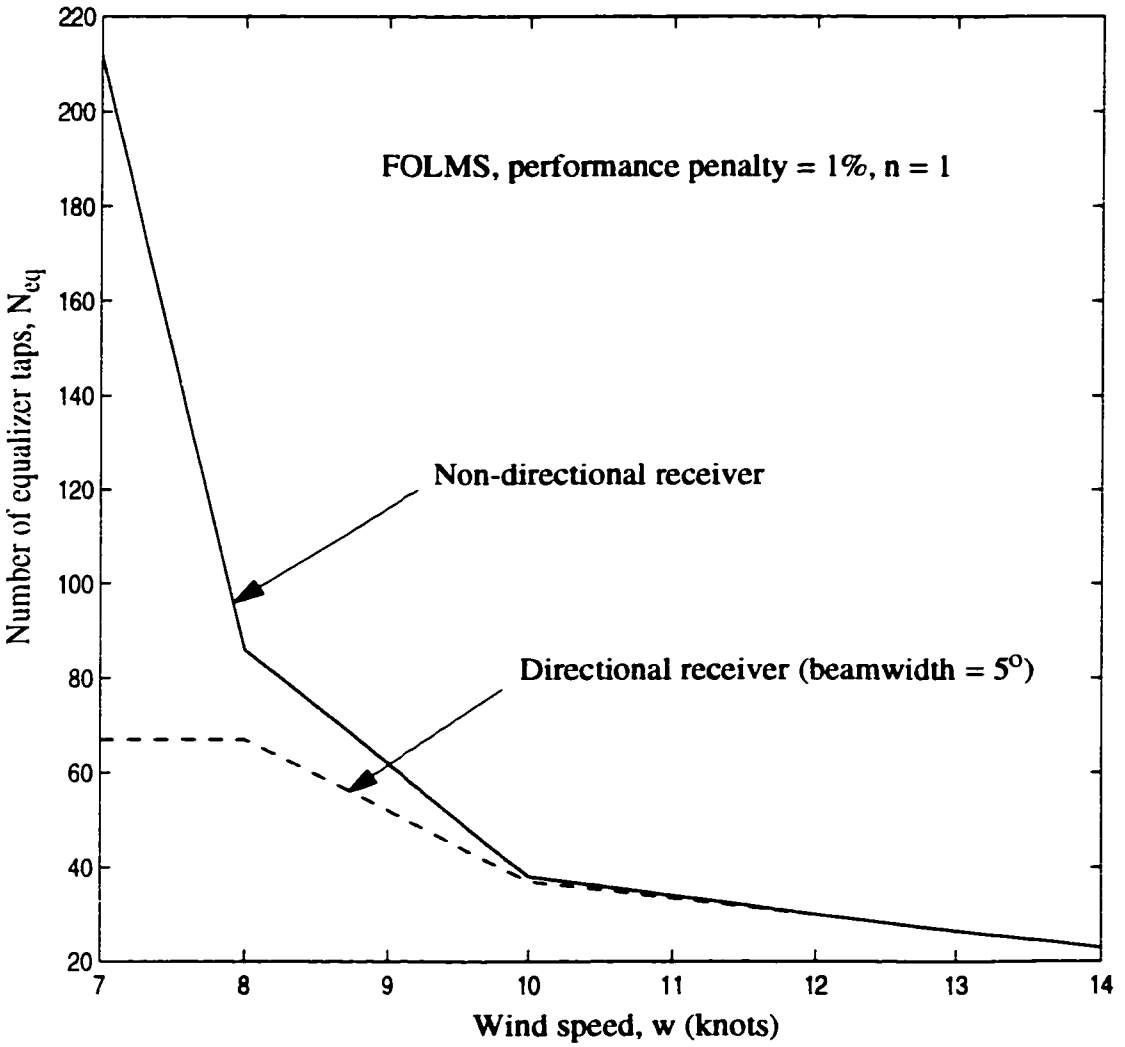

Figure 6.14: Number of equalizer taps vs. wind speed

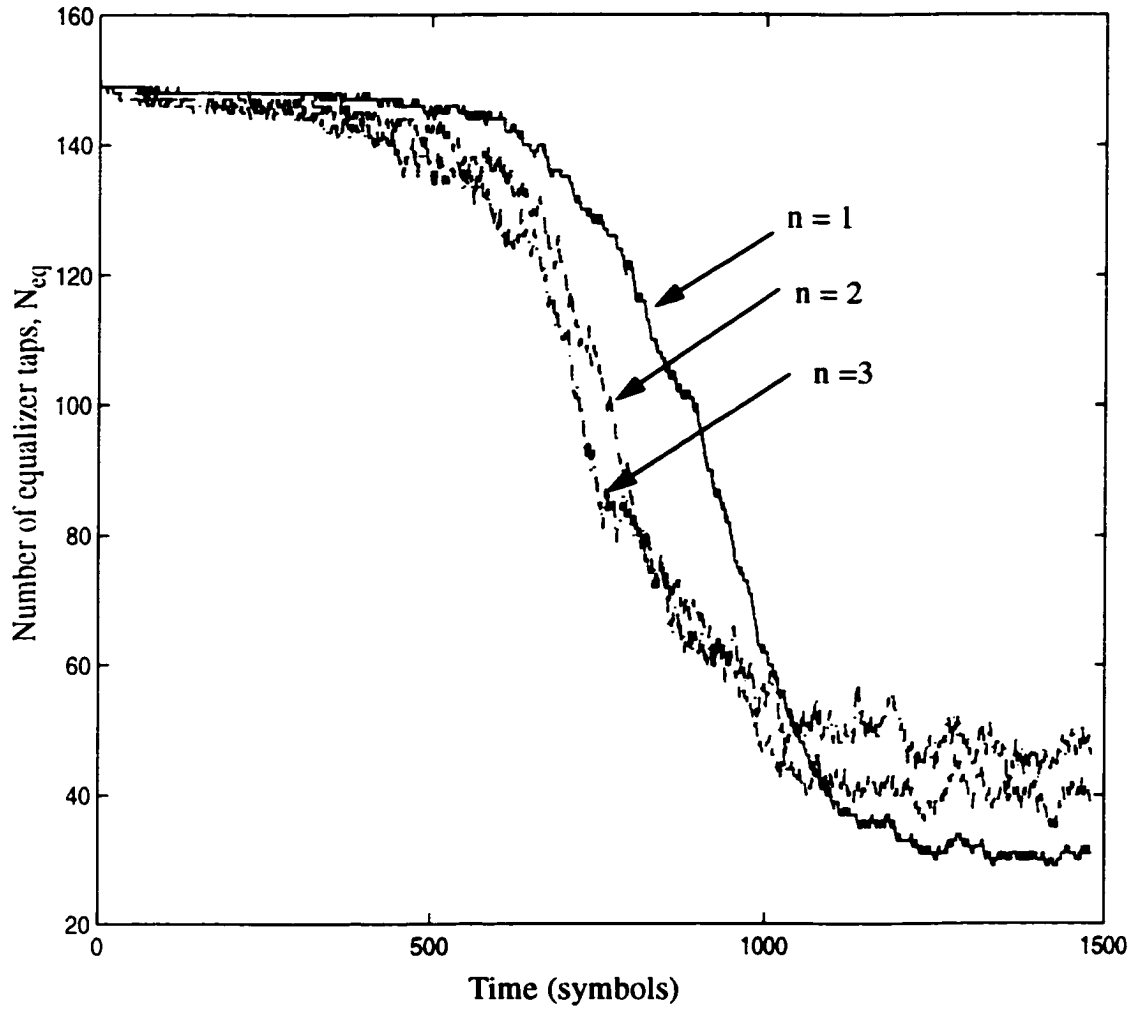

Figure 6.15: The effects of number of equalizer taps on size of increase/decrease

6.5 Summary

In this chapter, the time variation of underwater acoustic channels was considered. The effect of the time variation of wind speed on system impulse response was studied. The stronger the wind speed, the shorter the system impulse response.

A novel equalizer with an adaptive number of coefficient taps, depending on sea-state, was proposed and its performances were studied on a time-varying underwater acoustic channel. Adaptively adjusting to a smaller number of taps at high wind speeds resulted in less computation to update coefficients. As a result, less power consumption, a desirable outcome for a remotely operated system, can be obtained. It also potentially provides the ability to utilize a faster rate transmission rate or a larger number of phase N for N-ary phase shift keying (N-ary PSK) modulated signals.

Chapter 7

Summary and Future Research Considerations

7.1 Summary

In this chapter, the contributions described in this dissertation are summarized and suggestions for future research are presented. The goal of this research is the development of a reliable, coherent communication system which offers good bandwidth utilization and transmission performance in a shallow water channel. In order to achieve this goal, a simple model of a shallow underwater acoustic channel was developed. The method of computation of signal attenuation and delay based on channel geometry, environmental conditions and system parameters is described. To limit the number of terms in the computation of a received signal, the condition for finding the number of terms with significant amplitudes is derived. For the time-variant channel, the effect of the Doppler shift due to the relative motion between a transmitter and a receiver was considered. A case of the channel model was studied to investigate signal attenuation

and arriving angles with respect to time delay and wind speed. As the difference in time delay between direct and reflected signals increases, the arrival angles between reflected signals becomes larger, allowing us to limit the number of multipath signals using a directional receiver.

Relevant characteristics of the underwater acoustic communication channel were briefly described to investigate the achievable transmission range at given channel conditions and system requirements. The achievable transmission range as a function of the wind speed was investigated. We also investigated the acoustic power required for a certain transmission range at given SNR values. The effect of system impulse response when a directional receiver is employed at the receiver was investigated at different wind speeds. Communication over several kilometres with carrier frequency $f = 50$ kHz and several tens of kilometres with $f \leq 10$ kHz might be possible using only 75 watts of acoustic power.

A new method of performance evaluation for multipath corrupted signals was proposed by introducing the signal-to-multipath ratio (SMR). Using this tool, an analysis of an acoustics system was performed. Analysis results showed that a high transmission rate may be possible over a very shallow water channel using phase-shift-keying modulation. Such transmission is possible in the presence of constructive interference between direct- and multi-path signals. The robustness of the transmission depends on the sea state; it improves with rough sea conditions. Alternatively, higher transmission rates can be achieved by using a larger number of phases to modulate the signal. The channel model used in this study approximates an actual channel in which both the amplitude and delay of multi-path signals will randomly fluctuate. However, it is postulated here that these variations are negligible within the duration of the signalling element. Their effects on the phase detector can therefore be eliminated by using differential phase modulation.

An equalizer is used as a means to counter the effects of multipath propagation in a long-range shallow water channel. To study the effectiveness of an equalization tech-

nique, a channel condition which has severe intersymbol interference was chosen. Results show that adaptive equalization for digital acoustic communication in a long-range, shallow water channel is feasible. Data rates in excess of 12 k-bits/s might be possible over a 20 km distance with a system utilizing 4 ksymbols/s as transmission rate and 8-PSK as modulation method. For simplicity, perfect synchronization was assumed. A N-ary PSK modulated signal was studied due to its good bandwidth utilization. Convergence characteristics and steady state performance of the equalizer with least mean square (LMS), fast self-optimized LMS (FOLMS) and recursive least square (RLS) algorithms were investigated. Hardware complexity to implement the equalizer with those algorithms were determined. For a shallow underwater channel with large signal delay spread, LMS and FOLMS algorithms can be implemented with relatively low hardware complexity while a RLS algorithm requires extensive hardware and is difficult to implement in many cases.

As an anti-multipath technique for a time variant underwater acoustic channel, the modified structure of joint adaptive equalization and carrier synchronization for the q-PSK modulated signal is proposed. The procedure to update coefficients of the equalizer and synchronizer was described. A novel equalizer structure can change the number of equalizer taps adaptively depending on the sea state. Adaptive equalization allows us to design a computationally efficient and low-power-consumption system required for the prolonged battery life of a remotely operated system. Alternatively it can be used to increase the transmission rate at favorable channel conditions. This can be achieved by increasing signalling speed or by employing a larger number of phases for N-ary PSK modulated signals. The performance of the proposed structure was evaluated by computer simulation. Result of analysis indicates that the saving in computational load up to 60% can be achieved for a studied case. The effectiveness of a directional receiver with a proposed structure was also demonstrated.

7.2 Suggestions for Future Research

This section describes suggestions for future research which may lead to still better performance of the methods introduced in this dissertation.

The channel model used in this thesis was based on the assumption of a constant sound profile. To improve the accuracy of the model, a more reliable, layered sound profile can be incorporated. Utilizing a ray tracing algorithm with a layered sound profile, the channel model developed by the author can be generalized. A generalized model can be used for more accurate analysis of communication systems. This approach has already been taken by Bjerrum-Niese *et al.* [8].

An efficient communication system can explore time-variability by using an adaptive transmission rate. This can be achieved by varying the number of transmission phases in q-PSK modulation or by increasing the symbol rate at favorable channel conditions.

For a channel which varies slowly in time, it is possible to reduce the complexity of the equalizer. This is done by estimating the channel response to determine the values of the taps of the equalizer. These taps do not need to be updated as frequently, leading to simpler computations. Further computation complexity reduction is attainable by utilization of the fact that the occasionally estimated channel parameters can exclude those taps of an equalizer with negligible amplitudes. This in turn will allow us to use a more complex RLS algorithm with its superior performance.

Bibliography

[1] Albers, V.M., Underwater acoustic Handbook II, University park:Pensylvania state university press, 1965, p.346.

[2] Anderson, H.R., "Site-Specific BER Analysis in Frequency-Selective Channels Using a Ray-Tracing Propagation Model," *Proc. of Globecom 94*, Vol. 3, San Francisco, Nov. 1994, pp. 1441-1445.

[3] Bejani, E. and Beliore, J., "Multicarrier Coherent Communications for the Underwater Acoustic Channel," *Proc. Ocean 96*, Vol. III, Fort Lauderdale, FL, Sep. 1996, pp. 1125-1130.

[4] Bessios, A.G. and Caimi, F.M., "Multipath Compensation for Underwater Acoustic Communication," *Proc.of Oceans 94*, Vol. I, Brest, France, Sept. 1994, pp. 317-322.

[5] Beyer, W.H., CRC Standard Mathematical Tables, 26th edition, CRC press, 1981, p.8.

[6] Bierman, G.J., *Factorization Methods for Discrete Sequential Estimation*, New York: Academic, 1977.

[7] Billon, B. and Quellec, B., "Performance of High Data Rate Acoustic Underwater Communication Systems Using Adaptive Beamforming and Equalizing," *Proc. of Oceans 94*, Vol. III, Brest, France, Sept. 1994, pp. 507-512.

[8] Bjerrum-Niese, C. and Bjorno, L., "Simulated Design of an Acoustic Modem for an AUV in a Shallow Water Channel," *Proc. of Undersea Defense Technology*, London, UK, July 1996, pp. 20-24.

[9] Bjerrum-Niese, C., Bjorno L., Pinto, M.A. and Quellec, B., "A Simulation Tool for High Data-Rate Acoustic Communication in a Shallow-Water, Time-Varying Channel," *IEEE J. on Oceanic Engineering*, Vol. 21, No. 2, April 1996, pp. 143-149.

[10] Bozic, S.M., *Digital and Kalman filtering - An Introduction to Discrete-time Filtering and Optimum Linear Estimation*, Edward Arnord, 1979.

[11] Bragard, P. and Jourdain, G., "A Fast Self-optimized LMS Algorithm for Nonstationary Identification. Application to Underwater Equalization," *Proc. of ICASSP'90*, Albuquerque, NM, 1990, pp. 1425-1428.

[12] Brekhovskikh, L.M. and Lysanov, Y., *Fundamentals of Ocean Acoustics*, Springer-Verlag Berlin, 1982, pp. 21-22.

[13] Brekhovskikh, L.M. *Waves in Layered Media*, 1st ed., Academic press, 1960, pp. 325-331.

[14] Brekhovskikh, L.M., *Waves in Layered Media*, 2nd ed., Academic press, 1980, pp. 299-305.

[15] Brugel, H. and Driessen, P.F., "Variable Bandwidth DPLL Bit Synchronizer with Rapid Acquisition Implemented as a Finite State Machine," *IEEE Trans. Commun*, Vol. 42, No. 9, Sep. 1994, pp. 2751-2759.

[16] Brekhovskikh, L.M., *Waves in Layered Media*, 2nd ed., Academic press, 1980, pp. 299-305.

[17] Burdic, W.S., *Underwater Acoustic System Analysis*, 2nd ed., Prentice-Hall, Inc., 1991, pp. 93-95.

[18] Burdic, W.S., *Underwater Acoustic System Analysis*, 2nd ed., Prentice-Hall, Inc., 1991, pp. 130-131.

[19] Camp, L., *Underwater Acoustics*, Wiley-interscience, 1970, p.195.

[20] Capellano, V. and Jourdain, G., "Comparison of Adaptive Algorithms for Multichannel Adaptive Equalizers. Application to Underwater Acoustic Communications," *Proc. Ocean 98*, New York, NY, 1998, pp.1178-1182.

[21] Capellano, V., Loubet, G. and Jourdain, G., "Adaptive Multichannel Equalizer for Underwater Communications," *Proc. Ocean 96*, Vol. II, Fort Lauderdale, FL, Sep. 1996, pp.994-999.

[22] Captipovic, J., "Performance Limitations in Underwater Acoustic Telemetry," *IEEE J. on Oceanic Engineering*, Vol. 15, July 1990, pp. 205-216.

[23] Captipovic, J., Deffenbaugh, M., Freitag, L. and Frye, D., "An Acoustic Telemetry System for Deep Ocean Mooring Data Acquisition and Control," *Proc. of Oceans 89*, Seattle, WA, Oct. 1989, pp. 887-892.

[24] Carlson, N.A., "Fast Triangular Formulation of the Square Root Filter," *AIAA Journal*, Vol. 11, No.9, Sept. 1973, pp.1259-1265.

[25] Coates, R., Gazey B. and Smith B., *Underwater Acoustics and Sonar Systems*, Continuing Education Course in School of Electronic and Electrical Engineering, the University of Birmingham, UK, Vol. 1, Apr. 1991, p.21.

[26] Coates, R., *Underwater Acoustic Systems*, Mcmillan Education Ltd., 1990, pp. 13-14.

[27] Coates, R., *Underwater Acoustic Systems*, Mcmillan Education Ltd., 1990, pp. 26-28.

[28] Coates, R., *Underwater Acoustic Systems*, Mcmillan Education Ltd., 1990, pp. 92-93.

[29] Coates, R., "An Empirical Formula for Computing the Beckmann-Spizzichino Surface Reflection Loss Coefficient," *IEEE Trans. Ultrasonics, Ferro-electronics, and Frequency Control*, Vol. 35, No. 4, July 1988, pp. 522-523.

[30] Coates, R., Owens, R. and Tseng, M., "Underwater Acoustic Communications: A Second Bibliography and Review," in *Proc. of Institute of Acoustics*, Vol. 15, Part 9, Dec., 1993, pp.1-11.

[31] Coates, R., Tseng, M. and Wang, L., "BASS 300 PARACOM: A Model Underwater Parametric Communication System," *IEEE J. on Oceanic Engineering*, Vol. 21, No. 2, April 1996, pp. 225-232.

[32] Diamond, R., *Extend Users Manual*, Imagine That, Inc., San Jose, California, 1988.

[33] Driessen, P.F., "DPLL Bit Synchronizer with Rapid Acquisition Using Adaptive Kalman Filtering Techniques," *IEEE Trans. Commun*, Vol. 42, No. 9, Sep. 1994, pp. 2673-2675.

[34] Driessen, P.F., "Gigabits/s Indoor Wireless Systems with Directional Antennas," *IEEE Trans. Commun*, Vol. 44, No. 8, Aug. 1996, pp. 1034-1043.

[35] Eliaz, A., Tabrikian, J. and Messer, H., "Robust communication in Uncertain Shallow Water Acoustic Channels," Ninth IEEE Signal Processing Workshop on Statistical Signal and Array Processing, New York, NY, USA, 1998, pp.124-127.

[36] Essebbar, A., Loubet, G. and Vial, F., "Underwater Acoustic Channel Simulations for Communication," *Ocean 94*, Vol. III, pp. 495-500.

[37] Essebbar, A. and Vercelloni, E., "Simulation of Communication System for Underwater Acoustic," *Proc. of Oceans 95*, Oct. 1995, pp. 1204-1207.

[38] Falconer, D.D., "Jointly Adaptive Equalization and Carrier Recovery in Two-dimensional Digital Communication," *B.S.T.J.*, No.3, March 1976, pp.317-334.

[39] Falahati, A., Woodward, B. and Bateman, S.C., "Underwater Acoustic Channel Models For 4800 b/s QPSK Signals," *IEEE J. on Oceanic Engineering*, Vol. 16, No. 1, Jan. 1991, pp. 12-20.

[40] Fischer, J., Bennett, K., Reible, S., Cafarella J. and Yao I., "A High Rate, Underwater Acoustic Phone," *Proc. of Oceans 92*, Newport, RI, Oct. 1992, pp. 571-576.

[41] Freitag, L., Johnson, M. and Stojanovic M., "Efficient Equalizer Update Algorithms for Acoustic Communication Channels of Varying Complexity," *Proc. of Ocean 97*, Halifax, Nova Scotia, Canada, October 1997, pp.580-585.

[42] Galvin, R. and Coates, R.F.W, "Analysis of the Performance of an Underwater Acoustic Communications System and Comparison with a Stochastic Model," *Proc. of Oceans 94*, Brest, France, Sept. 1994, pp. III.478-III.482.

[43] Games, J and Barroso, V., "Blind Decision Feedback Equalization of Underwater Acoustic Channels," *Proc. of Ocean 98*, New York, NY, 1998, pp.810-814

[44] Geller, B., Capellano, V., Brossier, J., Essebbar, A. and Jourdain, G., "Equalizer for Video Rate Transmission in Multipath Underwater Communications," *IEEE J. on Oceanic Engineering*, Vol. 21, No. 2, April 1996, pp. 150-155.

[45] Geller, B., Brossier, J.M., and Capellano, V., "*Equalizer for high data rate transmission in underwater communications*," *Proc. of Oceans 94*, Brest, France, Sept. 1994, Vol. I, pp. 302-306.

[46] Gill, G.S. and Gupta, S.C., "On Higher-order Discrete Phase-locked Loops," *IEEE Trans., Aerosp. Electron. Syst.*, Vol. AES-8, Sept. 1972, pp. 615-623.

[47] Goalic, A., Labat, J., Trubuil, J., Saoudi, S. and Riouaten, D., "Toward a Digital Acoustic Underwater Phone," *Proc. of Oceans 94*, Brest, France, Sept. 1994, pp. III.489-III.494.

[48] Gray, C.A., Uehara, G.T. and Lin, S., "Bandwidth Efficient Modulation for Underwater Acoustic Data-Communications," *Proc. of Oceans 94*, Brest, France, Sept. 1994, pp. I.281-I.285.

[49] Hong, D. and Ingle, V.K., "Underwater Video Compression using the Wavelet Transform," *Proc. of Oceans 95*, San Diego, Oct. 1995, pp. 1141-1416.

[50] Howes, D. and Zielinski, A., "Multi-path Modeling for Acoustic Communication," *MTS-IEEE conf.*, Washington DC., Sep. 1982, pp. 217-222.

[51] Howe, G.S., Tarbit, P.S.D., Hinton, O.R., Sharif, B.S., and Adams, A.E., "Subsea Acoustic Remote Communications Utilizing an Adaptive Receiving Beamformer for Multipath Suppression," *Proc. of Oceans 94*, Brest, France, Sept. 1994, vol. I, pp. 313-316.

[52] Hsu, F.M., "Square Root Kalman Filtering for High-Speed Data Received over Fading Dispersive HF Channels," *IEEE Trans. on Information Theory*, vol. IT-28, no. 5, Sep. 1982, pp. 753-763.

[53] Jeruchim, M.C.,Balaban, P., Shanmugan, K.S., *Simulation of Communication Systems*, Plenum Press, New York, 1992, pp. 651-661.

[54] Johnson, M., Brady, D. and Grund, M., "Reducing the Computational Requirements of Adaptive Equalization in Underwater Acoustic Communications," *Proc. of Oceans 95*, pp. 1405-1410.

[55] Karam, G., Kervarec, J., Sari, H., and Vandamme, P., "All-Digital Implementation of the Carrier Recovery Loop in Digital Radio Systems," *ICC 91'*, June 1991, pp.175-179.

[56] Kaya, A. and Yauchi, S., "An Acoustic Communication System for Subsea Robot," *Proc.of Oceans 89*, Seattle, WA, Oct. 1989, pp. 765-770.

[57] Labat, J., "Real Time Underwater Communications," *Proc. of Oceans 94*, Brest, France, Sept. 1994, pp. III.501-III.506.

[58] Labat, J., Trubuil, L. and Nicot, M., "Blind Decision Feedback Equalization Application to Underwater Communication Systems," *Proc. of Oceans 98*, New York, NY, 1998, pp.805 - 809.

[59] Lee, J.C. and Un, C.K., "Performance Analysis of Digital Tanlock Loop for Tracking Suppressed-carrier N-ary PSK Signals," *IEEE Trans. Commun.*, Vol. COM-33, pp. 904-909, Sep. 1985.

[60] Lindsay, W.C. and Chie, C.M., "A Survey of Digital Phase-locked Loops," *Proc. IEEE*, Vol. 69, Apr. 1981, pp. 410-431.

[61] Lindsey, W.C. and Osbone, H.C., "Digital Phase-locked Loops for Suppressed Carrier Recovery," *Conf. Rec., Nat. Telecommun. Conf.*, Washington DC, Nov. 1979, pp. 24.3.1-24.3.6.

[62] Lindsey, W.C. and Seyl, S., "Characterization and Measurement of Phase-locked Loop Performance," *Conf. Rec., Nat. Telecommun. Conf.*, 1982, pp. E2.5.1-E2.5.6.

[63] Lo, N.W.K and Falconer, D.D., "Adaptive Equalization and Diversity Combining for Mobile Radio using Interpolated Channel Estimates," *IEEE Trans. Vehicular Technology.*, Vol. 40, No. 3, pp. 636-645, Aug. 1991.

[64] Merriam, S. and Porta, D., "DSP-based Acoustic Telemetry Modems," *Sea Technology*, May 1993.

[65] Meyr, H. and Ascheid, G., *Synchronization in Digital Communications*, A Wiley-Interscience Publication, 1990.

[66] Neasham, J. A., Thompson, D., Tweedy, A. D., Lawlor, M. A., Hinton, O. R., Adams, A. E. and Sharif, B. S., (1996), "Combined Equalization and Beamforming to Achieve 20kbits/s Acoustic Telemetry for ROVs," *Proc. Ocean 96*, Vol. II, Fort Lauderdale, FL, Sep. 1996, pp.988-993.

[67] Osborne, H.C., "Stability Analysis of an N-th Power Digital Phase-Locked Loop-Parts II," *IEEE Trans. Commun.*, Vol. COM-28, No. 8, pp. 1355-1364, Aug. 1980.

[68] Porta, D., "Underwater Acoustic Communications," *Sea Technology*, Feb. 1998, pp.49-55.

[69] Proakis, J.G., *Digital Communications*, McGraw-Hill Book Co., 1983, pp. 703-705.

[70] Proakis, J.G., *Digital Communications*, 2nd ed., McGraw-Hill Book Co., 1989, pp. 642-648.

[71] Proakis, J.G., "Coded Modulation For Digital Communications over Rayleigh Fading Channels," *IEEE J. on Oceanic Engineering.*, Vol. 16, No. 1, Jan. 1991, pp. 66-73.

[72] Proakis, J.G., "Adaptive Equalization Techniques for Acoustic Telemetry Channels," *IEEE J. on Oceanic Engineering*, Vol. 16, No. 1, Jan. 1991, pp. 21-31.

[73] Qureshi, S.U.H., "Adaptive equalization," *Proc. IEEE*, Vol. 73, Sep. 1985, pp. 1348-1388.

[74] Sandsmark, G.H. and Solstad, A., "Simulations of an Adaptive Equalizer Applied to High-speed Ocean Acoustic Data Transmission," *IEEE J. on Oceanic Engineering*, Vol. 16, No. 1, 1991, pp. 32-41.

[75] Soliman, S.S., "Synchronization Issues in Ocean Telemetry," *IEEE J. on Oceanic Engineering*, Vol. 16, No. 1, Jan. 1991, pp. 74-85.

[76] Stein, S. "Fading Channel Issues in System Engineering," *IEEE J. on Selected Areas Commun.*, Vol. SAC-5, Feb. 1987, pp. 68-89.

[77] Stojanovic, M., Catipovic, J.A. and Proakis, J.G., "Phase Coherent Digital Communications for Underwater Acoustic Channels," *IEEE J. on Oceanic Engineering*, Vol. 19, No. 1, Jan 1994, pp. 100-111.

[78] Stojanovic, M., "Recent Advances in High-Speed Underwater Acoustic Communications," *IEEE J. on Oceanic Engineering*, Vol. 21, No. 2, April 1996, pp. 125-136.

[79] Stojanovic, M. and Zvonar, Z., "Multichannel Processing of Broadband Multiuser communication Signals in Shallow Water Acoustic Channels," *IEEE J. on Oceanic Engineering*, Vol. 21, No. 2, April 1996, pp. 156-166.

[80] Suzuki, M. and Sasaki, T., "Digital Acoustic Image Transmission System for Deep Sea Research Submersible," *Proc. of Oceans 92*, Newport, RI, Oct. 1992, pp. 567-570.

[81] Tarbit, P.S.D., Howe, G., Hinton, O., Adam, A., and Sharif, B., "Development of a Real-time Adaptive Equalizer for a High-rate Underwater Acoustic Communication Link," *Proc. of Oceans 94*, Brest, France, Sept. 1994, pp. I.307-I.312.

[82] Tong, L., Xu, G. and Kailath, "Blind Identification and Equalization based on Second-order Statistics," *IEEE Trans. Inform. Theory*, Vol. 40, Mar. 1994, pp. 340-349.

[83] Tucker, D.G. and Gazey, B.K., *Applied Underwater Acoustics*, Pergamon Press, 1966, pp. 108-111.

[84] Urick, R.J., *Principles of Underwater Sound*, 3rd edition, McGraw-Hill Book Co., 1983.

[85] Urick, R.J., *Principles of Underwater Sound*, 1st edition, McGraw-Hill Book Co., 1975, p.165.

[86] Urick, R.J., "Intensity Summation of Modes and Images in Shallow-Water Sound Transmission," *The Journal of the Acoustical Society of America*, Vol. 46, No. 3, Apr.1969, pp. 780-788.

[87] Yarger, D.F., "The User Guide for the RAY-MODE Propagation Loss Program," *NUSC Technical memorandum*, 222-10-76, Aug. 1976, p. c-14.

[88] Yoon, Y. and Zielinski, A., "Simulation of the Equalizer for Shallow Water Acoustic Communications," *Proc. of Oceans 95*, San Diego, Oct. 1995, pp. 1197-1203.

[89] Yoon, Y. and Zielinski, A., "Adaptive Carrier Recovery for Underwater Acoustic Communication," *Proc. of XIIIth Symposium on Hydroacoustics*, Jurata, Poland, May 1996, pp. 12-20.

[90] Zielinski, A., Coates, R., Wang, L. and Saleh, A., "High Rate Shallow Water Acoustic Communication," *Proc. of Oceans 93*, vol. III, pp. 432-437.

[91] Zielinski, A., Yoon, Y. and Wu, L., "Performance Analysis of Digital Acoustic Communication in a Shallow Water Channel," *IEEE J. on Oceanic Engineering*, Vol. 20, No. 4, Oct. 1995, pp. 293-299,

[92] Zielinski, A. and Yoon, Y., "Simulation of Digital Communication System in a Shallow Water Channel," *XII Symposium on Hydroacoustics(SHA'95)*, May 1995, Jurata, Poland, pp. 299-308.

[93] Zielinski, A. and Yoon, Y., "High Rate Digital Acoustic Communication in Shallow Water Channel," contribution to a book *Recent Advances in Marine Science and Technology* -'94, June 1995, Townsville, Australia, PACON International, pp. 415-426.